MEASURING AND MODELING DEEP DRAINAGE, STREAMFLOW, AND SOIL MOISTURE IN OKLAHOMA

By

BRIANA M. WYATT

Bachelor of Science in Environmental Science
Oklahoma State University
Stillwater, OK
2013

Master of Science in Plant and Soil Sciences
Oklahoma State University
Stillwater, OK
2015

Submitted to the Faculty of the
Graduate College of the
Oklahoma State University
in partial fulfillment of
the requirements for
the Degree of
DOCTOR OF PHILOSOPHY
December 2019

MEASURING AND MODELING DEEP

DRAINAGE, STREAMFLOW, AND

SOIL MOISTURE IN OKLAHOMA

Dissertation Approved:

Tyson Ochsner

Dissertation Adviser

Chris Zou

Phillip Alderman

Henry Adams

ACKNOWLEDGEMENTS

First and foremost, this dissertation is dedicated to the Almighty God. I pray the years of work it represents have been a fragrant offering, a sacrifice acceptable and pleasing to Him. Secondly, I would like to thank my favorite person in the world, my wonderful husband, John, for his unending encouragement and support of my work over these past several years. I also want to extend my sincerest gratitude to my family, who has provided constant support throughout my graduate career. Finally, I want to thank my advisor, Dr. Tyson Ochsner, for his guidance over the past six years. His mentorship has taught me more than I would have thought possible and has given me an impeccable standard toward which to strive.

Name: BRIANA M. WYATT

Date of Degree: December 2019

Title of Study: MEASURING AND MODELING DEEP DRAINAGE, STREAMFLOW, AND SOIL MOISTURE IN OKLAHOMA

Major Field: SOIL SCIENCE

Abstract:

This dissertation examines multiple components of the Oklahoma water balance in order to answer three independent research questions:

i) Can long-term soil moisture monitoring data be used to estimate potential groundwater recharge rates? Daily drainage rates from the root zone were estimated for 78 sites using up to 17 years of soil moisture data from the Oklahoma Mesonet. Mean annual drainage rates ranged from 6 to 266 mm yr^{-1}, with a statewide median of 67 mm yr^{-1}. Drainage estimates were also modeled for four focus sites using HYDRUS1-D. Soil moisture-based drainage rates and HYDRUS1-D drainage rates agreed within 10 mm yr^{-1} at two drier sites but had discrepancies of >150 mm yr^{-1} at two sites with >1000 mm yr^{-1} precipitation.

ii) Does incorporating soil moisture information improve seasonal streamflow forecast accuracy? A modified version of the standard Natural Resources Conservation Service (NRCS) principal component analysis and regression (PCR) model was developed to forecast streamflow in four rainfall-dominated watersheds. This model incorporated antecedent precipitation and soil moisture data from long-term monitoring networks into PCR analysis to predict seasonal streamflow volumes at 0-, 1-, 2-, and 3-month lead times. Including soil moisture data improved forecast accuracy by more than 50% over precipitation-based forecasts.

iii) Can root zone soil moisture under diverse land cover types be effectively estimated by integrating ground-based meteorological data and remotely-sensed vegetation index data? Estimates of root zone soil moisture were made for four focus locations – a mixed hardwood forest, a loblolly pine plantation, cropland, and tallgrass prairie – by integrating ground-based meteorological data and basal crop coefficient curves derived from remotely-sensed vegetation index data within a soil water balance model. Results show that the model is able to estimate plant available water dynamics moderately well at the four focus locations, but needs further improvements before it can be used operationally.

TABLE OF CONTENTS

LIST OF TABLES

TABLES IN CHAPTER II

Table Page

TABLES IN CHAPTER III

Table Page

TABLES IN CHAPTER VI

Table Page

LIST OF FIGURES

FIGURES IN CHAPTER II

FIGURES IN CHAPTER III

Figure Page

FIGURES IN CHAPTER VI

Figure Page

CHAPTER I

GENERAL INTRODUCTION

Less than one percent of all water on Earth is fresh and accessible for use, and these scarce freshwater resources are increasingly threatened by overuse and changes in the hydrological cycle due to climate change (Shiklomanov, 1993). These impacts are especially clear in Oklahoma, which is located in a region known to have high levels of water scarcity, where frequent droughts and occasional severe flooding have the potential to cause both economic and ecological losses, as well as the loss of human life (Mekonnnen and Hoekstra, 2016). Natural disasters such as drought and floods are influenced not only by atmospheric conditions, but also by the soil water status (Berg and Sheffield, 2018; Seo et al., 2017). Soil strongly influences hydrological processes such as deep drainage (i.e., potential groundwater recharge) and streamflow generation by regulating fluxes of water between the deep subsurface, the land surface, and the atmosphere (Horton, 1931). Additionally, these fluxes impact and are impacted by plant water uptake and vegetation dynamics (Acharya et al., 2017). Because of the influence of soil moisture on these important hydrological processes, soil moisture data are able to provide important insight into the dynamics of deep drainage and may be used to improve streamflow forecasts. Also, due to the influence of vegetation dynamics on soil moisture,

it is important to understand the dynamics of soil moisture under diverse vegetation types. This dissertation seeks to determine how soil moisture influences deep drainage, how soil moisture data may be used to improve streamflow forecasts in rainfall-dominated watersheds, and how soil moisture varies under diverse vegetation types by addressing the following issues:

i) Groundwater levels in the state of Oklahoma have declined in recent years due to a number of factors including overpumping and drought (Sallee, 2015). Soil moisture levels influence the amount of water that percolates beneath the root zone (i.e., potential groundwater recharge), and it has recently been shown that it is possible to use soil moisture data to calibrate models used to estimate potential groundwater recharge over large areas (Andreasen et al., 2013; Wang et al., 2016). Oklahoma is home to one of the world's longest-running soil moisture monitoring networks, with soil moisture data recorded at over 100 locations in the state since 1996 (McPherson et al., 2007). The second chapter of this dissertation discusses how these long-term soil moisture monitoring data may be used to estimate state-wide potential groundwater recharge rates.

ii) Streamflow forecasts are essential for providing critical information to surface water managers regarding the potential amount of water available for distribution in upcoming months. However, unlike the well-established seasonal forecasts used in the snow-dominated Western U.S., streamflow forecasting methods currently used in the central and eastern U.S. are used primarily to predict flash floods at short lead times (i.e., <6 days) rather than to inform surface water management decisions at long lead times (i.e., months in advance). This lack of seasonal forecasts increases the vulnerability of surface water resources, which are subject to frequent droughts and an increasingly variable

climate (Krueger et al., 2017; Christian et al., 2015). Recent work has shown that incorporating antecedent soil moisture data into statistical streamflow forecasts used in the snow-dominated West increases forecast accuracy by ~8% (Harpold et al., 2017). The third chapter of this dissertation discusses how this method may be used to predict future streamflow volumes in rainfall-dominated watersheds, and whether these forecasts are able to be made at longer lead times than current forecasting models in the state.

iii) Current soil moisture monitoring networks have stations installed almost exclusively in locations where grasses are the dominant vegetation types, leading to uncertainties regarding the soil moisture status under other vegetation types, such as croplands and forests. Recent work has shown that there can be significant differences between soil moisture measured by sensors under grass and in neighboring winter wheat fields (Patrignani and Ochsner, 2018). It has also been shown that it may be possible to estimate soil moisture across diverse vegetation types by integrating satellite-based vegetation index data and ground-based meteorological data into a soil water balance model (Sanchez et al., 2010; Sanchez et al., 2012). The fourth chapter of this dissertation applies this methodology to four study locations to determine how effectively the water balance model estimates soil moisture under four different major vegetation types in Oklahoma.

DISSERTATION ORGANIZATION

This dissertation consists of a total of five chapters. The first and last chapters are a general introduction (**Chapter I**) and conclusion (**Chapter V**). These chapters provide a broad overview of the topics discussed in the dissertation and its most important findings. The remaining chapters address the issues stated above regarding the influence of soil moisture on various hydrological processes in Oklahoma.

Chapter II describes a novel method of estimating potential groundwater recharge using 17 years of soil moisture monitoring data from 78 Oklahoma Mesonet stations across the state. Comparisons are made between soil moisture-based potential groundwater recharge rates and recharge rates reported in prior studies, and with drainage rates estimated using a calibrated soil water flow model at four focus sites.

Chapter III discusses the application of a well-known statistical streamflow forecasting method in four rainfall-dominated watersheds, and the improvements in streamflow forecast resulting from the inclusion of antecedent soil moisture data.

Chapter IV investigates the potential of integrating remotely sensed vegetation index data and ground-based meteorological data into a soil water balance model in order to accurately estimate soil moisture in a mixed hardwood forest, a loblolly pine plantation, cropland, and tallgrass prairie in Oklahoma.

REFERENCES

Acharya, B.S., T. Halihan, C.B. Zou, and R.E. Will. 2017. Vegetation controls on the spatio-temporal heterogeneity of deep moisture in the unsaturated zone: a hydrogeophysical evaluation. Scientific Reports 7(1).

Andreasen, M., L. A. Andreasen, K. H. Jensen, T. O. Sonnenborg, and S. Bircher. 2013. Estimation of regional groundwater recharge using data from a distributed soil moisture network. Vadose Zone J. 12. doi:10.2136/vzj2013.01.0035.

Berg, A. & Sheffield, J. 2018. Climate change and drought: the soil moisture perspective. Curr Clim Change Rep (2018) 4: 180. https://doi.org/10.1007/s40641-018-0095-0.

Christian, J., K. Christian, and J. Basara. 2015. Drought and pluvial dipole events within the great plains of the United States. Journal of Applied Meteorology and Climatology 54(9):1886-1898.

Harpold, A. A., et al. 2017. Does including soil moisture observations improve operational streamflow forecasts in snow-dominated watersheds? JAWRA Journal of the American Water Resources Association 53(1): 179-196.

Horton, R.E. 1931. The field, scope, and status of the science of hydrology. Eos, Transactions American Geophysical Union 12(1):189-202.

Krueger, E.S., Y.T. Yimam, and T.E. Ochsner. 2017. Human factors were dominant drivers of record low streamflow to a surface water irrigation district in the US southern Great Plains. Agricultural Water Management 185:93-104.

McPherson, R. A., C. A. Fiebrich, K. C. Crawford, J. R. Kilby, D. L. Grimsley, J. E. Martinez, J. B. Basara, B. G. Illston, D. A. Morris, and K. A. Kloesel. 2007. Statewide monitoring of the mesoscale environment: A technical update on the Oklahoma Mesonet. J. Atmos. and Ocean. Tech. 24:301-321.

Mekonnen, M.M., Hoekstra, A.Y., 2016. Four billion people facing severe water scarcity. Sci. Adv. 2, http://dx.doi.org/10.1126/sciadv.1500323.

Patrignani, A. and T. E. Ochsner. 2018. Modeling transient soil moisture dichotomies in landscapes with intermixed land covers. Journal of Hydrology 566: 783-794.

Sallee, B. 2015. Estimating groundwater recharge using the Oklahoma Mesonet. M.S. thesis. Oklahoma State Univ., Stillwater.

Sánchez, N., et al. 2010. Combining remote sensing and in situ soil moisture data for the application and validation of a distributed water balance model (HIDROMORE). agricultural water management 98(1): 69-78.

Sánchez, N., et al. 2012. Water balance at plot scale for soil moisture estimation using vegetation parameters. Agricultural and Forest Meteorology 166: 1-9.

Seo, D., T. Lakhankar, B. Cosgrove, R. Khanbilvardi, and X. Zhan. 2017. Applying SMOS soil moisture data into the National Weather Service (NWS)'s Research Distributed Hydrologic Model (HL-RDHM) for flash flood guidance application. Remote Sensing Applications: Society and Environment 8:182-192.

Shiklomanov, Igor. 1993. World Fresh Water Resources. Water in Crisis: A Guide to the World's Fresh Water Resources. Oxford University Press, New York.

USGS, U.S. Geological Survey. 2019. https://www.ers.usda.gov/topics/farm-practices-management/irrigation-water-use/#:~:targetText=USDA's%20Farm%20and%20Ranch%20Irrigation,fifths%20occurring%20in%20the%20West.&targetText=Agriculture%2C%20however%2C%20accounts%20for%20approximappro,of%20U.S.%20consumptive%20water%20use. Accessed 14 November 2019.

Wang, T., T. E. Franz, W. Yue, J. Szilagyi, V. A. Zlotnik, J. You, X. Chen, M. D. Shulski and A. Young. 2016. Feasibility analysis of using inverse modeling for estimating natural groundwater recharge from a large-scale soil moisture monitoring network. J. Hydrol. 533: 250-265.

CHAPTER II

Manuscript published in Vadose Zone Journal Vol. 16(6), 2017

USEFUL DRAINAGE ESTIMATES OBTAINED FROM A LARGE-SCALE SOIL MOISTURE MONITORING NETWORK BY APPLYING THE UNIT-GRADIENT ASSUMPTION

Briana M. Wyatt, Tyson E. Ochsner, Christopher A. Fiebrich, Christopher R. Neel, and David S. Wallace

ABSTRACT

Groundwater supplies ~20% of global freshwater withdrawals, and accurate information regarding groundwater recharge rates is needed for sustainable groundwater management. Recharge rates are often limited by the rates of drainage from the soil profile, which are influenced by soil moisture conditions. Soil moisture monitoring has expanded dramatically in recent decades with the advent of large-scale networks like the Oklahoma Mesonet, which has monitored soil moisture statewide since 1996. Using those data with site-specific soil hydraulic properties and a unit-gradient assumption, we estimated daily drainage rates at 60 cm for 78 sites for up to 17 years. Our working hypothesis is that these drainage rates are indicative of potential groundwater recharge rates. Mean annual drainage rates ranged from 6 – 266 mm yr^{-1}, with a statewide median

of 67 mm yr^{-1}. These rates agreed well with prior recharge estimates for major Oklahoma aquifers.

To provide a further independent check on our results, drainage was modeled using HYDRUS-1D for four focus sites across 17 years. Soil moisture-based drainage rates and HYDRUS-1D drainage rates agreed to within 10 mm yr^{-1} at the drier two sites but had discrepancies of >150 mm yr^{-1} at two sites with >1000 mm yr^{-1} precipitation. Simulations also showed that for a semi-arid site the unit-gradient assumption was likely violated at the 60-cm depth, highlighting the need for deeper soil moisture monitoring. Despite these limitations, this simple method for estimating drainage through long-term soil moisture monitoring shows unique potential to provide valuable information for hydrology and groundwater management.

INTRODUCTION

Groundwater aquifers supply approximately 20% of all freshwater withdrawals by humans globally, and the increasing number and severity of droughts projected due to climate change may lead to a heightened dependence upon these resources for agricultural production as well as for domestic, industrial, and municipal uses (World Water Assessment Programme, 2009). Plans for management of these vital natural resources are often based, in part, on estimates of groundwater recharge rates. However, given the complex nature of groundwater systems and the numerous interactions that occur in the groundwater-soil-atmosphere system, the quantification of recharge, especially over large areas, is difficult. A wide variety of methods have been used to estimate groundwater recharge, so recharge rates tend to differ between studies, even among those conducted on the same aquifer (Scanlon et al., 2002). Variations in estimated recharge rates between studies may also be caused by a number of other factors including: data availability, climate of the time period considered, and duration of the study. At large spatial scales, natural variations in soil type, climate, and topography also cause variability in recharge rates (Qu et al., 2014; Nolan et al., 2006).

Groundwater recharge estimates for major aquifers are often based upon short-term studies that only capture information over a few years' time, and frequently include decades-old data that may not reflect current climatological conditions. Additionally, ongoing changes in land cover and land use (e.g., woody plant encroachment) may impact groundwater recharge rates, making old estimates inaccurate (Kim and Jackson, 2012; Scanlon et al., 2006; Wine and Zou, 2012). In light of these challenges, methods to generate accurate and up-to-date information regarding current recharge rates are needed

to facilitate water resources planning and to advance hydrologic understanding of groundwater systems.

Groundwater recharge is often limited by the drainage rate from the soil profile, and that drainage rate is strongly influenced by the soil volumetric water content (hereafter referred to as soil moisture). Large-scale monitoring of soil moisture has expanded dramatically since the 1990's (Ochsner et al., 2013), yet the resulting data have not been widely utilized for estimating drainage rates. Two recent studies have shown that data from soil moisture monitoring networks can be used to optimize or calibrate the parameters of the soil hydraulic property functions in one-dimensional hydrologic models (Andreasen et al., 2013; Wang et al., 2016). The calibrated models can then be used with meteorological forcing data to estimate groundwater recharge. Here we add to this body of knowledge by demonstrating that the soil moisture data can be used directly to estimate drainage, without the complexities arising from reliance on a hydrologic model.

One of the earliest and most extensive large-scale soil moisture monitoring networks is the Oklahoma Mesonet (McPherson et al., 2007). The Oklahoma Mesonet has provided hydro-meteorological and soil matric potential data at >100 monitoring sites throughout the state since 1996 (Figure 1). Heat dissipation sensors located at depths of 5, 25, and 60 cm beneath the surface provide matric potential data every half hour (Illston et al, 2008; Scott et al., 2013). Using estimated soil hydraulic properties, these matric potential data can be converted to soil moisture data and then to hydraulic conductivity estimates. Assuming a unit gradient (i.e., gravity-driven flow) at the deepest measurement depth, these hydraulic conductivity values are numerically equivalent to the drainage rate (Nolan et al., 2006). These drainage rate estimates are expected to be

greater than or equal to the rate of groundwater recharge with a time lag that depends on vadose zone characteristics and depth to the water table.

The primary objective of this research was to determine the level of agreement between these soil moisture-based drainage estimates and independent estimates of drainage and recharge. Our over-arching goal is to create a method for providing long-term, updatable information on drainage rates, and thus potential groundwater recharge rates. To achieve this objective, daily drainage rates at the 60-cm depth were estimated using up to 17 years of soil moisture data for each of 78 Oklahoma Mesonet sites. Soil moisture was calculated from matric potential measurements made using heat dissipation sensors. The working hypothesis of this research was that these soil moisture-based drainage rates are indicative of the potential groundwater recharge rates for the underlying aquifer at each site, and that calculated drainage rates may act as an upper limit for actual recharge.

The potential benefits of this method over those used previously in the state of Oklahoma are three-fold: 1) soil moisture-based drainage rates incorporate long-term meteorological and soil moisture data that have been collected since 1996, including the effects of several extreme climatic events, 2) drainage estimates can be updated any time as long as the soil moisture monitoring system is intact, and 3) in addition to site-specific estimates of drainage, the large number of point measurements available may be used to indicate the spatial distribution of recharge across the entire state of Oklahoma, as opposed to single-aquifer studies that have been done in the past (Nolan et al., 2006). If the proposed approach shows merit, then it could be applied to other large-scale soil moisture monitoring networks in the US and around the world in future studies.

MATERIALS AND METHODS

Study area

The Oklahoma Mesonet spans the state of Oklahoma, which has an area of approximately 1.8×10^5 km^2 (Figure 1). The climate of the state ranges from humid subtropical in the southeast to semi-arid in the far west. Mean annual precipitation ranges from approximately 1420 mm in the southeast to 430 mm in the western Oklahoma Panhandle (Oklahoma Climatological Survey). Dominant land cover types vary from oak and pine forests and tallgrass prairies in the eastern portions of the state to shrublands and shortgrass prairie in the western portions, and encroachment by eastern redcedar (*Juniperus virginiana*) is pronounced in some areas (Tyrl et al., 2007). Additionally, approximately 2.4×10^4 km^2 of winter wheat are planted in the state each year, mostly in the west-central Oklahoma "wheat belt" (Oklahoma State University Small Grains Extension, 2015). The soils of Oklahoma vary from ultisols in the east to alfisols and mollisols in the central portion of the state to inceptisols and entisols in the west, with mollisols being the most common soil order in the state (Tyrl et al., 2007). Soil textures are highly variable, with sand contents ranging from 0.5% to 90% and clay contents ranging from 2.5% to 78% (Scott et al., 2013; Soil Survey Staff). The thickness of the vadose zone generally increases from east to west, with rock outcrops and shallow soils in the far southeast portion of the state and deep soils in the Panhandle.

Groundwater aquifers provided 37% of all water withdrawals in Oklahoma in 2005, with 63% of groundwater withdrawals used for agricultural irrigation (Tortorelli, 2009). The greatest irrigation withdrawals come from the Ogallala (High Plains) aquifer, portions of which underlie the Oklahoma Panhandle region (Luckey and Becker, 1999).

Another major source of water for irrigation is the Rush Springs aquifer in west-central Oklahoma (Becker and Runkle, 1998). The Garber-Wellington aquifer in central Oklahoma is heavily used for public and domestic water supply (Mashburn et al., 2014). Other major aquifers in the eastern half of the state, such as the Antlers aquifer in the southeast (Morton, 1992), the Arkansas River aquifer in east-central Oklahoma (Oklahoma Water Resource Board, 2012), and the Boone aquifer in the northeast (Czarnecki et al., 2009), are not heavily used at present; but they may come under increasing pressure due to population growth. Pre-existing recharge estimates for the above-mentioned major aquifers provide a primary means of evaluating the proposed soil moisture-based drainage estimation method.

Soil moisture-based drainage rates

Drainage rates were calculated for the years 1998-2014 using output from the Oklahoma Mesonet heat dissipation sensors (CS-229, Campbell Scientific, Inc., Logan, UT) and soil hydraulic property data for each site published by Scott et al. (2013). Heat dissipation sensors under grassland vegetation at each site are located at depths of 5, 25, and 60 cm and record the change in temperature that occurs within a porous ceramic matrix after a 21-s heat pulse is generated by a heater located inside the matrix. This temperature differential is measured and reported every 30 minutes and is normalized to account for inter-sensor differences (Illston et al., 2008). The 30-min resolution data were used to generate a daily mean reference (i.e., normalized) temperature differential, ΔT_{ref}. This daily mean was then used to determine the daily matric potential value using an empirical calibration equation:

$$\Psi_m = -c \exp(a\Delta T_{ref}) \quad (1)$$

where Ψ_m is the matric potential (kPa), and c and a are calibration constants with values of 0.717 kPa and 1.788° C^{-1}, respectively (Illston et al., 2008). The mean percent error for matric potential measurement with these sensors over the range from -10 to -35,000 kPa is 23% (Flint et al., 2002).

The daily matric potential data were then converted to soil volumetric water content values using the van Genuchten equation:

$$\theta = \theta_r + (\theta_s - \theta_r)[1 + (-\alpha\Psi_m)^n]^{-m} \quad (2)$$

where θ is soil volumetric water content (cm^3 cm^{-3}), θ_r is residual soil water content (cm^3 cm^{-3}), θ_s is saturated soil water content (cm^3 cm^{-3}), α and n are shape parameters estimated from the soil water retention curve, and m = 1-1/n (van Genuchten, 1980). Daily volumetric water content data at the 60-cm depth were then used to estimate hydraulic conductivity values by:

$$K(S_e) = K_0 S_e^L \{1 - [1 - S_e^{n/(n-1)}]^{1-1/n}\}^2 \quad (3)$$

where the effective saturation, S_e, is calculated by $S_e = (\theta-\theta_r)/(\theta_s-\theta_r)$, K_0 (cm d^{-1}) is a matching point conductivity value, and L is a unitless empirical coefficient (Schapp et al., 2001).

Values for θ_r, θ_s, α, n, K_0, and L for each Mesonet site and each sensor depth were determined by Scott et al. (2013). They used the most accurate sub-model within the Rosetta pedotransfer function to estimate soil hydraulic parameters based on soil texture (percent sand, silt, and clay) and bulk density, along with water retention measurements at -33 kPa and -1500 kPa (Schaap et al., 2001). The database containing these hydraulic parameters is called the MesoSoil database, and the version produced by Scott et al.

(2013) is MesoSoil version 1.1. Subsequently, the MesoSoil database has been updated with the inclusion of data for additional monitoring stations and improved quality control procedures, resulting in newer versions. MesoSoil version 1.2b, which can be downloaded at http://soilphysics.okstate.edu/data, was used for this study.

Assuming unit-gradient flow conditions (i.e., gravity-driven flow), the daily drainage rate at 60 cm was set equal to the hydraulic conductivity for that day. While the Oklahoma Mesonet does have sensors installed at 75 cm at some sites, there are not sensors at this depth at every site. As of 2007, there were 76 sites with sensors at 60 cm but only 53 with sensors at 75 cm. Additionally, starting in January 2011, sensors at the 75-cm depth began to be decommissioned (Scott et al., 2013). For these reasons, we chose to use the 60-cm depth. The unit-gradient assumption employed here has been used in a number of previous recharge studies that also incorporate Darcian flow methods (Chong et al., 1981; Gardner, 1964; Sisson, 1987; Nolan et al., 2006; Ahuja et al., 1988).

In preliminary studies, we tested a variety of more complex alternative approaches for estimating drainage from the soil moisture data that attempted to estimate and correct for vertical gradients in matric potential and unsaturated hydraulic conductivity. In the first alternative method, the matric potential gradient was approximated based on the difference in matric potential between adjacent sensor depths (i.e. 5 to 25, and 25 to 60 cm), and the hydraulic conductivity for the soil between two adjacent sensor depths was estimated by the arithmetic mean of the hydraulic conductivity at those depths. However, this method yielded unreasonable and widely variable results. For example, at the Fittstown Mesonet site in south-central Oklahoma for the years 2006-2009, this method produced drainage estimates ranging from -52 to +99

cm yr^{-1}, neither of which is physically plausible at this site which received 99 cm yr^{-1} of precipitation during that time frame.

In the second alternative method, the average hydraulic conductivity across two depths was estimated using the harmonic mean, as suggested by Darcy's law for layered soils. Although better than the first method, this second method again yielded unreasonable and widely variable drainage estimates, ranging from -11.8 to +4.7 cm yr^{-1} at the Fittstown site, with an average of -4.4 cm yr^{-1}. Such sustained upward flow is extremely unlikely to occur in this context. The third method used the simple unit-gradient approach, and was the only evaluated method that proved to produce reasonable drainage estimates when compared to previous recharge studies in the region. At the Fittstown site the unit-gradient approach resulted in drainage estimates ranging from 5.4 to 12.7 cm yr^{-1}, with an average of 9.6 cm yr^{-1}. These values are consistent with the recharge rate of 11.9 cm yr^{-1} determined by the Oklahoma Water Resources Board for the underlying Arbuckle-Simpson aquifer. Based on these preliminary findings, we chose to apply the unit-gradient assumption for the remainder of the study.

After calculating drainage for all sites with the necessary data, statistical outliers in long-term mean annual drainage rates were identified using a box plot, which resulted in the exclusion of four sites- Washington, Bixby, Lane, and Foraker- from subsequent analyses. Additional quality control included removing site-years with 30 or more missing days from analysis. To visualize spatial patterns in drainage, the mean annual drainage rate for the state was mapped using ordinary kriging with a 1 km x 1 km grid size. A Gaussian model was used for the variogram, with the kriging neighborhood

restricted to the ten nearest observation points and a maximum search distance of 300 km.

HYDRUS-1D model calibration and validation

Site-specific, independent drainage estimates were developed using HYDRUS-1D (PC-Progress, Prague, Czech Republic) for four focus sites: Goodwell, Miami, Tipton, and Wister (Figure 1.) These focus sites were selected for modeling because their locations represent a substantial portion of the variability in climatic and vegetative conditions across the state, with mean annual precipitation totals for years 1998 through 2014 ranging from 392 to 1144 mm (Table 1). HYDRUS-1D estimates water flow in saturated and unsaturated soil according to the Richards equation (Šimůnek et al., 2016; Richards, 1931).

In order to facilitate inverse estimation of soil hydraulic properties, soil profiles at each site were simplified and characterized by four soil layers associated with the depths of the heat dissipation sensors: 0-10 cm, 10-40 cm, 40-80 cm, and 80-300 cm. Previous studies involving inverse estimation of soil hydraulic properties based on in situ soil moisture data have also employed simplified soil profiles to limit the uncertainty arising from estimating large numbers of parameters (e.g. Scott et al., 2000). The 300-cm profile depth was considered adequate because it is unlikely that the root zone extends to 3 m in these locations (Sun et al., 1997; Jackson et al., 1996).

The main processes considered in HYDRUS-1D simulations were water flow and root water uptake. The van Genuchten-Mualem model for hydraulic properties (van Genuchten, 1980) was used to model water flow throughout the soil profiles. The -2 cm

air entry suction option was used at all sites except Tipton. This option is recommended for use at sites with fine-textured soils where the *n* parameter is < 1.2 (Vogel et al., 2001). Root water uptake was simulated using the model of Feddes et al. (1978). Critical pressure head values in the water stress response function were determined by values for pasture from Wesseling (1991). No data regarding root distribution or maximum rooting depths were available for these sites, so the Jackson et al. (1996) root density distribution model was used (Wang et al., 2016). Within this model, a β value for temperate grasslands of 0.943 and depth values from the HYRDUS-1D nodal depth distribution were used to calculate the root density. Upper boundary conditions were defined as atmospheric conditions with surface runoff, meaning that precipitation in excess of the soil's infiltration capacity would leave the site as runoff and not increase the pressure head at the top of the column. Lower boundary conditions were defined as free drainage.

The FAO Penman-Monteith method (also referred to as the FAO-56 method) was used to determine daily potential evapotranspiration values for each site within the HYDRUS-1D model (Allen et al., 1998). Meteorological parameters required for this calculation included site latitude, site elevation above mean sea level (m), angstrom values for short wave radiation, a factor regarding the effect of cloudiness on long wave radiation, coefficients for computing the cloudiness factor from solar radiation, coefficients for computing the emissivity effect on long wave radiation, and wind speed and temperature measurement heights (cm). All values except site latitude, site elevation, and wind speed and temperature measurement heights were set equal to suggested values given in HYDRUS-1D. Wind speed was measured at 200 cm above the ground surface and temperature was measured at 150 cm above the ground surface by the Oklahoma

Mesonet stations at each location. Crop data were considered to be constant, with a crop height of 150 mm, an albedo of 0.23, a surface cover fraction of 0.5, and a maximum rooting depth of 1000 mm. The leaf area index was computed from the surface cover fraction using a radiation extinction coefficient of 0.463. No rainfall interception was considered in our simulations.

Meteorological input data used to estimate potential evapotranspiration included daily maximum and minimum air temperature (°C), maximum and minimum relative humidity (%), precipitation (mm), wind speed (km d^{-1}), incoming solar radiation (MJ m^{-2} d^{-1}), and average vapor pressure deficit (Allen et al., 1998). These data, along with daily precipitation totals, were collected from the Oklahoma Mesonet. Additional upper boundary inputs included a factor termed hCritA, which is the minimum allowed pressure head at the soil surface, below which evaporation is decreased from the estimated potential evaporation rate. The hCritA value was set equal to -15,000 cm for our simulations, which is within the range suggested in the HYDRUS-1D documentation.

The inverse solution option of the HYDRUS-1D model was used to optimize soil hydraulic parameters of the top three soil layers based on daily field-measured matric potential data for the years 2006-2007 at each of the four focus sites. The fourth layer (80-300 cm) was left uncalibrated because no matric potential data were measured below 60 cm. The 2006-2007 time period was chosen because these years include extreme climatological phenomena (e.g., 2006 was an extremely dry year for Oklahoma, and 2007 was extremely wet). Calibration simulations also included the year 2005 as a spin-up year, but matric potential values for optimization were not included for 2005. Matric potential values calculated from the daily output of the heat dissipation sensors at depths

of 5, 25, and 60 cm were included in the objective function for the inverse solution. To obtain simulated matric potentials for the objective function, the daily output option was chosen within HYDRUS-1D, which uses a time-step weighted daily mean calculation.

Parameter optimization was done by running the inverse solution within the HYDRUS-1D model for each of the top three soil layers for each site, beginning with the uppermost layer and continuing downward (Turkeltaub et al., 2015; Wang et al., 2016). This approach breaks the optimization problem down into more manageable pieces, but it has the limitation that precludes possible interactions between parameters in separate layers that have the potential to change the optimized parameter values. To overcome this limitation, following the optimization of the individual soil layers, an additional optimization was done for the uppermost three layers (3 layers X 5 parameters/layer = 15 total parameters). Also, to reduce the influence of initial parameter values, optimizations were carried out twice for each site- once using Rosetta-estimated parameters from the MesoSoil database as the initial values and once using parameters values from Carsel and Parrish (1988) (Wang et al., 2016). In both cases, the initial values for L were taken from Rosetta. The matching point hydraulic conductivity (K_0) was used as the initial value for the saturated hydraulic conductivity (K_s) in the optimizations using Rosetta parameters. The set of optimized parameter values that led to the greatest agreement between measured and Hydrus-estimated matric potentials during the validation period was used for forward simulations. As suggested by prior studies, the following upper and lower bounds were placed on hydraulic parameters during optimization: θ_s = 0.3 - 0.5 cm^3 cm^{-3}, α = 0.01 – 10 kPa^{-1}, n = 1.01 - 3.0 (-), K_s = 1.0 – 10000 mm d^{-1}, and L = -2.0 – 2.0 (-) (Ries et al., 2015). All hydraulic parameters except for residual water content (θ_s, α, n, K_s,

and *L*) were calibrated for each of the top three layers, resulting in 15 optimized parameters per site. The θ_r parameter was not optimized because it has been shown by previous studies that this parameter is typically the least sensitive (Vrugt et. al., 2001; Šimůnek et al., 1998).

After calibrations were complete, validation simulations were carried out for each focus site in order to evaluate the soil moisture-based drainage estimates for those sites. Validation simulations were run using data for the years 1998-2014 and used the same input and boundary condition data as the calibration simulations. HYDRUS-1D outputs included, along with many other variables, estimations of pressure head, water content, and water flow at observation nodes 5, 25, and 60 cm below the surface. Water flow output data were analyzed to determine average annual drainage at the 60-cm depth.

To investigate the validity of the unit gradient assumption applied in the soil moisture-based drainage estimation method, a subset of pressure head profiles at the Goodwell site were examined. The Goodwell focus site was chosen for this analysis, as it is located in the semi-arid Oklahoma Panhandle region and may be the least likely of the focus sites to exhibit a unit gradient condition at the 60-cm depth. For soil profiles undergoing free drainage, a unit gradient is expected when the profile is near saturation, a condition which rarely, if ever, occurs at the Goodwell site. By default, HYDRUS-1D uses a variable time step to simulate soil water dynamics. The model automatically adjusts to small time steps (on the order of minutes) during times of sudden changes in soil water conditions, such as during rainfall infiltration, while larger time steps (on the order of days) are used during times of relatively stable soil water conditions. At each time step, model output included water flux at 60 cm. The outputs for each of these time

steps were ranked from largest to smallest in terms of drainage rate (downward flux) at the 60 cm depth, and the pressure head profiles corresponding to the top 1% of simulated drainage rates were plotted. This approach allowed us to visualize the pressure head (matric potential) gradients occurring at the times of maximum drainage to evaluate the validity of the unit-gradient assumption.

RESULTS AND DISCUSSION

Soil moisture-based drainage rates and prior recharge estimates

The soil-moisture based drainage estimates from the proposed method agreed well with prior recharge estimates. Mean annual soil moisture-based drainage rates for the period from 1998-2014 ranged from 6 mm yr^{-1} at Boise City in the Oklahoma Panhandle to 266 mm yr^{-1} at Bristow in northeast Oklahoma (Figure 2). This is similar to the range of recharge values found by prior studies in Oklahoma, with reported recharge rates ranging from 0.8 to 333 mm yr^{-1} (Pettyjohn and Miller, 1982; Veiux and Moreno, 2008). The state-wide median value of the mean annual soil moisture-based drainage rate for the years 1998-2014 was 67 mm yr^{-1}, which is approximately 7.7% of the median state-wide rainfall of 870 mm yr^{-1} for the same period. A similar percentage was found by Kim and Jackson (2012), who observed that an average of 8.3% of precipitation became recharge under grassland systems in their global analysis. Soil moisture-based drainage rates generally followed the precipitation gradient of the state, as expected, decreasing from east to west (Figure 2).

The most recent prior state-wide recharge rate map for Oklahoma, published by Pettyjohn et al. (1983), corresponds fairly well with the map of soil moisture-based

drainage rates (Figures 2 and 3). Although Pettyjohn et al. (1983) used the baseflow separation method and data from the 1970's, the maps are similar in several ways, including the trend that drainage and recharge rates decrease from east to west. Additionally, the maximum soil moisture-based drainage rate (266 mm yr^{-1}) and maximum Pettyjohn et al. (1983) recharge rate (254 mm yr^{-1}) are comparable. However, there are also some differences between the two maps. For instance, our calculated drainage rates in the Oklahoma Panhandle range from 6 to 27 mm yr^{-1} and are higher than the recharge rate of 2.5 mm yr^{-1} or less estimated for this region by Pettyjohn et al (1983). This difference is reasonable, given that the baseflow method used by Pettyjohn et al. (1983) underestimates recharge when there are upstream water losses due to groundwater evapotranspiration in riparian areas or groundwater pumping, both of which likely influence streamflow in the semi-arid, groundwater-irrigated Panhandle region (Scanlon et al., 2002). Also, there is a difference in the location of the maximum estimated drainage and recharge rates between the two studies. Pettyjohn et al. (1983) estimated that the greatest rates of groundwater recharge occur in the southeast portion of the state, near the Oklahoma-Arkansas border (Figure 3), while the maximum soil moisture-based drainage rates occurred in two areas: one in the northeast and one in the southeast (Figure 2). This may be caused, in part, by a relative lack of soil moisture sensors at the 60-cm depth in the far southeastern part of the state due to shallow bedrock, which leads to a lack of drainage rate estimates in that region.

Soil moisture-based drainage estimates summarized by aquifer compare well with previous recharge estimates for major Oklahoma aquifers (Table 3). These drainage values were found by computing the median value of the mean annual drainage rate for

aquifers with a minimum of three Mesonet sites above them, resulting in aquifer-scale drainage rate estimates for six Oklahoma aquifers. Aquifer-scale median soil moisture-based drainage rates fall within the range of previous recharge estimates, with the exception of the Arkansas River alluvial aquifer, which has only one prior recharge estimate. Though only one other study has estimated recharge for the Arkansas River alluvial aquifer, the soil moisture-based drainage estimate is within 30% of the estimated recharge rate found by that study. These results provide strong evidence that drainage estimates from a large-scale soil moisture monitoring network can be indicative of potential recharge rates at the spatial scales of an individual aquifer and an entire state.

HYDRUS-1D calibration results

Optimized soil hydraulic properties varied from the initial estimates in most cases and are shown in Table 4. Optimized K_s values were lower than the initial estimates for seven out of the twelve calibrated layers, while optimized θ_s values were higher in all but two cases. Optimized α values were lower than initial estimates at every site and depth, except for at Tipton, where the α and n values did not change during calibration. Optimized parameter values were limited in several instances by the upper or lower limits specified prior to optimization (e.g. all Goodwell θ_s values, Goodwell 25 cm L value). This same non-ideal behavior has been reported in prior studies and likely indicates some unresolved problems in the model structure or parameterization (Ries et al., 2015; Wang et al., 2016). Some of the deficiencies in the optimized parameters may result from using daily average matric potential data in the objective function, meaning that any changes in matric potential throughout the day were not captured. This would have the most impact

at sites with high sand contents, where rain events may lead to large changes during the day being "smoothed over" because of the use of mean daily matric potential data. Additionally, optimized parameters may not be physically meaningful because of model simplifications, such as a four-layer soil profile, and because of possible non-uniqueness issues.

Matric potential values estimated during the HYDRUS-1D calibration period (2006-2007) agreed reasonably well with measured matric potentials at the four focus sites (Figure 4). There were however extended periods during 2007, a year with unusually high precipitation, when the simulated matric potential at 25 and 60 cm was well below the measured matric potential for the Tipton site. The root mean square error (RMSE) values ranged from 88 to 329 kPa and generally were larger at the 60-cm depth than at the 5-cm depth, suggesting that the ability of the calibrated model to match the data decreased as depth increased (Table 5). Mean RMSEs at the 5-, 25-, and 60-cm depths were 184, 182, and 268 kPa, respectively.

The "goodness of fit" of simulated matric potentials can also be evaluated using the ratio of the RMSE to the standard deviation of the observed matric potentials. The value of this ratio, called the RMSE-observations standard deviation ratio (RSR) by Moriasi et al. (2007), can range from zero for a perfect model (RMSE = 0) to a large positive value. Moriasi et al. (2007) gave a list of performance ratings that categorize model outputs based on this RSR statistic, where $0.00 \leq RSR \leq 0.50$ indicates a very good model fit, $0.50 < RSR \leq 0.60$ indicates a good model fit, $0.60 < RSR \leq 0.70$ indicates a satisfactory model fit, and $RSR > 0.70$ indicates an unsatisfactory fit. The given RSR ranges are for simulations modeled at a monthly time step, and Moriasi et al.

(2007) noted that using smaller model time steps would widen the acceptable ranges. RSR values were calculated for matric potential data during the calibration period, and only two of the sites and depths were rated satisfactory or better based on the RSR ranges listed by Moriasi et al. (2007) (Table 5). The relatively poor RSR values during the calibration reflect the difficulty of accurately simulating matric potential, which can vary by orders of magnitude, in heterogeneous soil profiles with dynamic meteorological forcing.

The Nash-Sutcliffe Efficiency (NSE, Nash and Sutcliffe, 1970) values for estimated versus measured matric potential during the calibration period ranged from 0.581 to 0.685 (Table 5). This range of NSE values is favorable when compared to the range from -1.44 to 0.711 that was obtained when HYDRUS-1D was calibrated using three years of soil moisture data from monitoring sites in Nebraska (Wang et al., 2016). The negative NSE values found by Wang et al. indicate that using a constant value of the mean of the matric potential for that particular site and depth would provide a more accurate representation of the temporal dynamics than their calibrated model. There was a tendency for lower NSE values at 60 cm than at 5 cm, again suggesting that model accuracy decreases with depth. During the calibration period, mean bias in HYDRUS-1D estimated matric potential for each site-depth combination ranged from -277 kPa to +169 kPa (Table 5). The overall mean bias across sites for this period was -50 kPa. All but two sites and depths had a negative mean bias, meaning that conditions simulated by the model were drier than measured conditions overall, although there were times when the model predicted conditions much wetter than measured (Figure 4c, d).

One interesting pattern discernible in the measured matric potentials during the calibration period at Miami and Wister was the occurrence of prolonged periods of wetness during the fall and winter months with matric potentials around -10 kPa, near the upper measurement limit of the sensors (Fig. 4b and 4d). These wet periods end each spring due to the onset of the growing season and subsequent increases in plant water uptake. We hypothesize that these prolonged periods near saturation are partly caused by restriction of downward water movement due to the high clay contents (>60%) at the 60-cm depth at both sites (Table 1). These high clay contents at depth could greatly reduce the rate of water leaving the soil profile, producing the prolonged periods of high measured matric potential values. Ries et al. (2015) showed somewhat similar patterns at a depth of 80 cm after rainfall events, with water contents near saturation (albeit for shorter durations) occurring in that case due to a restriction of water flow by underlying shallow bedrock. These times of near saturation could potentially lead to errors in the estimated drainage rates if the heat dissipation sensors' upper measurement limit of -8.5 kPa is exceeded (Illston et al., 2008) or if the hydraulic gradient becomes substantially less than the assumed unit gradient.

Comparison of HYDRUS-1D and soil moisture-based drainage rates

Agreement between simulated and measured matric potential was in most cases slightly poorer during the validation simulations (1998-2014) than during calibration, with RMSE values ranging from 72 to 426 kPa (Table 5). The RSR values during this time ranged from 0.54 to 1.89, with agreement for eight of the twelve layers classified as unsatisfactory (RSR > 0.70) according to the categories defined by Moriasi et al. (2007).

However, the categories of Moriasi et al. (2007) are for simulations using a monthly time step, and they noted that a less strict performance rating is warranted for smaller time steps. The NSE values were slightly lower during the validation simulations than they were during calibration years, ranging from 0.47 to 0.59.

The validation period NSE values were generally better than the values ranging from -16.9 to 0.754 observed by Wang et al. (2016), who calibrated HYDRUS-1D using three years of soil water content data. The bias in simulated matric potential during the validation simulations was negative at all but four sites and depths. The mean bias at 60 cm during the validation period was -93 kPa. This general trend of HYDRUS-1D to underestimate matric potential at 60 cm is shown in Figure 4 for all but the Wister site. The simulated matric potential at the Wister site displayed a positive bias at every depth. As a whole, the statistics for the validation period indicate that our simulations have accuracy comparable to those in the most similar recent study (Wang et al., 2016) but still explain less than 60% of the variance in measured matric potential. Thus, significant uncertainty remains regarding the accuracy of the simulated drainage rates.

Drainage estimates for the calibration period from the soil moisture-based method and from HYDRUS-1D are shown in Figure 5. While there was a general correspondence between the methods in the timing of largest drainage events, the magnitudes of HYDRUS-1D drainage peaks were larger than those of the SMB method, especially at the Wister site, where HYDRUS-1D drainage estimates often exceeded SMB drainage rates by ~30 mm d^{-1}. This discrepancy was likely due to the unrealistically high value (62 mm d^{-1}) of the optimized K_s value for the 60-cm soil layer at Wister, which has a clay

content of 74%. Additionally, HYDRUS-1D drainage estimates indicated times of upward flow that were not captured by the SMB method.

Mean annual drainage rates at 60 cm resulting from HYDRUS-1D simulations for 1998-2014 ranged from 6 mm yr^{-1} at Goodwell to 301 mm yr^{-1} at Wister (Table 6). Differences between soil moisture-based and HYDRUS-1D mean annual drainage rates for the validation period ranged from -239 mm yr^{-1} at Wister to +158 mm yr^{-1} at Miami. For the two sites with annual precipitation <1000 mm, Tipton and Goodwell, the soil-moisture based and HYDRUS-1D estimated mean annual drainage rates agreed to within 10 mm. Plotting annual drainage rate estimates versus annual precipitation also reveals similar relationships for both the soil moisture-based method and HYDRUS-1D estimates at Goodwell and Tipton (Fig. 6a, c). This is evidence that both the soil moisture-based method and the calibrated HYDRUS-1D model provide reliable drainage estimates at the 60-cm depth at these sites with annual precipitation <1000 mm. However, the annual soil moisture-based drainage rates were consistently higher than the HYDRUS-1D estimates across all precipitation levels at Miami and lower at Wister (Fig. 6b, d). It is not immediately clear how much of the discrepancy to attribute to errors in the soil moisture-based drainage estimates and how much to attribute to errors in the simulated drainage.

At Miami, where the soil moisture-based mean annual drainage rate is 158 mm yr^{-1} greater than the HYDRUS-1D estimate, the HYDRUS-1D estimates may be somewhat more reliable. The most recent groundwater modeling study encompassing this region, Czarnecki et al. (2009), reviewed prior recharge estimates from the literature and calibrated a groundwater flow model by adjusting the recharge rates, resulting in a mean annual recharge of 46 mm yr^{-1} for the area encompassing the Miami site. This is

consistent with the 59 mm yr^{-1} drainage rate at 60-cm depth estimated by HYDRUS-1D. The pre-existing groundwater recharge map based on the baseflow separation method (Fig. 3) puts the estimated recharge at Miami near 152 mm yr^{-1}, approximately mid-way between the soil moisture-based and HYDRUS-1D drainage estimates.

At Wister, where the soil moisture-based mean annual drainage rate is 239 mm yr^{-1} less than the HYDRUS-1D estimate, the soil moisture-based estimate may be somewhat more reliable. The optimized K_s value of 62 mm d^{-1} for the 60-cm depth at Wister is relatively high for a soil with a clay content of 73%. For comparison, the 60-cm depth at the Miami site with 63% clay had an optimized K_s value of only 1.3 mm d^{-1}. If the optimized K_s value is too high, then the HYDRUS-1D mean annual drainage rate of 301 mm yr^{-1} may be an overestimate. Furthermore, the Richards equation that HYDRUS-1D uses to model water flow may not simulate field conditions accurately in soils with high clay contents, such as the Wister site (Beven and Germann, 2013; Vereecken et al., 2016). On the other hand, the pre-existing groundwater recharge map based on the baseflow separation method (Fig. 3) puts the estimated recharge at Wister between 203-254 mm yr^{-1}, between the soil moisture-based and HYDRUS-1D drainage estimates but closer to the HYDRUS-1D estimates. As a whole, the simulation results at both Miami and Wister suggest increased uncertainty in drainage rates when applying the soil moisture-based drainage estimation method at sites with >1000 mm yr^{-1} annual precipitation.

The unit-gradient assumption applied in the soil moisture-based drainage estimates has been evaluated previously and has been shown to be an adequate approximation for some but not all situations (Chong et al., 1981; Libardi et al., 1980;

Sisson, 1987). Using HYDRUS-1D, we were able to simulate the matric potential profile for the focus sites. The matric potential profiles associated with the top 1% of simulated drainage rates at 60-cm for the Goodwell are shown in Figure 7. For these model time steps, at the 60-cm depth there was a substantial matric potential gradient, which was not dissipated until near the 100-cm. The depth at which the unit-gradient condition is approached is likely dependent upon the specified rooting depth and distribution. These matric potential profiles indicate that the unit gradient assumption was clearly violated during times of maximum drainage at the 60-cm depth. Still, the soil moisture-based drainage estimate for the site was within 4 mm yr^{-1} of the HYDRUS-1D simulated value, so the soil moisture-based method may not be overly sensitive to violations of the unit-gradient assumption.

Overall, the results of the HYDRUS-1D simulations provided further evidence for the reliability of the soil moisture-based drainage estimates at the two drier sites, Tipton and Goodwell, while indicating potentially large errors in the soil moisture-based drainage estimates at wetter sites. At the two simulated sites with annual precipitation >1000 mm, the discrepancy between soil moisture-based drainage estimates and HYDRUS-1D modeled drainages rates was >150 mm yr^{-1}. The saturated hydraulic conductivity estimates from the underlying Rosetta pedotransfer function have an uncertainty of approximately one order of magnitude (Schaap et al., 2001), so a relatively large uncertainty in mean annual drainage for wet sites is perhaps to be expected.

Limitations and advantages of the soil moisture-based drainage estimation method

Some limitations of the soil moisture-based drainage estimation method include a lack of data in places where shallow bedrock prevents sensor installation, such as in the southeastern part of Oklahoma. Quality control of the drainage estimates can also be challenging if data from a large number of sites are being processed. In this study, a simple box plot approach was used to identify sites that were outliers and remove them from analysis. Understanding the cause of these outliers would likely require more careful examination of the sensor performance and estimated soil hydraulic properties, as well as site visits to evaluate possible confounding local factors such as site disturbance and site topography. Additionally, the soil moisture-based drainage estimation method is prone to overestimate potential groundwater recharge if substantial root water uptake occurs below the 60-cm depth or if there is a shallow groundwater table resulting in less than unit-gradient conditions in the field. Soil moisture measurements at a deeper depth would generally be preferable for estimating drainage, as would collocated measurements of water table depth. Finally, the heat dissipation sensors used in this study are not ideal for use in estimating drainage because they have limited sensitivity under near-saturated conditions. The manufacturer specifies -10 kPa as the upper measurement limit for matric potential, although the Oklahoma Mesonet calibration procedures result in a slightly higher upper limit of -8.5 kPa. Sensors using other measurement principles might be better suited to detect small changes in soil moisture near saturation, leading to improved drainage estimates for wet sites.

Despite these limitations, the benefits of estimating drainage and potential groundwater recharge using data from in situ soil moisture monitoring networks are

substantial. First, soil moisture-based drainage estimates from networks like the Oklahoma Mesonet can incorporate increasingly long-term soil moisture data, 17 years in this study. In contrast, many groundwater studies are based on field data collected over periods of just a few years, which may be less likely to show the effects of extreme climatic events. Second, soil moisture-based drainage estimates can be updated simply, frequently, and automatically with minimal recurring cost as long as the soil moisture monitoring system is intact. Other methods for estimating recharge typically cannot be readily updated without substantial investment of time and money. Third, the relatively large number of measurement sites available within a monitoring network like the Oklahoma Mesonet can provide valuable information on the spatial distribution of potential groundwater recharge across an entire region.

CONCLUSION

The results of this study reinforce the insight of Black et al. (1969), who wrote "…it is a characteristic of the unsaturated flow equation that fluxes into and out of a system may be estimated with surprising precision using very gross approximations…". Soil moisture-based drainage estimates can be made by applying a simple unit-gradient assumption to daily soil moisture data from long-term in situ monitoring stations. The primary weaknesses of this approach in the present study were: 1) the relatively shallow measurement depth used, i.e., 60 cm and 2) the increased uncertainty in the drainage estimates for wetter sites. It appears likely that the unit-gradient assumption is often violated at 60 cm and that some root water uptake occurs beneath that depth. It also appears that uncertainty in saturated hydraulic conductivity values and the limited wet-

end sensitivity of the heat dissipation sensors used here increase the uncertainty of the drainage estimates for wet sites. Despite these weaknesses, our results provide evidence that in many cases the drainage rates at 60 cm are estimated with reasonable accuracy and that these drainage rates are indicative of potential groundwater recharge rates. Spatial patterns of the estimated drainage rates tended to follow the state's precipitation gradient, decreasing from east to west. Additionally, median aquifer-scale drainage rates compare well with previous estimates of recharge in all available cases. The map of mean annual drainage rates across the state of Oklahoma, as well as yearly drainage maps and other maps related to soil moisture conditions in Oklahoma, are available online at http://soilmoisture.okstate.edu under the "Projects" tab. Future research should apply, evaluate, and refine the method proposed here using data from other large-scale soil moisture monitoring networks around the world. Doing so is likely to produce new information about potential groundwater recharge rates that will be valuable for advancing hydrologic understanding with the ultimate goal of improving management of groundwater resources, resources that are increasingly critical for societies worldwide.

ACKNOWLEDGEMENTS

Support for this work was provided by the Oklahoma Water Resources Center, the Oklahoma Water Resources Board, the US Geological Survey 104b Grant Program, and the Oklahoma Mesonet. This work was also supported by the USDA National Institute of Food and Agriculture Hatch project OKL02918, the W-3188 Multi-State Research Project, and the Division of Agricultural Sciences and Natural Resources at Oklahoma State University. We would like to thank the staff of the EPA Kerr lab in Ada, OK and

the USDA-NRCS office in Woodward, OK for their assistance in completing fieldwork related to this project.

REFERENCES

Ahuja, L. R., B. B. Barnes, D. K. Cassel, R. R. Bruce, and D. L. Nofziger. 1988. Effect of assumed unit gradient during drainage on the determination of unsaturated hydraulic conductivity and infiltration parameters. Soil Science. 145:235-243.

Allen, R. G., L. S. Pereira, D. Raes, and M. Smith. 1998. Crop evapotranspiration - guidelines for computing crop water requirements - FAO irrigation and drainage paper 56. Food and Agricultural Organization of the United Nations, Rome.

Andreasen, M., L. A. Andreasen, K. H. Jensen, T. O. Sonnenborg, and S. Bircher. 2013. Estimation of regional groundwater recharge using data from a distributed soil moisture network. Vadose Zone J. 12. doi:10.2136/vzj2013.01.0035.

Becker, M. F. and D. L. Runkle. 1998. Hydrogeology, water quality, and geochemistry of the Rush Springs aquifer, western Oklahoma. US Geological Survey, Water Resources Division; Branch of Information Services.

Beven, K., and P. Germann. 2013. Macropores and water flow in soils revisited. Water Resour. Res. 49:3071–3092. doi:10.1002/wrcr.20156

Black, T., W. Gardner, and G. Thurtell. 1969. The prediction of evaporation, drainage, and soil water storage for a bare soil. Soil Sci. Soc. Am. J. 33: 655-660.

Carsel, R. F. and R. S. Parrish. 1988. Developing joint probability distributions of soil water retention characteristics. Water Resour. Res. 24: 755-769.

Chong, S. K., R. E. Green, and L. R. Ahuja. 1981. Simple in situ determination of hydraulic conductivity by power function descriptions of drainage. Water Resour. Res. 17:1109-1114.

Czarnecki, J. B., J. A. Gillip, P. M. Jones, and D. S. Yeatts. 2009. Groundwater- flow model of the Ozark Plateaus aquifer system, northwest Arkansas, southeastern Kansas, southwestern Missouri, and northeastern Oklahoma. U.S. Geological Survey Scientific Investigations Report 2009-5148: 62p.

Dugan, J. and J. Peckenpaugh. 1986. The effects of climate on consumptive water use and ground-water recharge in parts of Arkansas, Colorado, Kansas, Missouri, Nebraska, Oklahoma, South Dakota, and Texas. US Geological Survey Water-Resources Investigations Report: 85-4326.

Feddes, R. A., P. J. Kowalik, and H. Zaradny. 1978. Simulation of field water use and crop yield. Centre for Agricultural Publishing and Documentation.

Gardner, W. 1964. Water movement below the root zone. Proc 8th Int. Congr. Soil Sci., Bucharest. 31:317-320.

Hart, D. L. Jr., G. L. Hoffman, and R. L Geomaat. 1976. Geohydrology of the Oklahoma Panhandle, Beaver, Cimarron and Texas Counties. U.S. Geological Survey Water Resources Investigation 25-75. 72p.

Hart, D. L. and R. E. Davis. 1981. Geohydrology of the Antlers aquifer (Cretaceous), southeastern Oklahoma, University of Oklahoma Press. 81.

Illston, B. G., J. B. Basara, C. A. Fiebrich, K. C. Crawford, E. Hunt, D. K. Fisher, R. Elliot, and K. Humes. 2008. Mesoscale monitoring of soil moisture across a statewide network. J. Atmos. Ocean. Tech. 25:167-182.

Imes, J. L., 1989. Analysis of the effect of pumping on groundwater flow in the Springfield Plateau and Ozark aquifers near Springfield, Missouri: U.S. Geological Survey Water Resources Investigations Report 89-4079, 63p.

Imes, J. L. and L. F. Emmett. 1994. Geohydrology of the Ozark Plateaus aquifer system in parts of Missouri, Arkansas, Oklahoma, and Kansas. U.S. Geological Survey Professional Paper 1414-D. 127p.

Jackson, R. B., J. Canadell, J. R. Ehleringer, H. S. Mooney, O. E. Sala, and E. D. Schulze. 1996. A global analysis of root distributions for terrestrial biomes. Oecologia 108:389-411.

Kim, J. H. and R. B. Jackson. 2012. A global analysis of groundwater recharge for vegetation, climate and soils. Vadose Zone J. 11. doi:10.2136/vzj2011.0021RA.

Libardi, P. L., K. Reichardt, D. R. Nielsen, and J. W. Biggar. 1980. Simple field methods for estimating soil hydraulic conductivity. Soil Sci. Soc. of Am. J. 44:3-7.

Luckey, R. L. and M. F. Becker. 1999. Hydrogeology, water use, and simulation of flow in the High Plains aquifer in northwestern Oklahoma, southeastern Colorado, southwestern Kansas, northeastern New Mexico, and northwestern Texas. U.S. Geological Survey, Water Resources Investigation Report 99-4104.

Mashburn, S. L., D. W. Ryter, C. R. Neel., S. J. Smith, and J. S. Magers. 2014. Hydrogeology and simulation of groundwater flow in the Central Oklahoma (Garber-Wellington) Aquifer, Oklahoma, 1987 to 2009, and simulation of available water in storage, 2010–2059. U.S. Geological Survey, Water Resources Investigations Report 2013-5219.

McPherson, R. A., C. A. Fiebrich, K. C. Crawford, J. R. Kilby, D. L. Grimsley, J. E. Martinez, J. B. Basara, B. G. Illston, D. A. Morris, and K. A. Kloesel. 2007. Statewide monitoring of the mesoscale environment: A technical update on the Oklahoma Mesonet. J. Atmos. and Ocean. Tech. 24:301-321.

Moriasi, D. N., J. G. Arnold, M. W. van Liew, R. L. Binger, R. D. Harmel, T. L. Veith. 2007. Model evaluation guidelines for systematic quantification of accuracy in watershed simulations. Trans. ASABE 50:885-900.

Morton, R. B. 1980. Digital-model projection of saturated thickness and recoverable water in the Ogallala aquifer, Texas County, Oklahoma. U.S. Geological Survey Open-file Report 79-565. 34p.

Morton, R. B. 1992. Simulation of ground-water flow in the Antlers aquifer in southeastern Oklahoma and northeastern Texas. US Department of the Interior, US Geological Survey Water Resources Investigation.

Nash, J.E. and J.V. Sutcliffe. 1970. River flow forecasting through conceptual models part I—A discussion of principles. J. Hydrol. 10: 282-290.

Nolan, B. T., R.W. Healy, P. E. Taber, K. Perkins, K. J. Hitt, and D. M. Wolock. 2006. Factors influencing ground-water recharge in the eastern United States. J. Hydrol. 332:187-205.

Ochsner, T. E., M. H. Cosh, R. H. Cuenca, W. A. Dorigo, C. S. Draper, Y. Hagimoto, Y. H. Kerr, E. G. Njoku, E. E. Small, and M. Zreda. 2013. State of the art in large-scale soil moisture monitoring. Soil Sci. Soc. Am. J. 77:1888-1919.

Oklahoma Climatological Survey. Climate of Oklahoma. Oklahoma Climatological Survey webpage. <

http://climate.ok.gov/index.php/site/page/climate_of_oklahoma>. Accessed [02/09/2016].

Oklahoma State University Small Grains Extension. 2015. Oklahoma State University Department of Plant and Soil Sciences. <wheat.okstate.edu>. Accessed [02/09/2016].

Oklahoma Water Resources Board (OWRB). 2011. Oklahoma Comprehensive Water Plan Physical Water Supply Availability Report.

Oklahoma Water Resources Board (OWRB). 2012. Oklahoma Comprehensive Water Plan 2012 Executive Report.

Parkhurst, D. L., S. C. Christenson, and G. N. Breit. 1996. Ground-water-quality assessment of the central Oklahoma Aquifer, Oklahoma: geochemical and geohydrologic investigations. United States Geological Survey Water Supply Paper 2357-C. 101p.

Pettyjohn, W. A. and A. Miller. 1982. Preliminary estimate of effective ground-water recharge rates in central Oklahoma. Oklahoma Water Resources Research Institute.

Pettyjohn, W.A., H. White, and S. Dunn. 1983. Water atlas of Oklahoma. University Center for Water Research, Oklahoma State University, Stillwater, OK.

Qu, W., H. R. Bogena, J. A. Huisman, G. Martinez, Y. A. Pachepsky, and H. Vereecken. 2014. Effects of soil hydraulic properties on the spatial variability of soil water content: evidence from sensor network data and inverse modeling. Vadose Zone J. 13(12).

Richards, L. A. 1931. Capillary conduction of liquids through porous mediums. J. Appl. Phys. 1: 318-333.

Ries, F., J. Lange, S. Schmidt, H. Puhlmann, and M. Sauter. 2015. Recharge estimation and soil moisture dynamics in a Mediterranean, semi-arid karst region. Hydrol. Earth Syst. Sc. 19:1439-1456.

Scanlon, B. R., R. W. Healy, and P. G. Cook. 2002. Choosing appropriate techniques for quantifying groundwater recharge. Hydrogeol. J. 10:18-39.

Scanlon, B. R., K. E. Keese, A. L. Flint, L. E. Flint, C. B. Gaye, W. M. Edmunds, and I. Simmers. 2006. Global synthesis of groundwater recharge in semiarid and arid regions. Hydrol. Process. 20:3335-3370.

Schaap, M. G., F. J. Leij, and M. T. van Genuchten. 2001. Rosetta: A computer program for estimating soil hydraulic parameters with hierarchical pedotransfer functions. J. Hydrol. 251:163-176.

Scott, R. L., W. J. Shuttleworth, T. O. Keefer, and A. W. Warrick. 2000. Modeling multiyear observations of soil moisture recharge in the semiarid American Southwest. Water Resour. Res. 36:2233-2247.

Scott, B. L., T. E. Ochsner, B. G. Illston, C. A. Fiebrich, J. B. Basara, and A. J. Sutherland. 2013. New Soil Property Database Improves Oklahoma Mesonet Soil Moisture Estimates. J Atmos. Ocean. Tech. 30:2585-2595.

Šimůnek, J., M.T. van Genuchten, and O. Wendroth .1998. Parameter estimation analysis of the evaporation method for determining soil hydraulic properties. Soil Sci. Soc. Am. J. 62: 894-905.

Šimůnek, J., M.T. van Genuchten, and M. Šejna. 2016. Recent developments and applications of the HYDRUS computer software packages. Vadose Zone J. 15. doi: 10.2136/vzj2016.04.0033.

Sisson, J. B. 1987. Drainage from layered field soils: Fixed gradient models. Water Resour. Res. 23:2071-2075.

Soil Survey Staff. Natural Resources Conservation Service. United States Department of Agriculture. Official Soil Series Descriptions. Available online. Accessed [02/09/2016].

Sun, G., D. P. Coffin, and W. K. Lauenroth. 1997. Comparison of root distributions of species in North American grasslands using GIS. J. Veg. Sci. 8:587-596.

Tanaka, H. H. and L. V. Davis. 1963. Ground Water: Rush Springs Sandstone. Norman, Oklahoma: Oklahoma Geological Survey, Circular 61.

Tortorelli, R.L. 2009. Water Use in Oklahoma 1950–2005. U.S. Geological Survey Scientific Investigations Report 2009–5212. 49 p.

Turkeltaub, T., D. Kurtzman, G. Bel, and O. Dahan. 2015. Examination of groundwater recharge with a calibrated/validated flow model of the deep vadose zone. J. Hydrol. 522:618-627.

Tyrl, R. J., T. G. Bidwell, R. E. Masters, R. D. Elmore, and J. R. Weir. 2014. Oklahoma's Native Vegetation Types. Oklahoma State University Extension Fact Sheet E-993, 14p.

van Genuchten, M. T. 1980. A closed-form equation for predicting the hydraulic conductivity of unsaturated soils. Soil Sci. Soc. of Am. J. 44:892-898.

Vereecken, H., A. Schnepf, J.W. Hopmans, M. Javaux, D. Or, T. Roose, J. Vanderborght, M.H. Young, W. Amelung, M. Aitkenhead, S.D. Allisson, S. Assouline, P. Baveye, M. Berli, N. Brüggemann, P. Finke, M. Flury, T. Geiser, G. Govers, T. Ghezzehei, P. Hallett, H.J. Hendricks Franssen, J. Heppel, R. Horn, J.A. Huisman, D. Jacques, F. Jonard, S. Kollet, F. Lafolie, K. Lamorski, D. Leitner, A. McBratney, B. Minasny, C. Montzka, W. Nowak, Y. Pachepsky, J. Padarian, N. Romano, K. Roth, Y. Rothfuss, E. C. Rowe, A. Schwen, J. Šimůnek, A. Titak, J. van Dam, S. E. A. T. M. van der Zee, H.J. Vogel, J.A. Vrugt, T. Wöhling, and I.M. Young 2016. Modeling soil processes: Review, key challenges, and new perspectives. Vadose Zone J. 15, 57 p. doi: 10.2136/vzj2015.09.0131

Vieux, B. E. and M. A. Moreno. 2008. Arbuckle-Simpson Hydrology Study. Distributed water resources assessment: Final report submitted to the Oklahoma Water Resources Board, University of Oklahoma School of Civil Engineering and Environmental Science, 44p.

Vogel T., M. Th. van Genuchten, and M. Cislerová, 2001. Effect of the shape of the soil hydraulic functions near saturation on variably-saturated flow predictions. Adv. Water Resour. 24:133-144.

Vrugt, J. A., W. Bouten, and A. H. Weerts. 2001. Information content of data for identifying soil hydraulic parameters from outflow experiments. Soil Sci. Soc. Am. J. 65:19-27

Wang, T., T. E. Franz, W. Yue, J. Szilagyi, V. A. Zlotnik, J. You, X. Chen, M. D. Shulski and A. Young. 2016. Feasibility analysis of using inverse modeling for estimating

natural groundwater recharge from a large-scale soil moisture monitoring network. J. Hydrol. 533: 250-265.

Wesseling, J. G., J. A. Elbers, P. Kabat, and B. J. van den Broek. 1991. SWATRE: instructions for input, Internal Note, Winand Staring Centre, Wageningen, the Netherlands.

Wine, M. L. and C. B. Zou. 2012. Long-term streamflow relations with riparian gallery forest expansion into tallgrass prairie in the Southern Great Plains, USA. Forest Ecol. Manag. 266:170-179.

World Water Assessment Programme. 2009. The United Nations World Water Development Report 3: Water in a Changing World. Paris: UNESCO, and London: Earthscan.

Table 1. Mean annual precipitation (*P*), mean annual temperature (*T*), and soil physical properties for the four focus Mesonet sites at which drainage was modeled using HYDRUS-1D. Precipitation and temperature data are averages from 1998-2014.

Site	*P*	*T*	Depth	Sand	Silt	Clay	Bulk density
	mm	°C	cm	———	%	———	g cm^{-3}
Goodwell	397	12.1	5	36.6	34.6	28.8	1.37
			25	28.2	34.0	37.8	1.51
			60	34.8	29.4	35.8	1.42
Miami	1062	10.0	5	15.6	60.5	23.9	1.20
			25	23.4	62.2	14.4	1.43
			60	9.5	28.0	62.5	1.38
Tipton	573	10.6	5	42.6	41.6	15.8	1.48
			25	43.9	38.4	17.6	1.58
			60	43.1	35.4	21.5	1.45
Wister	1130	8.3	5	17.5	61.8	20.8	1.51
			25	9.9	61.2	28.9	1.45
			60	8.8	17.9	73.7	1.34

Table 2. Initial values for soil hydraulic parameters for the four focus sites at which drainage was modeled using HYDRUS-1D. θ_r is the residual volumetric water content, θ_s is the volumetric water content at saturation, α and n are shape parameters, K_s is the saturated hydraulic conductivity (from Carsel and Parrish), K_o is a matching point hydraulic conductivity (from Rosetta), and L is an empirical coefficient related to the pore connectivity. Sites marked with a † indicate locations where Carsel and Parrish (1998) initial values resulted in better calibration than the Rosetta initial values.

Site	**Depth**	**θ_r**	**θ_s**	**α**	***n***	***K_o* or *K_s***	***L***
	cm	$cm^3\ cm^{-3}$	$cm^3\ cm^{-3}$	kPa^{-1}	-	$mm\ d^{-1}$	-
Goodwell†	5	0.095	0.410	0.204	1.31	62.4	-0.93
	25	0.095	0.410	0.204	1.31	62.4	-1.02
	60	0.095	0.410	0.204	1.31	62.4	-1.73
	300	0.095	0.410	0.204	1.31	62.4	-1.73
Miami	5	0.032	0.422	0.043	1.65	22	0.91
	25	0.028	0.366	0.043	1.65	19	0.61
	60	0.081	0.510	0.028	1.35	7	0.90
	300	0.081	0.510	0.028	1.35	7	0.90
Tipton	5	0.032	0.368	0.139	1.39	66	-0.42
	25	0.034	0.349	0.194	1.35	88	-0.89
	60	0.041	0.388	0.238	1.36	116	-0.99
	300	0.041	0.388	0.238	1.36	116	-0.99
Wister†	5	0.067	0.450	0.204	1.41	108.0	0.65
	25	0.089	0.430	0.102	1.23	16.8	-0.38
	60	0.068	0.380	0.082	1.09	48.0	-1.13
	300	0.068	0.380	0.082	1.09	48.0	-1.13

Table 3. Summary of soil moisture-based drainage rates by aquifer. Aquifer name, number of Mesonet sites located above the aquifer, median value of the mean annual soil moisture-based drainage rate, a range of previous recharge estimates, and the number of publications contributing to that range.

Aquifer	Sites	Drainage	Recharge	Sources
		mm yr^{-1}	mm yr^{-1}	
Boone	3	74	2.3-267	4†
Arkansas River	5	165	127	1‡
Garber-Wellington	3	113	0.8-211	4§
Rush Springs	5	66	5.1-89	4¶
Antlers	4	63	7.6-76	3#
Ogallala	8	19	1.5-56	4‡‡

†Czarnecki et al. (2009); Dugan & Peckenpaugh (1985); Imes (1989); Imes and Emmett (1994).
‡ Oklahoma Water Resources Board (2012).
§ Pettyjohn and Miller (1982); Mashburn et al. (2014); Parkhurst et al. (1996); Oklahoma Water Resources Board (2011).
¶ Becker and Runkle (1998); Tanaka and Davis (1963); Pettyjohn et al. (1983); Oklahoma Water Resources Board (2012).
# Oklahoma Water Resources Board (2012); Hart and Davis (1981); Morton (1992).
‡‡ Luckey and Becker (1999); Hart et al. (1976); Morton (1980); Oklahoma Water Resources Board (2012).

Table 4. Optimized soil hydraulic parameters for the four focus sites at which drainage was modeled using HYDRUS-1D. θ_r is the residual volumetric water content, θ_s is the volumetric water content at saturation, α and *n* are shape parameters, K_s is the saturated hydraulic conductivity, and *L* is an empirical coefficient related to the pore connectivity. Sites marked with a † indicate locations where Carsel and Parrish (1998) initial parameter values were used.

Site	**Depth**	**θ_r**	**θ_s**	**α**	***n***	**K_s**	***L***
	cm	$cm^3\ cm^{-3}$	$cm^3\ cm^{-3}$	kPa^{-1}	-	$mm\ d^{-1}$	-
Goodwell†	5	0.095	0.500	0.126	1.27	2.5	-0.81
	25	0.095	0.500	0.061	1.10	623	-2.00
	60	0.095	0.500	0.039	1.12	18	-1.77
	300	0.095	0.410	0.204	1.31	62	-1.73
Miami	5	0.032	0.499	0.036	1.87	29	1.13
	25	0.028	0.472	0.012	1.98	1.2	0.38
	60	0.081	0.500	0.010	1.04	1.3	1.78
	300	0.081	0.510	0.028	1.35	7.0	0.90
Tipton	5	0.032	0.377	0.139	1.39	24	0.00
	25	0.034	0.366	0.194	1.35	104	1.11
	60	0.041	0.500	0.238	1.36	145	-1.19
	300	0.041	0.388	0.238	1.36	116	-0.99
Wister†	5	0.067	0.500	0.031	1.82	107	1.99
	25	0.089	0.484	0.012	2.07	18	-1.05
	60	0.068	0.302	0.013	1.01	62	-1.68
	300	0.068	0.380	0.102	1.09	48	-1.13

Table 5. Root mean square error (RMSE), RMSE-observations standard deviation ratio (RSR), Nash-Sutcliffe Efficiency (NSE), and bias for measured versus simulated matric potential for the HYDRUS-1D calibration (2006-2007) and validation periods (1998-2014). Sites marked with a † indicate locations where Carsel and Parrish (1998) initial parameter values were used.

		Calibration				Validation			
Site	**Depth**	**RMSE**	**RSR**	**NSE**	**Bias**	**RMSE**	**RSR**	**NSE**	**Bias**
	cm	kPa	-	-	kPa	kPa	-	-	kPa
Goodwell†	5	238	0.895	0.653	-151	272	1.190	0.527	-203
	25	324	1.338	0.594	-277	426	1.886	0.484	-384
	60	168	0.741	0.620	-83	335	1.315	0.466	-241
Miami	5	140	0.738	0.674	-10	96	0.617	0.558	-21
	25	99	0.870	0.685	-42	72	0.693	0.587	-26
	60	315	0.968	0.581	169	158	0.802	0.589	28
Tipton	5	271	2.230	0.643	-195	238	1.031	0.515	-123
	25	213	0.839	0.661	-124	309	1.195	0.507	-206
	60	329	1.060	0.594	-41	332	1.122	0.465	-241
Wister†	5	88	0.561	0.680	-6	95	0.538	0.573	1
	25	91	0.601	0.660	-4	107	0.624	0.558	8
	60	258	0.996	0.622	159	196	0.830	0.550	83

Table 6. Mesonet site name, soil moisture-based (SMB) drainage rates, and HYDRUS-1D drainage rates at 60 cm for the calibration (2006-2007) and validation periods, and difference for the validation period (1998-2014).

	Calibration		Validation		
Site	**SMB**	**HYDRUS**	**SMB**	**HYDRUS**	**Difference**
	mm yr^{-1}		mm yr^{-1}		mm yr^{-1}
Goodwell	19	-12	10	6	4
Miami	159	55	217	59	158
Tipton	25	12	26	16	10
Wister	34	274	62	301	-239

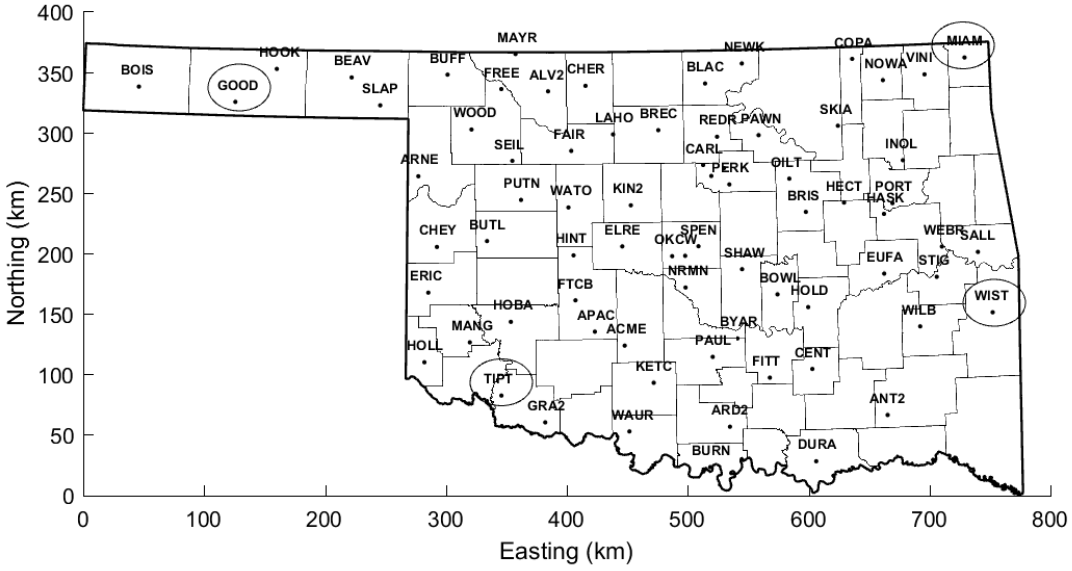

Figure 1. Mesonet site name abbreviations and locations for sites where drainage estimates were made. Labels for three sites (Stillwater, Marena, and Oklahoma City East) were excluded for clarity. Modeled focus site locations [Goodwell (GOOD), Miami (MIAM), Tipton (TIPT), and Wister (WIST)] are circled.

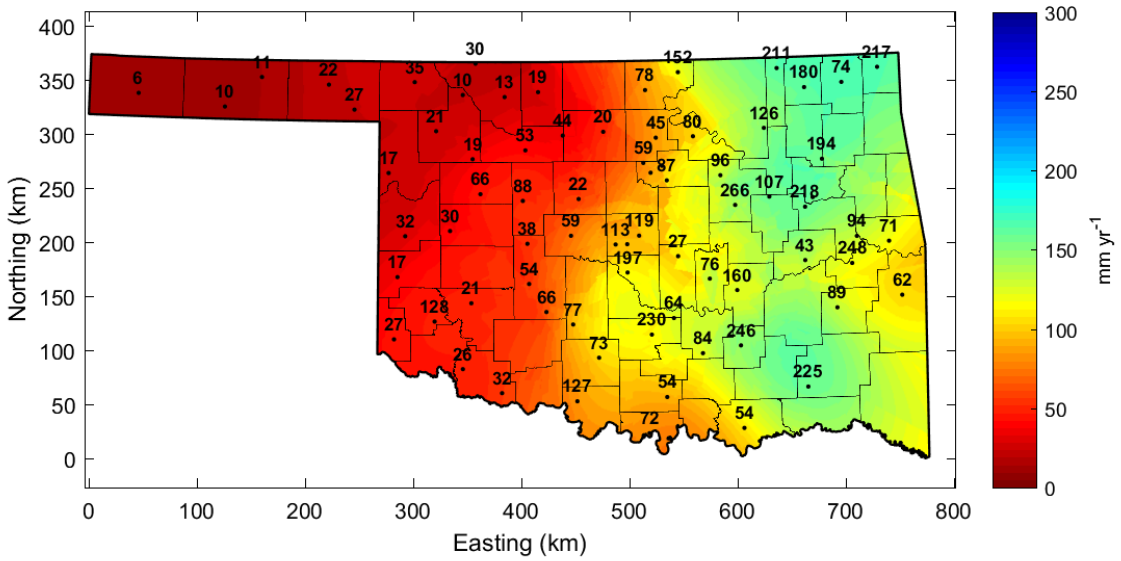

Figure 2. Statewide mean annual soil moisture-based drainage rates for the years 1998-2014. Drainage rate labels for the Stillwater, Oklahoma City East, Porter, and Marena sites were excluded for clarity, but were 214, 82, 166, and 66 mm yr^{-1}, respectively.

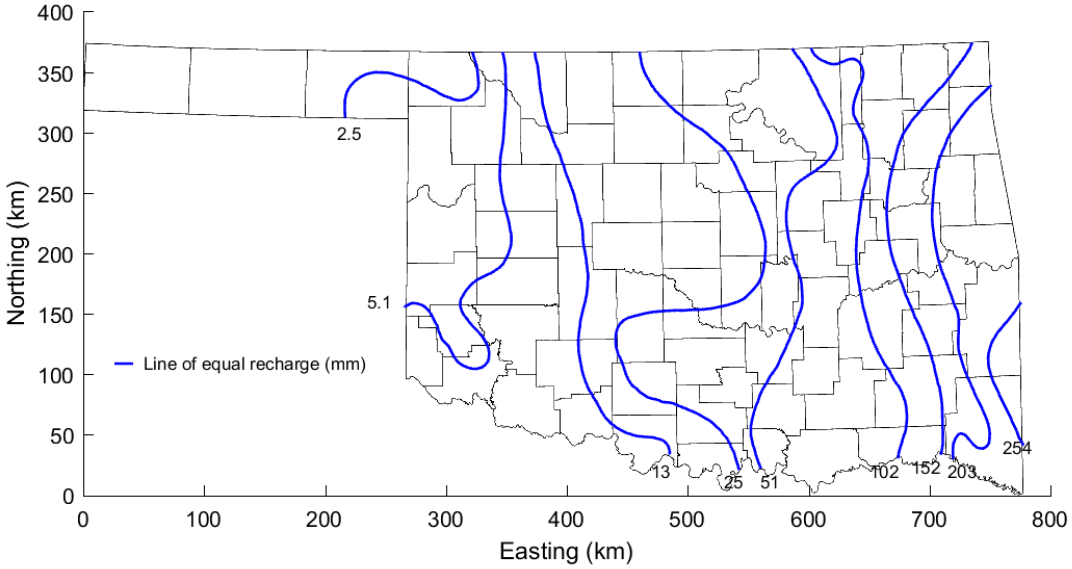

Figure 3. Previously published state-wide recharge map made using the stream baseflow method of recharge estimation. Adapted from original publication by Pettyjohn et al. (1983).

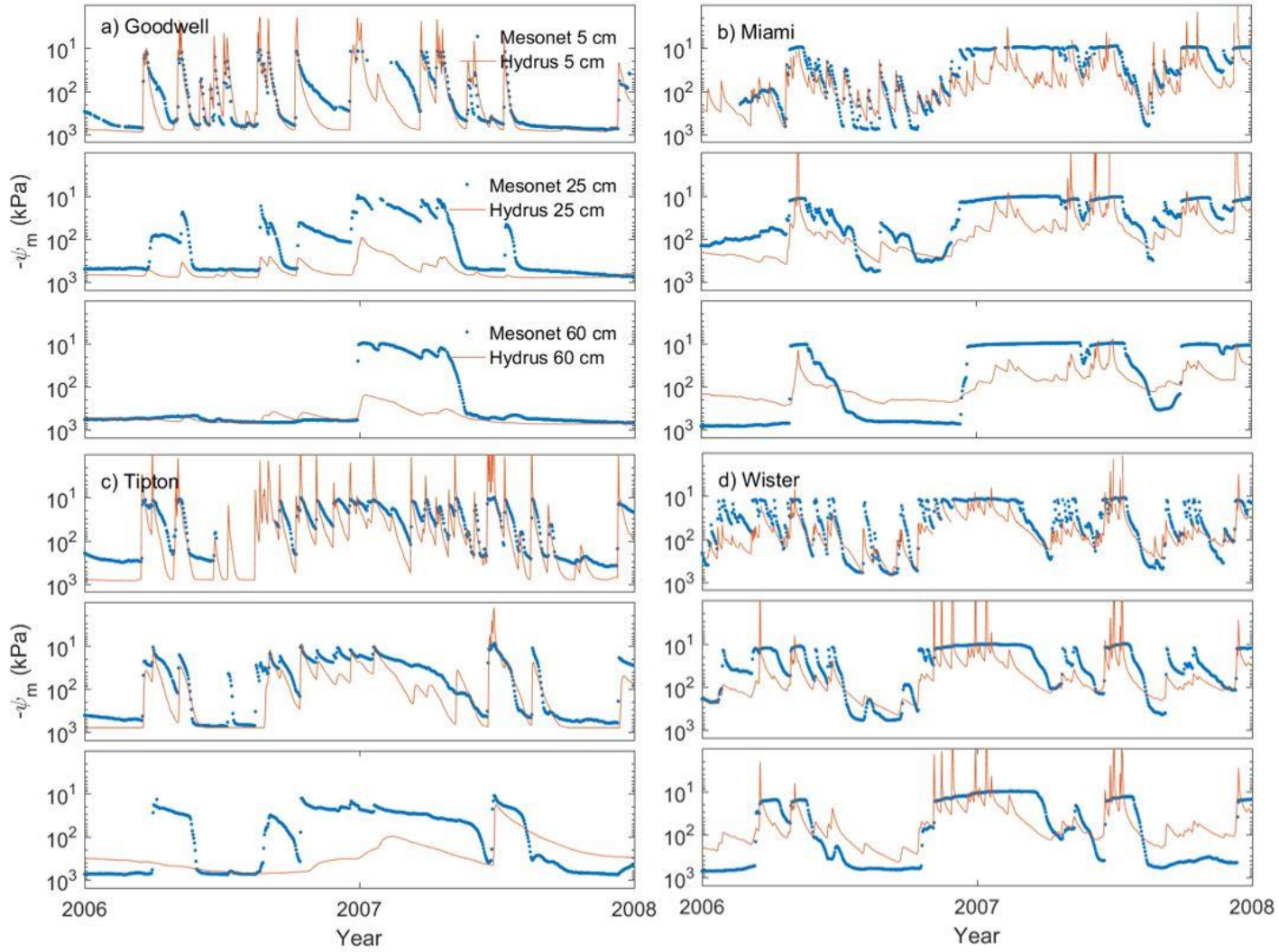

Figure 4. Mesonet-measured daily matric potential (dots) and HYDRUS-1D simulated matric potential (solid line) at 5, 25, and 60 cm during the calibration period for Goodwell (a), Miami (b), Tipton (c), and Wister (d).

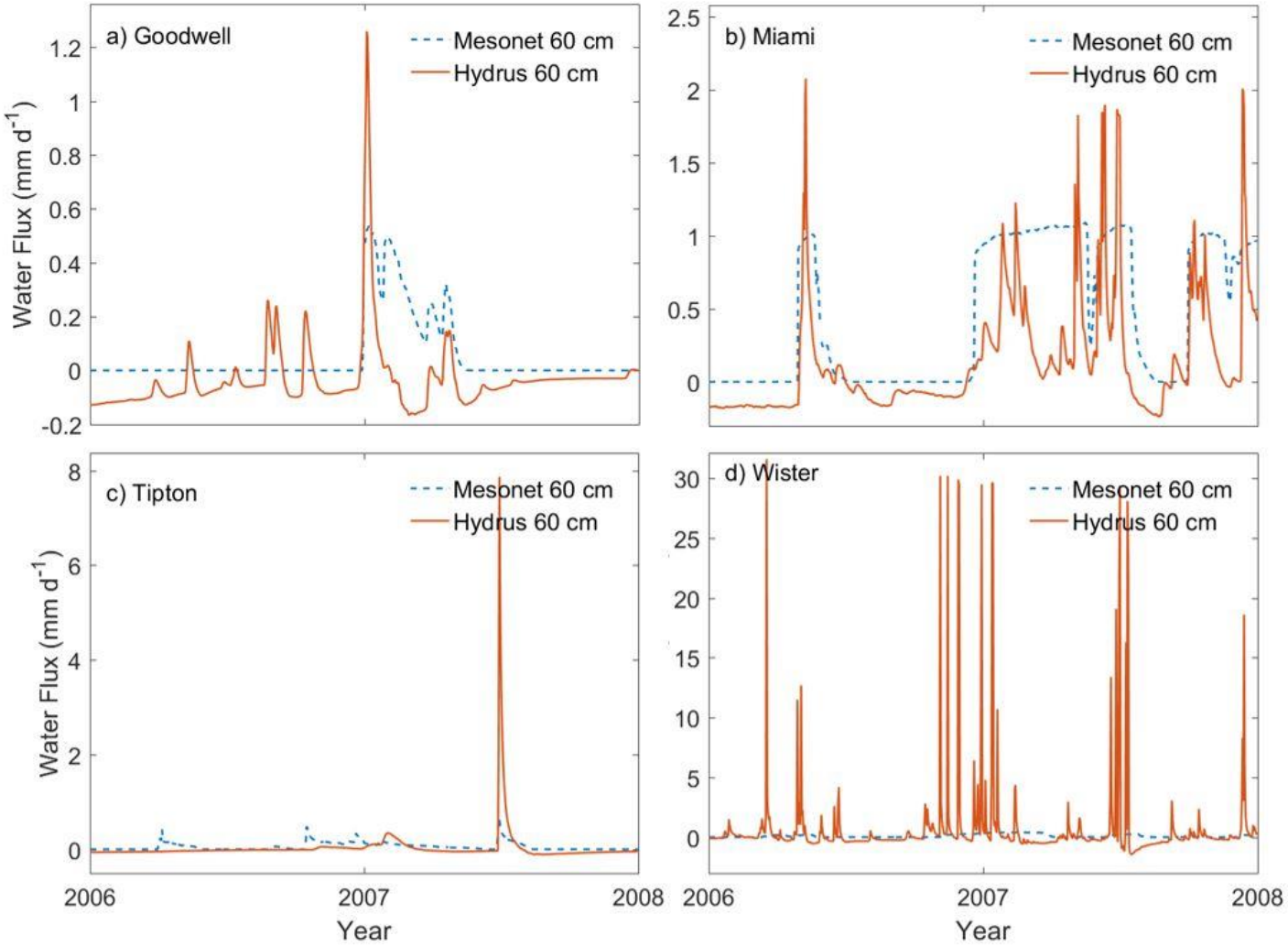

Figure 5. Daily soil moisture-based drainage estimate (dashed line) and HYDRUS-1D estimated drainage for the 60-cm depth during the calibration period at Goodwell (a), Miami (b), Tipton (c), and Wister (d).

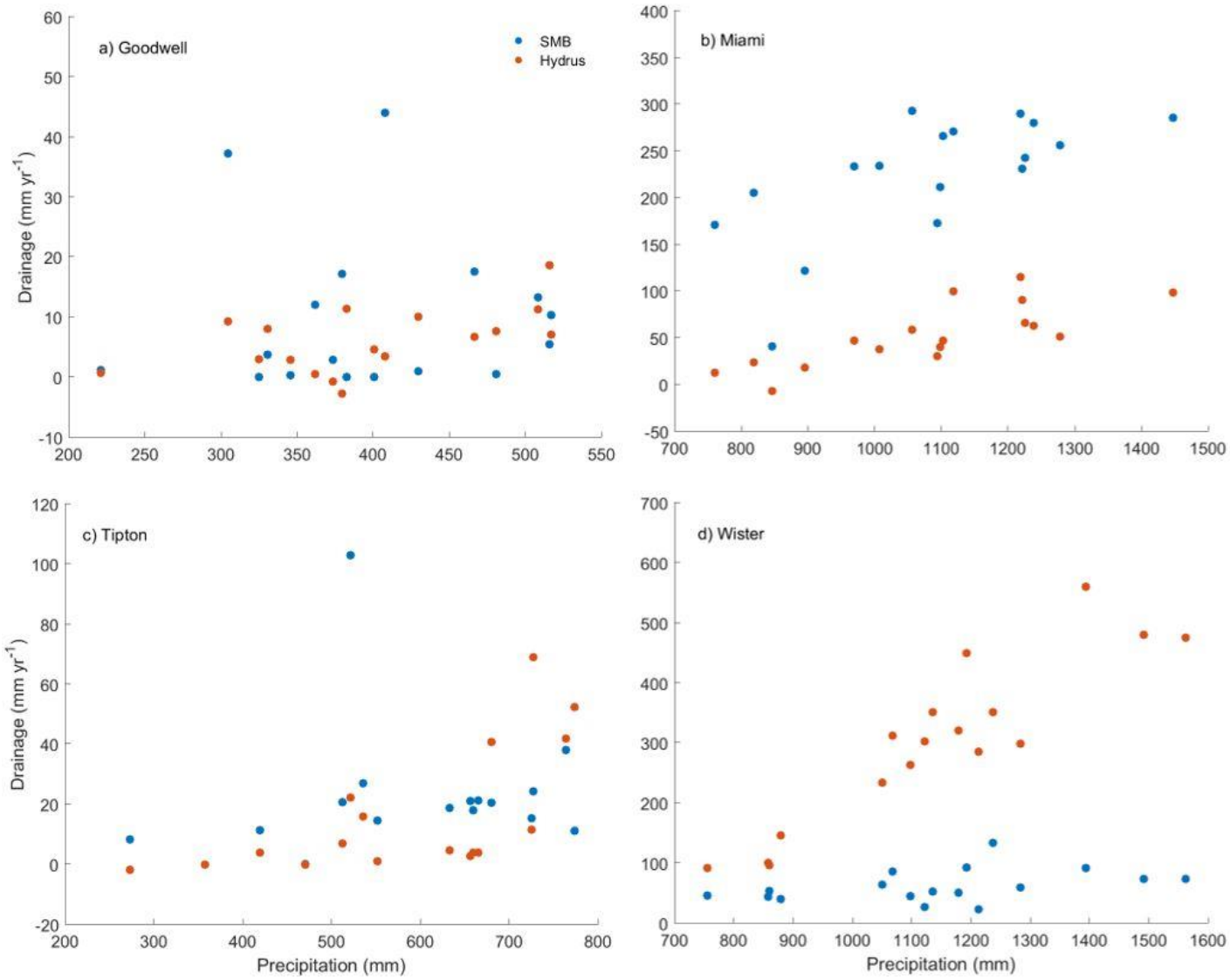

Figure 6. Annual soil moisture-based (SMB) drainage estimates (blue dots) and HYDRUS-1D estimated drainage (orange dots) at the 60-cm depth versus annual precipitation during the validation period at Goodwell (a), Miami (b), Tipton (c), and Wister (d).

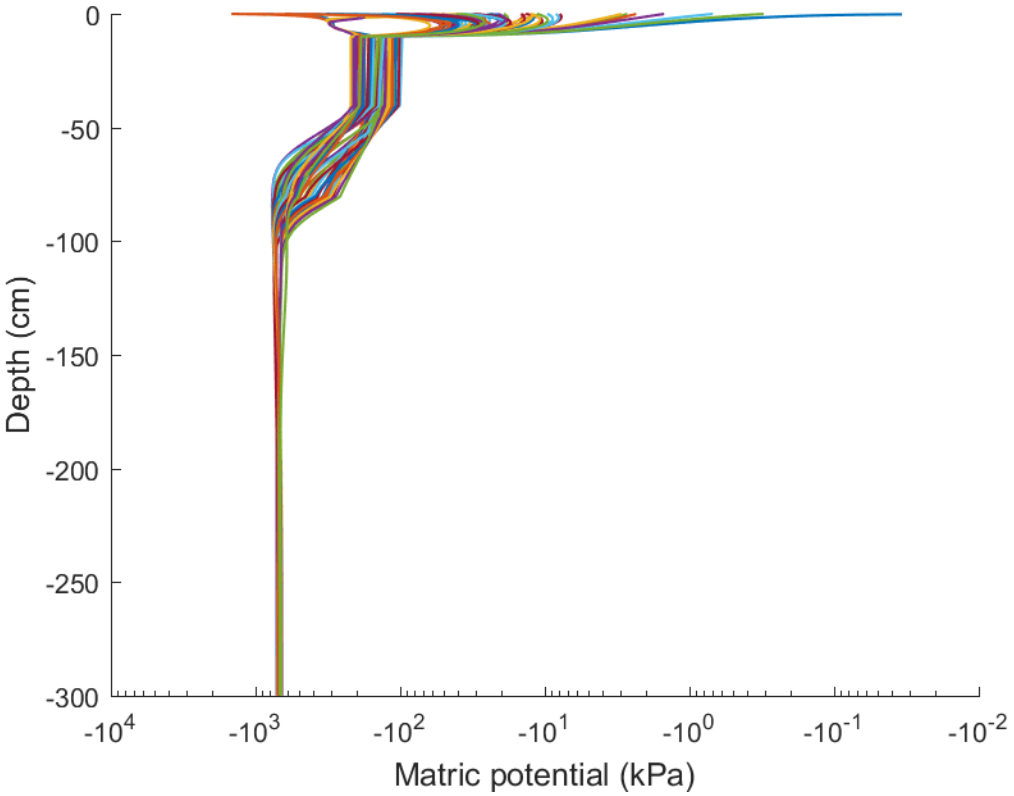

Figure 7. Simulated matric potential profiles associated with the top 1% of simulated drainage rates at the 60-cm depth for Goodwell focus site from 1998-2014.

CHAPTER III

Manuscript undergoing revision for resubmission to Water Resources Research

IN-SITU SOIL MOSITURE DATA IMPROVE SEASONAL STREAMFLOW FORECAST ACCURACY IN RAINFALL-DOMINATED WATERSHEDS

Briana M. Wyatt, Tyson E. Ochsner, Erik S. Krueger, and Eric T. Jones

ABSTRACT

The security and sustainability of surface water resources are threatened by an increasingly variable climate and by the growing water demands of a rising world population. While seasonal streamflow forecasting methods for snow-dominated regions are well-developed, forecasting methods used in rainfall-dominated areas remain less skillful, limiting their usefulness for water resource management. Recent work has shown that including soil moisture data in a principal component analysis and regression forecasting model (hereafter referred to as PCR) can improve seasonal streamflow forecasts in snow-dominated catchments, but its impact on forecast performance in rainfall-dominated watersheds remains unknown. Therefore, our objective was to evaluate the potential improvements gained by including in-situ soil moisture data in PCR-based streamflow forecasts in rainfall-dominated watersheds.

Precipitation and soil moisture data from multiple long-term monitoring watersheds were incorporated into a modified PCR model to predict seasonal streamflow totals at 0-, 1-, 2-, and 3-month lead times. We found that forecasts derived from antecedent precipitation alone were often statistically insignificant, explaining at best 27% of the variability in seasonal streamflow. Conversely, forecast models that included soil moisture information explained 67% to 83% of seasonal streamflow variability at the 0-month lead time. Due to the incorporation of measured soil moisture data, the PCR method applied here produces seasonal streamflow forecasts for rainfall-dominated watersheds with accuracies comparable to those previously reported in snow-dominated watersheds. This new forecast method shows strong potential for use in surface water management in rainfall-dominated regions.

INTRODUCTION

An increasingly variable climate and the growing water demands of a rising world population continually threaten the security and sustainability of surface water resources essential for agricultural production, domestic and industrial water use, recreation, and other beneficial uses (Brekke et al., 2010; Wood, 2007; Garbrecht et al., 2004). These threats are amplified by the relatively low skill of many forecasting systems for predicting future streamflows (Nash and Sutcliffe, 1970). While operational models applied in snow-dominated watersheds have been widely studied and improved (Pagano et al., 2004), seasonal forecasting methods (i.e., forecasts which estimate streamflow volumes over several months) for rainfall-dominated watersheds remain less skillful, reducing their efficacy for water resource management (Cuo et al., 2011; Pagano et al., 2004). Increasing the accuracy of seasonal streamflow forecasts in rainfall-dominated watersheds is critical for improving reservoir operations, drought management, sustainable water use, hydropower production, and irrigated agriculture (Raff et al., 2013; Maurer and Lettenmaier, 2004).

Existing operational streamflow forecasting models used in rainfall-dominated regions of the U.S. are generally used to produce probabilistic streamflow forecasts at short lead times (i.e., < 1 week) and were developed for the purpose of flood forecasting rather than for long-term water resource management and planning (Anderson et al., 2006; Cuo et al., 2004; Sorooshian et al., 1993). The most widely-used streamflow forecasting model in this context is the Sacramento Soil Moisture Accounting model (SAC-SMA), a lumped model used by the National Weather Service River Forecast Centers to predict river flows up to six days in advance (Sorooshian et al., 1993). This relatively small lead time makes the model suitable for predicting flooding events, but

prevents the model from providing useful seasonal streamflow forecast information. Additionally, the conceptual nature of the model requires the use of a generic "soil wetness" variable, and there is often a weak correlation between modeled and observed soil moisture values (Anderson et al., 2006). This can lead to inaccurate model representations of the soil moisture state within the model domain (Koster et al., 2009). Because soil moisture is a key variable in determining the rainfall-runoff behavior of soils (Castillo et al., 2003), it is especially important that soil moisture data used in streamflow forecasting models be accurate.

An alternative forecasting method commonly used to predict streamflow in the snow-dominated, mountainous Western U.S. is principal component analysis and regression (or simply principle components regression, hereafter referred to as PCR), a statistical method utilized by the Natural Resources Conservation Service (NRCS) (Garen, 1992; Garen and Pagano, 2007). The goal of PCR is to find one or more linear combination(s) of predictor variables which explains the greatest amount of variability in a given response variable (Shlens, 2014), where each of these linear combinations is called a principal component. PCR is well-suited for exploring the potential benefits of including soil moisture data in streamflow forecasts in rainfall-dominated regions because it is far simpler than mechanistic models and because it requires no data from the forecast period, allowing forecasts to be made months in advance, providing water managers ample time for decision making. PCR has often been employed using snow water equivalent (SWE) data as the primary input variable (i.e., predictor) used to predict seasonal streamflow volumes (i.e., response) (Garen, 1992). However, Harpold et al. (2017) showed that the inclusion of soil moisture data in PCR analysis improved

operational streamflow forecast skill in 12 snow-dominated watersheds in the Western U.S.

Soil moisture data are underutilized in streamflow forecasting, despite the well-understood influence of soil moisture on infiltration capacity, soil profile storage capacity, and surface runoff (Aubert et al., 2003; Rosenberg et al., 2013; Akbar et al., 2018). In the few instances when soil moisture information has been included in streamflow forecasting models, the information was often based on model-derived soil moisture values, such as those produced by the SAC-SMA model, rather than in-situ measurements (e.g., Koster et al., 2010; Maurer and Lettenmaier, 2004). The use of model-based soil moisture information may lead to potentially large differences between estimated and actual soil moisture and, in turn, streamflow values (Koster et al., 2009). Due to recent increases in the number of state- and nation-wide soil moisture monitoring networks, in-situ soil moisture data are readily available in many locations throughout the U.S. (Ochsner et al., 2013). However, despite the increasing availability of in-situ soil moisture data in many areas and the well-known influence of soil moisture on rainfall-runoff partitioning, these data have not been used operationally by the NRCS, nor is any information available regarding the performance of PCR streamflow forecasting models using these data in rainfall-dominated watersheds (Rosenberg et al., 2013).

We seek to address this knowledge gap by incorporating long-term soil moisture monitoring data from multiple rainfall-dominated watersheds into a PCR methodology similar to that used by Harpold et al. (2017) in order to answer a practical question of great importance in hydrology: How does the inclusion of soil moisture data influence seasonal streamflow forecast accuracy in regions where rainfall is the primary driver of

surface runoff? Therefore, our objective was to evaluate the potential improvements from including in-situ soil moisture data in PCR-based streamflow forecasts in rainfall-dominated watersheds. To achieve this, we (1) developed and tested a modified PCR model which incorporates precipitation and soil moisture data to predict seasonal streamflow volumes in several watersheds with differing seasonal streamflow characteristics; (2) quantified the forecast accuracy improvement provided by the inclusion of soil moisture data, if any; and (3) determined how seasonal streamflow forecast improvements vary across different forecast lead times.

MATERIALS AND METHODS

*Site Description*s

This study focuses on the analysis of four watersheds in rainfall-dominated regions of the U.S.- one in Arizona, two in Oklahoma, and one in Georgia. The Walnut Gulch (hereafter abbreviated as AZ-WG) watershed in Arizona is home to the USDA-Agricultural Research Service (USDA-ARS) Southwest Watershed Research Center, which has collected precipitation data at 88 locations and soil moisture data at two soil profiles since 1990 (Figure 1a). All data from AZ-WG used in the current study are available for download at https://www.tucson.ars.ag.gov/dap/.

The Little Washita (hereafter abbreviated as OK-LW) and Fort Cobb (hereafter abbreviated as OK-FC) watersheds in Oklahoma contain USDA-ARS Micronets, in-situ monitoring networks with long-term soil moisture and precipitation measurement stations which are overseen by the Grazing Lands Research Laboratory (Figure 1b and 1c). At each monitoring location, daily precipitation and soil moisture data have been collected

continuously since 2005 (OK-FC) and 2006 (OK-LW). All precipitation and soil moisture data from OK-FC and OK-LW used in the current study are available for download at http://ars.mesonet.org/form/ars-data-request.

The Little River (hereafter abbreviated as GA-LR) watershed in Georgia has been monitored by the USDA-ARS Southeast Watershed Research Laboratory since 1968, with precipitation data available from 46 rain gauges beginning in 1968 and soil moisture data from 29 measurement locations beginning in 2001 (Figure 1d). Data for the GA-LR watershed are available at http://www.tifton.uGA-LR.edu/sewrl/radio/lrdata.htm. A summary of watershed characteristics, instrumentation, and study-specific meteorological and hydrological information can be found in Table 1.

The AZ-WG watershed has an area of 149 km^2, a mean elevation of 1428 m a.s.l., and soils that range from clay loams to gravelly loams (Keefer et al., 2008). Long-term mean annual precipitation in the watershed is 312 mm, with approximately 60% of annual rainfall occurring in the summer monsoon months of July, August, and September (Goodrich et al., 2008; USDA-ARS Southwest Watershed Research Center webpage). The mean annual temperature of the watershed is 18° C and the primary vegetative cover types are shrubs and grasses (Keefer et al., 2008). The OK-FC watershed has an area of 786 km^2 (area above the dam, Figure 1b), a mean elevation of 467 m a.s.l., and the dominant soil type is Pond Creek fine sandy loam (Moriasi et al., 2014). The long-term mean annual precipitation is 816 mm and the long-term mean annual temperature is 16° C (USDA-ARS Grazing Lands Research Laboratory). The primary land uses are cropland and grassland (Starks et al., 2014b). The OK-LW watershed has an area of 610 km^2, a mean elevation of 393 m a.s.l., and soils ranging from fine sand to silty loam (Moriasi et

al., 2014a; Allen and Naney, 1991). The watershed's long-term mean annual precipitation is 760 mm and its long-term mean annual temperature is 16° C (USDA-ARS Grazing Lands Research Laboratory). The primary land uses are range, pasture, and cropland (Steiner et al., 2008; Starks et al., 2014b). The GA-LR watershed has an area of 334 km^2, a long-term mean annual precipitation of 1200 mm, mean annual temperature of 19° C, and is dominated by Tifton loamy sand (36%), Alapaha loamy sand (12%), and Kinston and Osier fine sandy loam soil types (Bosch et al., 2007a; Sullivan et al., 2007; CEAP Project Plan, 2005; Sheridan, 1997). Land use in the watershed is estimated to be 50% woodland, 31% row crops, 10% pasture, and 2% water based on Landsat remote sensing imagery (Sullivan et al., 2007).

Precipitation Input Data

In the AZ-WG watershed, precipitation data were collected at one-minute intervals using digital rain gauges (Goodrich et al., 2008). These data were combined to produce daily precipitation totals. In the OK-FC and OK-LW watersheds, precipitation measurements have been collected in 15-minute intervals at each of the monitoring stations using tipping-bucket rain gauges since 2000 (Starks et al., 2014a). Precipitation measurements were collected every 5 minutes in the GA-LR watershed, using weighing rain gauges from the inception of the stations until 1993, when weighing rain gauges were replaced with tipping-bucket rain gauges (Bosch et al., 2007b).

Watershed mean precipitation data were used in the current study for all watersheds, with no elevation or area weighting, following the method of Harpold et al. (2017). While no precipitation data were missing at the AZ-WG watershed due to the

relatively low frequency of rainfall, there were some missing precipitation records in the other study watersheds. Quality control procedures for the OK-LW and OK-FC watersheds included filling missing precipitation records with data from the nearest Oklahoma Mesonet station (McPherson et al., 2007). Quality control procedures for the GA-LR watershed included filling in missing precipitation records with data from the nearest or second nearest monitoring station with data available on the missing date. If the two nearest stations had no data available on the missing date, the mean value of the remaining sites in the watershed was used to fill the missing data point.

Soil Moisture Input Data

At AZ-WG, voltage differential data were collected using a Delta-T ThetaProbe (Delta-T Devices, Ltd., Cambridge, UK) at two locations and converted to volumetric water content using methods described in Keefer et al. (2008). At both measurement locations in the watershed, soil moisture measurements were made at six depths- 5, 15, 30, 50, 75, and 100 cm; however, only the top three depths were used in our analysis in order that the effective soil profile depth be comparable to those of the other study watersheds. Daily depth-weighted mean volumetric water content data were calculated by assuming soil moisture sensors were located at the center of a given soil layer (i.e., the data recorded by the sensor at 5 cm is representative of the condition of the layer from 0-10 cm, etc.), resulting in an effective soil profile depth of 40 cm for the watershed. Quality control procedures for soil moisture data at all sites in all watersheds included the removal of any unrealistic volumetric water content values (< 0.0 m^3 m^{-3} or > 0.60 m^3 m^{-3}) and filling gaps using linear interpolation.

Soil volumetric water content data for all other watersheds (OK-FC, OK-LW, and GA-LR) were collected using Stevens HydraProbe sensors (Stevens Water Monitoring Systems, Inc., Portland, Oregon). Sensors were installed at 5-, 25-, and 45-cm depths in the OK-LW and OK-FC watersheds. Mean daily volumetric water content data for OK-LW and OK-FC were downloaded for each sensor depth from http://ars.mesonet.org/form/ars-data-request. Data were depth-weighted in the same fashion as described above, resulting in an effective soil profile depth of 50 cm for the OK-FC and OK-LW watersheds.

Soil moisture sensors were added at 29 of the existing precipitation monitoring locations in the GA-LR watershed beginning in 2001 (Bosch et al., 2007b). Soil moisture measurements were collected at 5, 20, and 30 cm below the surface at one-minute intervals. One-minute data were summarized by data loggers at each station to provide mean soil moisture values every half-hour. Daily volumetric water content data were calculated by summing 30-minute data over 24 hours and daily depth-weighted means were calculated by assuming data from the 5-cm sensors were representative of the 0-10 cm layer, and that the mean value of the 20- and 30-cm sensors was representative of the layer from 10-40 cm, yielding an effective profile depth of 40 cm. As with the precipitation data, mean watershed soil moisture metrics values were calculated with no area or distance weighting.

Streamflow Input Data

Streamflow data in the AZ-WG watershed were measured using specialized flumes. Digital runoff records from the flume at the outlet of the watershed began in 2000

and were used here (Figure 1a) (Stone et al., 2008). Streamflow data for the OK-LW watershed were collected from USGS monitoring gauge #07327550, the gauge in the watershed with the largest contributing area (Figure 1b). Gauge #07327550 has reported instantaneous streamflow data every 15 minutes from 1992-present. Daily streamflow volume totals were calculated from 15-minute data by assuming reported values were representative of flow rates for the entire 15-minute time interval prior to measurement and summing time-weighted streamflow records for each 24-hour period. Periods of missing data, which accounted for ~20% of the daily data record, were filled using an area-weighted mean of one upstream gauge (#07327442) and one downstream gauge (#07328100), similar to the method described by Shu and Ouarda (2012). Using this approach, daily streamflow estimates were unsatisfactory when compared to available data from the target gauge (#07327550). However, when the same method was used to estimate total monthly streamflow volumes, results showed a strong correlation (R^2 = 0.92) with available measured total monthly streamflow records at the target gauge. Thus, estimated monthly streamflow total data were used to infill months with fewer than 25 days of streamflow records at the target gauge. Since the PCR model is used to predict total streamflow during the forecast period, the use of monthly data rather than daily data has no effect on the model or its inputs.

There are several USGS streamflow gauges in the OK-FC watershed, but none captures streamflow from the entire watershed area above the Fort Cobb Reservoir. For this reason, we used estimated daily inflow volumes to the Fort Cobb Reservoir as a proxy for daily streamflow volumes. Daily inflow volume data for the Fort Cobb Reservoir are provided by the Army Corps of Engineers and are estimated using a daily

reservoir water balance calculation (http://www.swt-wc.usace.army.mil/FCOB.lakepage.html). Lake water levels, changes in lake storage, precipitation data, and potential evapotranspiration values are used to estimate the total daily inflow to the reservoir. Daily reservoir inflow data are available from November 1994 until the present at http://www.swt-wc.usace.army.mil/FCOBcharts.html.

Mean daily streamflow data are collected at several locations in the GA-LR watershed by USDA-ARS monitoring gauges. Data from a gauge near the watershed outlet (gauge B, Figure 1d) are available for the years 1971-2015 and were used here. Precipitation, soil moisture, and streamflow data were gathered for all watersheds and all available water years. Data were retained only for water years when all data types were available and only for precipitation and soil moisture stations which reported data for the entirety of those water years, resulting in 9 water years of data (2009-2017) from 2 soil moisture profiles and 88 rain gauges at AZ-WG, 12 water years of data (2007-2018) from 9 co-located soil moisture and precipitation sites at OK-LW, 13 water years of data (2006-2018) from 13 co-located soil moisture and precipitation sites in the OK-FC watershed, and 12 water years of data (2004-2015) from 14 co-located soil moisture and precipitation sites at GA-LR. Study periods and additional data for each watershed are summarized in Table 1.

Soil Moisture Metrics

In addition to volumetric water content (θ_v; $m^3\ m^{-3}$), four other soil moisture metrics were calculated and included in PCR analyses following the approach of Harpold et al. (2017): percent saturation (%), total soil water storage (mm), available storage (mm), and the soil

moisture index (SMI; unitless). The procedures described below were used to estimate these soil moisture metrics for all study watersheds.

Percent saturation was calculated as the ratio of daily θ_v to the satiated water content of the dominant soil type at each soil moisture monitoring location as reported in the NRCS SSURGO database. Daily percent saturation values were calculated for each soil layer and then depth-weighted according to the procedures described in section 2.2.1. Total soil water storage is the depth of water currently stored in a soil profile. Storage for each soil layer was calculated by multiplying the daily θ_v of the layer by the thickness of the layer according to the depth-weighting scheme used. Total storage was calculated as the sum of storage of each soil layer.

Available storage was calculated as the maximum available storage minus the total depth of water currently stored in the profile. Maximum available storage was estimated by multiplying the satiated water content of each soil layer as reported in the NRCS SSURGO database by the thickness of the layer and adding together the maximum storage values for each soil layer, similar to the calculation for total storage. If SSURGO data were unavailable for a certain soil layer, the soil properties were assumed to be the same as the overlying layer. If SSURGO data were unavailable for a location, the soil properties were estimated using the mean values of soil properties at the other locations within that watershed for which SSURGO data were available.

The SMI was calculated by:

$$SMI = -5 + 10(\theta_v - \theta_{wp})/(\theta_{fc} - \theta_{wp}) \quad (1)$$

where θ_v was the reported volumetric water content for a given day, θ_{wp} is the volumetric water content at wilting point (-1500 kPa), and θ_{fc} is the volumetric water content at field

capacity (-33 kPa) (Hunt et al., 2009). Daily SMI values were found for each soil depth and then depth-weighted. θ_{fc} and θ_{wp} values for each site were taken from the SSURGO database and unavailable data were estimated as described above.

PCR Forecasts

Principal component analysis and regression is a well-known multivariate technique for incorporating data from multiple monitoring sites into a statistical model while minimizing the effects of intercorrelation between measured variables (Shlens, 2014). Briefly, principal component analysis finds one or more non-correlated linear combination(s) of some intercorrelated predictor variables. Each of these linear combinations is called a principal component, and these non-correlated principal components are used to develop a linear regression which is then used to estimate the value of the response variable given a set of input variables. In terms of linear algebra, the fundamental mechanism of PCR is a change of basis and re-projection of some orthogonal linear combination(s) of the original predictor variable data into a new phase space which, in most cases, captures a large amount of the observed variability in the original predictor variables. A thorough introduction to the statistical procedures involved in PCR analysis is given by Shlens (2014), a summary of the use of PCR models in standard NRCS streamflow forecasts is provided in Garen and Perkins (2011), and additional applications of the method in hydrology are discussed in Haan (1977).

We developed a PCR methodology similar to that used by Harpold et al. (2017), which is an adaptation of the standard NRCS forecasting method described by Garen (1992). Harpold et al. (2017) incorporated antecedent precipitation, snow water

equivalent, and soil moisture data as input data in their PCR analysis of 12 snow-dominated watersheds in Utah and California. Because snowmelt runoff is negligible in our study watersheds, the snow water equivalent input variable used in traditional NRCS forecasts and by Harpold et al. (2017) was not used in the present study. Similar to Harpold et al. (2017), we chose to use a two-step PCR analysis in order to distinguish the presumably first-order control of antecedent precipitation on streamflow from the presumably second-order control of soil moisture. In our case, this involved an initial PCR analysis using only antecedent precipitation data as inputs (hereafter called the "baseline" scenario) to estimate seasonal streamflow totals and a secondary PCR (hereafter called the "two-step" scenario) which estimated the residuals between estimated and observed streamflow volumes from the baseline scenario using the soil moisture metrics described in section 2.3.

Baseline PCR Forecasts

Baseline PCR forecasts were made for each water year using mean cumulative watershed precipitation data accumulated from the beginning of the water year until the forecast date (i.e., antecedent precipitation). These data were calculated by averaging the cumulative precipitation from the beginning of each water year until the forecast date for all precipitation measurement stations within each individual watershed. These antecedent precipitation values were used as the predictor variables in the baseline PCR analyses. The response variable in the baseline PCR analyses was total streamflow volume during the forecast target period. For the three wetter watersheds, the forecast target period was the four months of greatest median monthly streamflow (Figure 2b-d).

Due to extremely low streamflow volumes in the AZ-WG watershed, the forecast target period was the four months of greatest mean monthly streamflow (Figure 2a). This led to target forecast periods of September-December for the AZ-WG watershed, April-July for the OK-FC watershed, February-May for OK-LW, and January-April in the GA-LR watershed (Table 1). In the baseline scenario, principal components were only retained by the model if their regression coefficients were positively correlated with the response variable (i.e., higher cumulative precipitation leads to greater seasonal streamflow volumes) and significantly different from zero based on a *t*-test (*p*-value < 0.1). These are the same criteria used by Harpold et al. (2017), and forecasts were only considered statistically valid if the underlying PCR model satisfied these criteria.

Two-step PCR Forecasts

Two-step forecasts were made by adding a second PCR analysis after the baseline scenario which utilized mean depth-weighted soil moisture metrics as described in section 2.3 to estimate the residuals between predicted and observed seasonal streamflow totals from the baseline scenario for each water year. In order to account for the different magnitudes of the five soil moisture metrics and to prevent the model from favoring any one metric based on its magnitude, all soil moisture metrics were normalized using their *z*-score prior to being input into the PCR model (Haan, 1977). Finally, the baseline scenario total streamflow volume estimates and step two streamflow residual estimates were summed for each water year, yielding final streamflow volume estimates for each year.

Because PCR analysis requires a single value of each predictor variable for each water year, daily soil moisture metric data must be summarized into a single value which, in theory, should represent the general soil moisture condition of each watershed over the portion of the year during which soil moisture most strongly influences streamflow during the subsequent forecast target period. Here, we chose to use the mean value of each soil moisture metric over some optimal time period prior to the forecast date, similar to Harpold et al. (2017). To determine which time period provided the best results, eight different soil moisture metric averaging periods were tested at the 0-month lead time for each watershed. These averaging periods were modeled after those used by Harpold et al. (2017). While the length of each averaging period and its temporal relation to the target forecast period is the same across all watersheds, the periods were shifted between watersheds because of the different target forecast periods. The averaging periods used capture a range of soil moisture conditions both near the beginning of the forecast period, over longer time periods, and in prior seasons.

In addition to testing these eight soil moisture averaging periods at the 0-month lead time, we also tested using soil moisture metrics from the first day of the forecast period (SM1, Figure 3) at all lead times in order to determine whether using data nearer the beginning of the forecast period resulted in greater model accuracy. A generalization of all averaging time periods relative to the forecast period is shown in Figure 3. For each watershed and lead time, results of forecasts made using the soil moisture averaging period which included only data prior to the forecast date and which provided the best results at the 0-month lead time were compared to model results from forecasts made using soil moisture metrics from the first day of the forecast period at all lead times.

Forecasts with the highest accuracy were used and are reported in Table 2, as are the soil moisture averaging periods used for each watershed/lead time combination.

Like baseline forecasts, two-step PCR forecasts also retained only principal components with a *t*-test *p*-value of < 0.1. However, the qualification that regression coefficients be positive was not applied in the second step because it is not necessarily true that residuals between observed streamflow values and estimated values from the baseline forecast must be positively correlated with soil moisture.

Baseline and two-step forecasts were evaluated for each watershed for all available water years with lead times of 0-3 months. Each scenario and lead time combination was run independently for each watershed, for a total of 32 model runs (2 scenarios X 4 watersheds X 4 lead times). All PCR and statistical analyses were carried out using a series of custom MATLAB scripts and functions. Forecast accuracy was quantified using the root mean square error (RMSE), the coefficient of determination (R^2), the RMSE to observation standard deviation ratio (RSR), and bias.

RESULTS AND DISCUSSION

Weather and streamflow during study period

The markedly differing precipitation and streamflow totals across watersheds (Tables 1 and 2) are representative of the watershed characteristics in their respective regions, and this diversity was a primary reason for their inclusion in our study. Water year precipitation during the study period ranged from 119-388 mm yr^{-1} at AZ-WG, 320-1155 mm yr^{-1} at OK-FC, 360-1328 mm yr^{-1} at OK-LW, and from 766-1571 mm yr^{-1} at GA-LR (Table 1). Mean water year precipitation during the study period was 307 mm yr^{-}

^{1} at AZ-WG, 750 mm yr^{-1} at OK-FC, 847 mm yr^{-1} OK-LW, and 1131 mm yr^{-1} at GA-LR. There was substantial variability in annual precipitation levels for OK-FC and OK-LW, including a multi-year drought beginning in the fall of 2010 which corresponds to the lowest water year total precipitation values of 320 mm and 360 mm for those watersheds, respectively.

Streamflow volumes were normalized by watershed area and are presented here as a depth (mm). Seasonal streamflow volumes during the target forecast period ranged from 0.0-1.8 mm at AZ-WG, 12-94 mm at OK-FC, 6.6-102 mm at OK-LW, and 8.0-349 mm at GA-LR with mean seasonal streamflow (Q) values of 0.41 mm at AZ-WG, 31.3 mm at OK-FC, 33.0 mm at OK-LW, and 187 mm at GA-LR (Table 1). Mean depth-weighted volumetric soil water content from October 1 to the forecast date for the 0-month lead time forecast ranged from 0.022-0.033 $m^3\ m^{-3}$ at AZ-WG, 0.018-0.097 $m^3\ m^{-3}$ at OK-FC, 0.007-0.116 $m^3\ m^{-3}$ at OK-LW, and 0.015-0.152 $m^3\ m^{-3}$ at GA-LR, with mean values of 0.027 $m^3\ m^{-3}$, 0.052 $m^3\ m^{-3}$, 0.054 $m^3\ m^{-3}$, and 0.062 $m^3\ m^{-3}$, respectively. The low mean volumetric water contents reported for the watersheds are likely due to the relatively high sand contents of the dominant soil mapping units in the watersheds as reported by the NRCS SSURGO database (Table 1).

Baseline forecasts

Baseline forecasts, those based on antecedent precipitation alone, had little predictive power. Statistically valid baseline forecasts could be made only for the OK-FC and GA-LR watersheds, and only at the 0-month lead time (Table 2, Figure 4b,d). All other baseline forecast scenarios resulted in no principal components being retained due

to the qualifications for retaining principal components discussed in section 2.4.1. The 0-month lead time forecasts at OK-FC had an RMSE of 18.2 mm, and an R^2 value of 0.27, indicating that the forecast had a relatively high amount of error and explained only 27% of the variability in observed seasonal streamflow. On average, the model over-predicted seasonal streamflow in the OK-FC baseline scenario, with a bias of 2.56 mm and a range in annual bias of -45.6 mm to 40 mm. RSR performance criteria described by Moriasi et al. (2007) normalize model RMSE by the standard deviation of the observed data, allowing comparisons to be made across watersheds. RSR values in the range of 0.00-0.50 are considered to be very good, 0.51-0.60 to be good, 0.61-0.70 to be satisfactory, and >0.70 to be unsatisfactory. Using these criteria, the RSR value of the OK-FC baseline forecast was 0.82, which is considered unsatisfactory.

Similar results were found for the 0-month lead time at GA-LR, which had a relatively high amount of error (RMSE = 102 mm), and captured little of the variability in observed seasonal streamflow (R^2 = 0.19) (Table 2). On average, the model predicted seasonal streamflow in the GA-LR baseline scenario without bias, but had a large range in annual bias of -212 mm to 113 mm. Additionally, the RSR value of this forecast was 0.86, which is considered unsatisfactory based on the RSR performance criteria described above.

Observed and estimated seasonal streamflow totals for all baseline forecasts are shown in Figure 4, where each point represents the estimated and observed streamflow volumes during the forecast period for each water year. While only the OK-FC and GA-LR watersheds (Figure 4b,d) had statistically valid forecasts in the baseline scenario, baseline results are shown for all watersheds in order to demonstrate the inability of

antecedent precipitation data alone to produce accurate forecasts and to show the improvements gained due to the inclusion of soil moisture data. The deviation from the 1:1 line and high degree of scatter of data points for AZ-WG and OK-LW (Figure 4a,c) are a reflection of the absence of predictive power of baseline forecasts for these watersheds. Even when baseline forecasts were statistically significant (Figure 4b,d), the model underestimated flow during wet years and overestimated flow during dry years, an indication of low baseline forecast skill.

Our results differ from those of Harpold et al. (2017), whose streamflow forecasts without soil moisture data accounted for, on average, 77% of the observed variability in streamflow in snow-dominated watersheds. However, those forecasts relied primarily on snow water equivalent data, whereas our baseline forecasts rely solely on antecedent precipitation data. The low accuracy of the baseline forecast observed here is not entirely unexpected, as Garen and Perkins (2011) state that even in the snow-dominated Western U.S. the ability of standard operational NRCS streamflow prediction models to produce accurate forecasts decreases as snowpack decreases and as precipitation inputs to watersheds increase. The general inability of the baseline PCR model to produce meaningful streamflow forecasts for the rainfall-dominated watersheds presented here suggests that precipitation data alone do not provide adequate information to predict streamflow in such environments, and that additional PCR model predictor inputs may be necessary to provide accurate forecasts. Thus, the inclusion of soil moisture data may be considerably more influential for streamflow forecasts developed in rainfall-dominated regions than for those used in snow-dominated ones.

Testing soil moisture averaging periods

Following Harpold et al. (2017), we tested eight different soil moisture averaging periods at the 0-month lead time in order to determine which averaging period provided the most accurate forecasts. Definitions of the eight soil moisture averaging periods for each watershed and the results of testing each averaging period within the two-step PCR model are given in Table 3, and the averaging periods are generalized and shown relative to the forecast period for each watershed in Figure 3. In addition, we also tested the use of soil moisture metrics from the first day of the forecast period at all lead times. The results of these forecasts are given for each watershed in Table 4, and the generalized averaging periods are shown as gray stars in Figure 3.

Forecast results at the 0-month lead time varied among the different soil moisture averaging periods in each watershed, indicating that the two-step PCR model is sensitive to changes in the soil moisture metric inputs (Table 3). The 0-month lead time forecasts generally performed best when soil moisture data relatively near the forecast date were used (Table 3). At AZ-WG, the period from July-August (averaging period 3) provided the best 0-month forecast results. At OK-FC, the period from September-November (averaging period 7) provided the best 0-month forecast results. At OK-LW, the day of February 1 (averaging period 1) provided the best 0-month forecast results. At GA-LR, the day of January 1 (averaging period 1) provided the best 0-month forecast results.

Two-step forecasts

The inclusion of soil moisture metrics in the two-step forecasts led to at least one principle component being retained in all scenarios, which allowed forecasts to be made

at all lead times in all watersheds (Table 2). For the 0-month lead time, the soil moisture averaging periods which provided the best forecast results in each watershed were used (Table 3). At longer lead times, we tested two types of averaging periods: 1) the soil moisture averaging period from Table 3 which yielded the most accurate results at the 0-month lead time and which included only soil moisture data prior to the forecast date, or 2) the soil moisture metrics on the forecast date (SM1, Figure 3). Whichever of these two soil moisture averaging periods provided the most accurate forecast at each lead time was used. All watershed/lead time/averaging period combinations are shown in Table 2.

RMSE was lowest for all watersheds at the 0-month lead time, and generally increased as lead time increased at OK-FC and OK-LW. The increases in RMSE seen at the 1- and 3-month lead time at AZ-WG may be due to the changes in soil moisture averaging period from the averaging period of the prior lead time. The decrease in RMSE observed at the 3-month lead time at GA-LR is a result of an increased number of retained principle components as compared to the 1- and 2-month lead times (Table 2). R^2 values were highest at the 0-month lead time for all watersheds and generally decreased as lead time increased (Table 2). The 0-month lead time two-step forecasts explained, on average, 78% of the variability in seasonal streamflows in the study watersheds. The R^2 values resulting from the present two-step forecasts are comparable to the 0-month lead time results found by Harpold et al. (2017) for snow-dominated watersheds. However, the improvement in 0-month lead time forecast accuracy when soil moisture data are included was nearly an order of magnitude higher for these rainfall-dominated watersheds (mean R^2 improvement of 0.67) than for the snow-dominated watersheds in the Harpold et al. (2017) study (mean R^2 improvement of 0.07).

Forecast accuracy generally decreased with increasing lead time in all of the study watersheds. One-month lead time forecasts explained, on average, 62% of seasonal streamflow variability; 2-month lead time forecasts explained, on average, 56% of seasonal streamflow variability; and 3-month forecasts explained, on average, 50% of seasonal streamflow variability. This trend has also been observed in a number of prior streamflow forecasting studies (Pagano and Garen, 2005; Mahanama et al., 2012; Mahanama et al., 2008). However, despite the fact that forecast accuracy decreased at the longer lead times, the lowest performing two-step forecast still explained more variability in streamflow (35%) than the two 0-month lead time baseline forecasts (27% and 19%).

Bias was zero for all two-step forecasts (Table 2), indicating that on average, the PCR model tended to predict seasonal streamflow volumes accurately. However, in all watersheds, there is a wide range in bias, with all forecasts having simulation years with both negative and positive bias (Table 2). In general, the magnitude of the maximum bias is similar to that of the minimum bias, leading to overall bias values of zero.

Unlike the unsatisfactory results of the 0-month lead time baseline forecasts at OK-FC and GA-LR and the insignificant baseline forecasts in other watersheds, all 0-month lead time two-step forecasts were rated as good or very good based on the RSR performance criteria described previously (Table 2). Across all lead times, five two-step forecasts (31%) were classified as very good, four (25%) as good, five (31%) as satisfactory, and two (13%) as unsatisfactory (Table 2). Thus, 87% of the two-step forecasts developed using the current method provide results which are at least satisfactory and provide meaningful information regarding future streamflow volumes.

In all but the AZ-WG watershed, a considerable decrease in forecast accuracy is observed between certain lead times (i.e., OK-FC at 2- to 3-month lead times, OK-LW at 0- to 1-month lead times, GA-LR at 1- to 2-month lead times). This is most likely due to the decrease in the number of principal components retained by the PCR model in all of the cases mentioned above (Table 2). This decrease in the number of principle components used in the model consequently reduces the amount of predictive information included in the model, thus reducing model accuracy.

Observed and estimated seasonal streamflow totals for all two-step forecasts are shown in Figure 4, where each point represents one water year's streamflow volumes. In all watersheds, the inclusion of soil moisture data in the PCR model led to drastically improved model accuracy as compared to baseline forecasts. This is especially true for years when baseline forecasts had a large residual, regardless of whether the baseline forecast overestimated or underestimated seasonal streamflow totals.

Soil moisture averaging periods at longer lead times

Half of forecasts at lead times of one month or more had the most accurate results when using soil moisture averaging period 7 (six and seven months prior to forecast), while the other half performed best using either water year mean soil moisture metrics (averaging period 8) or soil moisture metrics from the first day of the forecast period (averaging period 1, longer lead times) (Figure 3, Table 3, Table 2). Coupling between soil moisture, groundwater, and streamflow may provide one pathway by which soil moisture conditions 6 to 7 months prior could influence streamflow during the target

forecast period. Increases in soil water stored in these watersheds may eventually lead to increased groundwater discharge, which would contribute to baseflow later in the year.

The majority (83%) of soil moisture averaging periods used at lead times of one month or greater summarize soil moisture data from a one- or two-month period or from a single day, rather than from longer time periods. These results are the opposite of those found by Harpold et al. (2017), who found that using a longer soil moisture averaging period provided the greatest forecast improvements in their snow-dominated watersheds. Our results suggest that there may be relatively short time periods, sometimes months in advance of the periods of peak streamflow, when soil moisture data are particularly beneficial for inclusion in the current streamflow forecasting method. However, while it is plausible that these results may be caused by physical processes as described above, due to the purely statistical nature of the PCR model and the relatively small number of watersheds studied here, a conclusive physical explanation regarding the importance of the soil moisture averaging periods requires further investigation.

Comparison with other forecasting methods

Our observed increases in model accuracy due to the incorporation of soil moisture data align with numerous prior studies which have employed land surface models (Crow et al., 2018; Mahanama et al., 2008), conceptual models (Aubert et al., 2003), and statistical models (Harpold et al., 2017) to demonstrate improved streamflow forecast accuracy using soil moisture data. Our results are consistent with a growing body of literature showing that the ability of even a small number of in-situ soil moisture monitoring locations in a watershed provide beneficial information about antecedent

moisture conditions leading to improved streamflow forecasts (Harpold et al., 2017; Aubert et al., 2003). However, to the authors' knowledge, the present study is the first to show that incorporating in-situ soil moisture data into a PCR model produces substantial improvement in accuracy of seasonal streamflow forecasts in rainfall-dominated watersheds.

Limitations

We recognize that factors not considered in the present analysis may have a significant impact on the ability of the PCR model to accurately predict streamflow. For example, the relatively poor performance of the PCR model at longer lead times in the OK-LW watershed may be due to the relatively large number of surface water retention structures located within the watershed (Moriasi et al., 2014b). While the majority of these structures are small, the large number of retention dams in the watershed likely has a significant impact on observed streamflow volumes. The impact of these structures was not considered directly in the present study, but the PCR method still provided accurate forecasts at the 0- and 1-month lead times for OK-LW.

The relatively high sand contents of the soils in the watersheds considered here is an additional limitation. The sand content of the study watersheds ranges from 43% to 84%, and AZ-WG has gravelly soils as well (see Table 1). It is not clear how these high sand contents impacted our results or how the PCR model might perform in less sandy areas, although some conclusions might be drawn by comparing the two Oklahoma watersheds. Despite being in close geographic proximity and having similar annual precipitation and total seasonal streamflow, OK-FC (average sand content of 43%) and

OK-LW (84% sand) displayed differing seasonal streamflow patterns (Figure 2) and model performance at lead times longer than 0-months (Table 2). Streamflow in OK-LW was higher earlier in the year when soil moisture tends to be higher (Krueger et al., 2016), whereas peak streamflow was later for OK-FC. Likewise, model performance at lead times greater than 0-months was poorer for OK-LW. Each of these trends are indicative of a sandy soil that is able to retain less soil moisture compared with heavier textured soils in the OK-FC watershed. Future studies should assess the impact of soil type by applying the PCR forecasting methodology used here across watersheds with a broader range of soil types.

Additional hydrological variables such as groundwater contributions to streamflow and the groundwater table depth were not considered in the present study, but may provide additional skill for PCR forecasts in watersheds where groundwater/surface water interactions are known to occur. While the statistical PCR model presented requires fewer inputs than a physically-based model would, the results of our analysis suggest that this type of model may still provide useful information for predicting future streamflow volumes at multiple lead times in rainfall-dominated watersheds.

CONCLUSION

The control of soil moisture on rainfall-runoff partitioning is well known, yet current operational streamflow forecasting systems have failed to take advantage of increasingly available soil moisture data. Harpold et al. (2017) showed that forecast accuracy in snow-dominated watersheds was improved by incorporating soil moisture data. Even greater improvements were achieved here for rainfall-dominated watersheds,

adding to the growing body of evidence in support of the inclusion of soil moisture data in operational streamflow forecasts. This study provides clear evidence of the usefulness of the PCR streamflow forecasting method in rainfall-dominated regions, as well as proof of seasonal streamflow forecast accuracy improvement in these regions due to the incorporation of measured soil moisture data. Forecasts which incorporated soil moisture were able to provide seasonal streamflow forecasts at lead times up to three months and, compared with forecasts including only precipitation data, improved model R^2 values by 0.66 at the 0-month lead time, 0.62 at the 1-month lead time, 0.56 at the 2-month lead time, and 0.50 at the 3-month lead time.

While the present study focused only on four watersheds, those watersheds spanned a wide range of hydrological, ecological, and meteorological conditions, suggesting that our methods could be broadly applicable to rainfall-dominated watersheds worldwide. Future development of this method should include expansion to additional watersheds in other geographical, climatological, and physiographic regions. There is also potential to explore the use of remotely-sensed soil moisture data, such as those from the SMOS or SMAP satellites (Entekhabi et al., 2010; Kerr et al., 2010), in the place of in-situ soil moisture data; however, their relatively short data records may be a limitation. The results presented here demonstrate that the PCR method can produce accurate seasonal streamflow forecasts in rainfall-dominated regions and that including soil moisture data in the PCR model increases forecast accuracy over forecasts made using antecedent precipitation data alone.

ACKNOWLEDGEMENTS

Support for this work was provided by the USGS 104(b) program and the Oklahoma Water Resources Center Berry Fellows Program. The authors would like to thank David Bosch of the USDA-ARS Southeast Watershed Research Lab; Daniel Moriasi and Patrick Starks of the USDA-ARS Grazing Lands Research Laboratory; and Joel Biederman, Russ Scott, and Mark Kautz of the USDA-ARS Southwest Watershed Research Center for their help in accessing and downloading data that were essential to the completion of this project and for sharing their expert knowledge of the study watersheds.

REFERENCES

Akbar, R., et al. 2018. Hydrological storage length scales represented by remote sensing estimates of soil moisture and precipitation. Water Resources Research 54(3): 1476-1492.

Allen, P.B. and J.W. Naney. 1991. Hydrology of the Little Washita River Watershed: Oklahoma- Data and Analyses. USDA-ARS Report ARS-90.

Aubert, D., et al. 2003. Sequential assimilation of soil moisture and streamflow data in a conceptual rainfall–runoff model. Journal of hydrology 280(1): 145-161.

Bosch D.D., et al. 2007a. Precipitation, soil moisture, and climate database, Little River Experimental Watershed, Georgia, United States. Water Resources Research 43(9).

Bosch D.D., et al. 2007b. Little River Experimental Watershed database. Water Resources Research 43(9).

Brekke, L. D., D. Garen, K. Werner, and D. Laurine. 2010. Projecting climate change impacts on seasonal water supply forecasting error. Preprints, 18th Conf. on Applied Climatology/22nd Conf. on Climate Variability and Change/ 24th Conf. on Hydrology, Atlanta, GA-LR, Amer. Meteor. Soc., J15.4. [Available online at https://ams.confex.com/ams/90annual/techprogram/paper_162386.htm.]

Castillo, V.M., Gómez-Plaza, A., Martinez-Mena, M., 2003. The role of antecedent soil water content in the runoff response of semiarid catchments: a simulation approach. J. Hydrol. 284, 114–130, http://dx.doi.org/10.1016/S0022-1694(03)00264-6.

Cuo, L., T.C. Pagano, and Q.J. Wang. 2011. A review of quantitative precipitation forecasts and their use in short- to medium-range streamflow forecasting. Journal of Hydrometeorology 12:713-728.

Entekhabi, D., E.G. Njoku, P.E. O'Neill, K.H. Kellogg, W.T. Crow, W.N. Edelstein, et al. 2010. The soil moisture active passive (SMAP) mission. Proc. IEEE 98:704–716. doi:10.1109/JPROC.2010.2043918.

Garbrecht, J., et al. 2004. Trends in precipitation, streamflow, and evapotranspiration in the Great Plains of the United States. Journal of Hydrologic Engineering 9(5): 360-367.

Garen, D. C. 1992. Improved techniques in regression-based streamflow volume forecasting. Journal of Water Resources Planning and Management 118(6): 654-670.

Garen, D. C. and T. Perkins. 2011. Water Supply Forecasting. National Engineering Handbook Part 622(Chapter 7).

Garen, D.C., and T. C. Pagano, 2007: Statistical techniques used in the VIPER water supply forecasting software. NRCS-USDA Engineering-Snow Survey and Water Supply Forecasting Tech. Note 210-2, 18 pp. [Available online at http://www.wcc.nrcs.usda.gov/ ftpref/downloads/factpub/wsf/technotes/Tech_ note_statistical_techniques_in_Viper.pdf.]

Goodrich, D. C., et al. 2008. Long-term precipitation database, Walnut Gulch Experimental Watershed, Arizona, United States. Water Resources Research 44: 5.

Haan, C. T. 1977. Statistical methods in hydrology. Iowa State University Press, Ames, Iowa.

Harpold, A. A., et al. 2017. Does including soil moisture observations improve operational streamflow forecasts in snow-dominated watersheds? JAWRA Journal of the American Water Resources Association 53(1): 179-196.

Hunt, E. D., et al. 2009. The development and evaluation of a soil moisture index. International Journal of Climatology 29(5): 747-759.

J.L. Steiner, P.J. Starks, J.A. Daniel, J.D. Garbrecht, D. Moriasi, S. McIntyre, and J.-S. Chen. 2008. Environmental effects of agricultural conservation: A framework for research in two watersheds in Oklahoma's Upper Washita River Basin. Journal of Soil and Water Conservation. 63(6):443-452; doi:10.2489/jswc.63.6.443

Keefer, T. O., et al. 2008. Long-term meteorological and soil hydrology database, Walnut Gulch Experimental Watershed, Arizona, United States. Water Resources Research 44(5).

Kerr, Y.H., P. Waldteufel, J.P. Wigneron, S. Delwart, F. Cabot, J. Boutin, et al. 2010. The SMOS mission: New tool for monitoring key elements of the global water cycle. Proc. IEEE 98:666–687. doi:10.1109/JPROC.2010.2043032

Koster, R. D., et al. 2009. On the nature of soil moisture in land surface models. Journal of Climate 22(16): 4322-4335.

Koster, R. D., et al. 2010. Skill in streamflow forecasts derived from large-scale estimates of soil moisture and snow. Nature Geosci 3(9): 613-616.

Krueger, E.S., T.E. Ochsner, J.D. Carlson, D.M. Engle, D. Twidwell and S.D. Fuhlendorf. 2016. Concurrent and antecedent soil moisture relate positively or negatively to probability of large wildfires depending on season. International Journal of Wildland Fire 25:657-668.

Mahanama, S. P. P., et al. 2008. The role of soil moisture initialization in subseasonal and seasonal streamflow prediction – A case study in Sri Lanka. Advances in Water Resources 31(10): 1333-1343.

Mahanama, S., et al. 2012. Soil Moisture, snow, and seasonal streamflow forecasts in the United States. Journal of Hydrometeorology 13(1): 189-203.

Maurer, E. P. and D. P. Lettenmaier. 2004. Potential effects of long-lead hydrologic predictability on Missouri River main-stem reservoirs. Journal of Climate 17(1): 174-186.

McPherson, R. A., et al. 2007. Statewide monitoring of the mesoscale environment: A technical update on the Oklahoma Mesonet. Journal of Atmospheric and Oceanic Technology 24(3): 301-321.

Mohanty, B.P, M.H. Cosh, V. Lakshmi, and C. Montzka. 2017. Soil moisture remote sensing- State-of-the-Science. Vadose Zone Journal 16(1).

Moriasi, D. N., et al. 2014. Upper Washita River Experimental Watersheds: reservoir, groundwater, and stream flow data. Journal of Environmental Quality 43(4): 1262-1272.

Moriasi, D. N., et al. 2014. Upper Washita River Experimental Watersheds: physiography data. Journal of Environmental Quality 43(4): 1298-1309.

Moriasi, D., et al. 2007. Model evaluation guidelines for systematic quantification of accuracy in watershed simulations. Trans. Asabe 50(3): 885-900.

Nash, J. E. and J. V. Sutcliffe. 1970. River flow forecasting through conceptual models part I — A discussion of principals. Journal of hydrology 10(3): 282-290.

Ochsner, T. E., et al. 2013. State of the art in large-scale soil moisture monitoring. Soil Science Society of America Journal 77(6): 1888-1919.

Pagano, T. and D. Garen. 2005. A recent increase in Western U.S. streamflow variability and persistence. Journal of Hydrometeorology 6(2): 173-179.

Pagano, T., D. Garen, and S. Sorooshian. 2004. Evaluation of official Western U.S. seasonal water supply outlooks, 1922–2002. Journal of Hydrometeorology 5(5):896-909.

Raff, D., L. Brekke, K. Werner, A.W. Wood and K. White. 2013. Short-term water management decisions: User needs for improved climate, weather, and hydrologic information. In: U.S. Army Corps of Engineers, Bureau of Reclamation and National Oceanic and Atmospheric Administration, editors, National Technical Information Service, Springfield, Virginia. p. 233.

Rosenberg, E. A., et al. 2013. Informing hydrometric network design for statistical seasonal streamflow forecasts. Journal of Hydrometeorology 14(5): 1587-1604.

Sheridan, J.M. 1977. Rainfall-streamflow relations for coastal plains watersheds. Applied Engineering in Agriculture 13(3):333-344.

Shlens, J. 2014. A tutorial on principal component analysis. CoRR.

Shu, Chang and T.B.M.J. Ouarda. 2012. Improved methods for daily streamflow estimates at ungauged sites. Water Resources Research 48(2).

Soil Survey Staff, Natural Resources Conservation Service, United States Department of Agriculture. Web Soil Survey. Available online at the following link: https://websoilsurvey.sc.egov.usda.gov/. Accessed June 2018.

Sorooshian, S., et al. 1993. Calibration of rainfall-runoff models: Application of global optimization to the Sacramento Soil Moisture Accounting Model. Water Resources Research 29(4): 1185-1194.

Starks, P. J., et al. 2014. Upper Washita River Experimental Watersheds: meteorologic and soil climate measurement networks. Journal of Environmental Quality 43(4): 1239-1249.

Starks, P. J., et al. 2014. Upper Washita River Experimental Watersheds: land cover data sets (1974–2007) for two southwestern Oklahoma agricultural watersheds. Journal of Environmental Quality 43(4): 1310-1318.

Stone, J. J., et al. 2008. Long-term runoff database, Walnut Gulch Experimental Watershed, Arizona, United States. Water Resources Research 44: 5.

Sullivan, D.G., Batten H. L., Bosch D., Sheridan J., and Strickland T. 2007. Little River Experimental Watershed, Tifton, Georgia, United States: A historical geographic database of conservation practice implementation. Water Resources Research 43(9).

Thierfelder, T. K., et al. 2003. Inferring the location of catchment characteristic soil moisture monitoring sites. Covariance structures in the temporal domain. Journal of hydrology 280(1): 13-32.

USDA-ARS Grazing Lands Research Laboratory, ARS Overview. Accessed on 26 June 2019. http://ars.mesonet.org/node/23.

USDA-ARS Southwest Watershed Research Center. Accessed on 26 June 2019. https://www.tucson.ars.ag.gov/swrc_site/research/wgew.

Wood, A. W. 2007. The effects of climate change on water supply forecasting in the Feather River basin. Preprints, Fourth Annual California Climate Change Conf., Sacramento, CA, California Energy Commission.

Table 1. Watershed area, number of precipitation (P) and soil moisture (SM) stations; watershed soil types, mean SSURGO database profile sand contents (standard deviation in parenthesis), and land uses/covers; water years considered in study; mean annual precipitation during study years; target forecast period; and mean seasonal streamflow (Q) during study years (minimum and maximum values in parentheses).

Watershed	State	Area	# P	# SM	Soil Types	Sand	Land Use/Cover	Water Years	Annual P	Forecast Period	Seasonal Q
		km^2				**%**			**mm**		**mm**
Walnut Gulch	AZ	149	88	2	clay loam, gravelly loam	67 (0)	shrubland, grassland	2009-2017	307	Sep-Dec	0.41
Fort Cobb	OK	786	13	13	sandy clay, sandy loam	43 (22)	cropland, pasture	2006-2018	750	Apr-Jul	31.3
Little Washita	OK	610	9	9	silty loam, fine sand	84 (4)	grassland, pasture	2007-2018	847	Feb-May	33.0
Little River	GA	334	14	14	sandy clay, loamy sand	49 (29)	woodland, cropland	2004-2015	1131	Jan-Apr	187

Table 2. Root mean square error (RMSE), coefficient of determination (R^2), bias, RMSE to observation standard deviation ratio (RSR), RSR performance rating, and number of retained principal components for baseline (ΣP) and two-step (ΣP + SM) PCR analyses at 0-, 1-, 2-, and 3-month lead times. Dashes indicate no forecast was made because no principal components were retained.

Watershed	Scenario	Lead Time months	SM period	RMSE mm	R^2 -	bias (min, max) mm	RSR -	RSR Performance Rating	# PCs
Walnut Gulch (AZ)	Baseline	0	-	-	-	-	-	-	0
		1	-	-	-	-	-	-	0
		2	-	-	-	-	-	-	0
		3	-	-	-	-	-	-	0
	Two-step	0	Jul-Aug (SM3)	0.30	0.73	0.00 (-0.37, 0.46)	0.49	Very good	1
		1	Oct 1- FD (SM8)	0.39	0.52	0.00 (-0.96, 0.51)	0.65	Satisfactory	1
		2	Oct 1- FD (SM8)	0.32	0.68	0.00 (-0.52, 0.46)	0.54	Good	1
		3	1-Jun (SM1)	0.42	0.46	0.00 (-0.71, 0.53)	0.69	Satisfactory	1
Fort Cobb (OK)	Baseline	0	-	18.2	0.27	2.56 (-45.6, 40)	0.82	Unsatisfactory	1
		1	-	-	-	-	-	-	0
		2	-	-	-	-	-	-	0
		3	-	-	-	-	-	-	0
	Two-step	0	Sep-Nov (SM7)	8.80	0.83	0.00 (-14.8, 15.1)	0.40	Very good	2
		1	Sep-Nov (SM7)	10.85	0.74	0.00 (-20.1, 19.2)	0.49	Very good	2
		2	Sep-Nov (SM7)	11.47	0.71	0.00 (-19.8, 20.8)	0.52	Good	2
		3	Sep-Nov (SM7)	15.52	0.47	0.00 (-32.0, 21.8)	0.70	Satisfactory	1
Little Washita (OK)	Baseline	0	-	-	-	-	-	-	0
		1	-	-	-	-	-	-	0
		2	-	-	-	-	-	-	0
		3	-	-	-	-	-	-	0
	Two-step	0	Dec-Jan (SM3)	16.0	0.67	0.00 (-34.8, 21.5)	0.55	Good	2
		1	Jul-Sep (SM7)	20.1	0.48	0.00 (-49.1, 35.4)	0.69	Satisfactory	1
		2	Jul-Sep (SM7)	21.7	0.39	0.00 (-53.2, 32.3)	0.75	Unsatisfactory	1
		3	Jul-Sep (SM7)	22.4	0.35	0.00 (-52.2, 28.2)	0.77	Unsatisfactory	1
Little River (GA)	Baseline	0	-	102	0.19	0.00 (-212, 113)	0.86	Unsatisfactory	1
		1	-	-	-	-	-	-	-
		2	-	-	-	-	-	-	-
		3	-	-	-	-	-	-	-
	Two-step	0	1-Jan (SM1)	41.0	0.87	0.00 (-95.6, 53.9)	0.35	Very good	2
		1	1-Dec (SM1)	57.51	0.74	0.00 (-91.3, 104)	0.49	Very good	2
		2	1-Nov (SM1)	83.11	0.46	0.00 (-98.7, 194)	0.70	Satisfactory	1
		3	1-Oct (SM1)	62.29	0.70	0.00 (-115, 145)	0.53	Good	2

Table 3. Soil moisture (SM) averaging periods tested at the 0-month lead time, months in each period, RMSE, R^2, bias, RSR, and number of retained principal components. Dashes indicate that no forecast could be made because no principal components were retained.

Watershed	SM period	Months	RMSE	R^2	bias (min, max)	RSR	# PCs
			(mm)	-	mm	-	
Walnut Gulch (AZ)	1	1-Sep	-	-	-	-	0
	2	Aug	0.34	0.65	0.00 (-0.55, 0.51)	0.56	1
	3	July-Aug	0.30	0.73	0.00 (-0.37, 0.46)	0.49	1
	4	June-Aug	-	-	-	-	0
	5	Mar-Aug	-	-	-	-	0
	6	Feb-Mar	-	-	-	-	0
	7	Feb-Apr	-	-	-	-	0
	8	Oct 1- FD	0.35	0.63	0.00 (-0.50, 0.69)	0.57	1
Fort Cobb (OK)	1	1-Apr	11.51	0.71	0.00 (-26.7, 12.7)	0.52	2
	2	Mar	13.42	0.60	0.00 (-26.7, 32.6)	0.61	1
	3	Feb-Mar	15.66	0.46	0.00 (-37.8, 34.9)	0.71	1
	4	Jan-Mar	14.98	0.51	0.00 (-35.2, 32.6)	0.68	1
	5	Oct-Mar	15.48	0.47	0.00 (-30.9, 32.4)	0.70	1
	6	Sep-Oct	14.92	0.51	0.00 (-35.5, 32.2)	0.67	1
	7	Sep-Nov	8.80	0.83	0.00 (-14.8, 15.1)	0.40	2
	8	Oct 1- FD	15.48	0.47	0.00 (-30.9, 32.4)	0.70	1
Little Washita (OK)	1	1-Feb	16.0	0.67	0.00 (-36.2, 24.5)	0.55	2
	2	Jan	-	-	-	-	0
	3	Dec-Jan	16.0	0.67	0.00 (-23.8, 32.4)	0.55	2
	4	Nov-Jan	22.3	0.36	0.00 (-35.9, 39.4)	0.77	1
	5	Aug-Jan	-	-	-	-	0
	6	July-Aug	21.2	0.42	0.00 (-48.6, 40.7)	0.73	1
	7	July-Sep	19.7	0.50	0.00 (-44.8, 39.6)	0.68	1
	8	Oct-FD	19.9	0.49	0.00 (-36.2, 27.8)	0.69	1
Little River (GA)	1	1-Jan	41.0	0.87	0.00 (-95.6, 53.9)	0.35	2
	2	Dec	80.8	0.49	0.00 (-201, 88.1)	0.68	1
	3	Nov-Dec	79.9	0.51	0.00 (-122, 120)	0.67	1
	4	Oct-Dec	75.5	0.56	0.00 (-139, 131)	0.64	1
	5	July-Dec	71.9	0.60	0.00 (-144, 100)	0.61	1
	6	June-July	69.1	0.63	0.00 (-152, 86.0)	0.58	1
	7	June-Aug	48.1	0.82	0.00 (-102, 58.4)	0.41	2
	8	Oct-FD	75.5	0.56	0.00 (-139, 131)	0.64	1

Table 4. Results of using soil moisture data from the first day of the forecast period in two-step simulations at all lead times. Columns show watershed name, lead time, RMSE, R^2, bias, RSR, and number of retained principal components. Dashes indicate that no forecast could be made because no principal components were retained.

Watershed	Lead Time	SM period	RMSE	R^2	RSR	bias (min, max)	# PCs
	(months)		(mm)	-	-	mm	
Walnut Gulch (AZ)	0	1-Sep	-	-	-	-	0
	1	1-Aug	-	-	-	-	0
	2	1-Jul	-	-	-	-	0
	3	1-Jun	0.42	0.46	0.69	0.00 (-0.71, 0.53)	1
Fort Cobb (OK)	0	1-Apr	11.51	0.71	0.52	0.00 (-26.7, 12.7)	2
	1	1-Mar	13.78	0.58	0.62	0.00 (-34.9, 18.0)	2
	2	1-Feb	15.99	0.44	0.72	0.00 (-31.1, 26.5)	1
	3	1-Jan	-	-	-	-	0
Little Washita (OK)	0	1-Feb	16.0	0.67	0.55	0.00 (-36.2, 24.5)	2
	1	1-Jan	22.6	0.34	0.78	0.00 (-34.1, 36.4)	1
	2	1-Dec	22.7	0.33	0.78	0.00 (-46.5, 24.2)	1
	3	1-Nov	22.6	0.34	0.78	0.00 (-55.3, 23.7)	1
Little River (GA)	0	1-Jan	41.00	0.87	0.35	0.00 (-95.6, 53.9)	2
	1	1-Dec	57.51	0.74	0.49	0.00 (-91.3, 104)	2
	2	1-Nov	83.11	0.46	0.70	0.00 (-98.7, 194)	1
	3	1-Oct	62.29	0.70	0.53	0.00 (-115, 145)	2

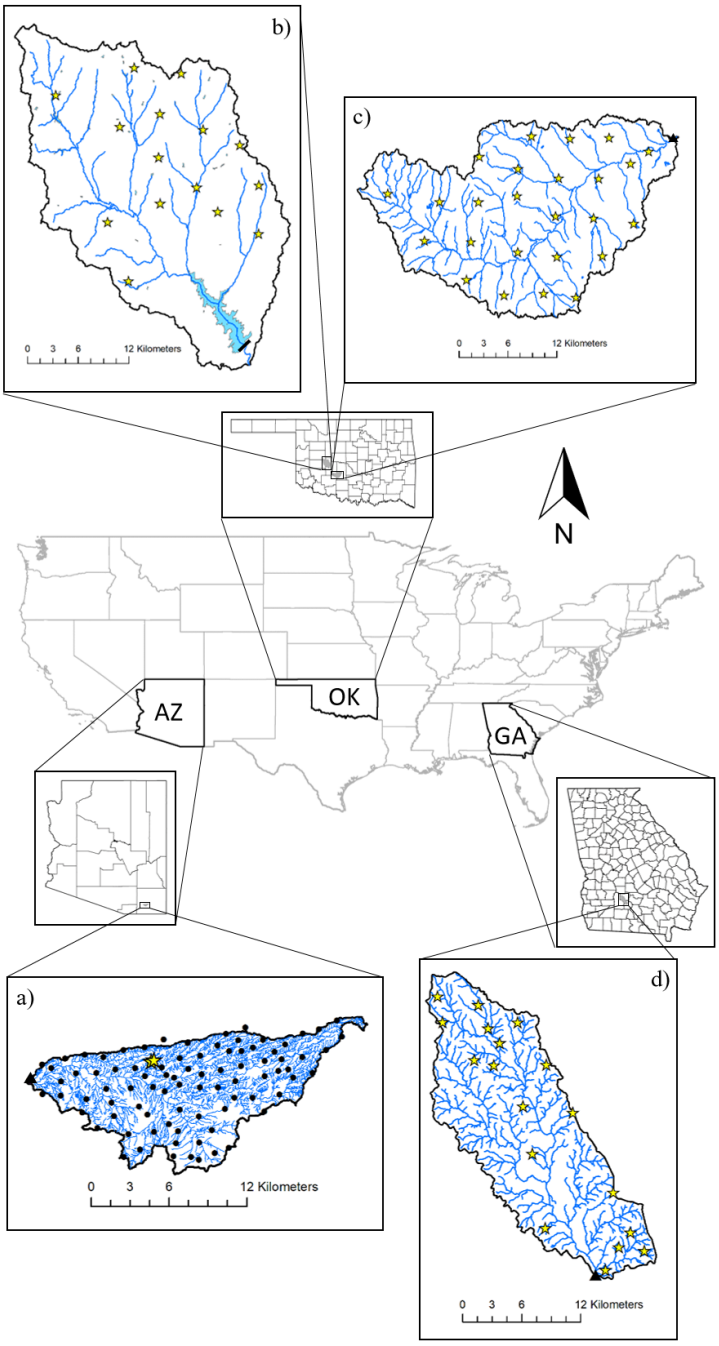

Figure 1. The Walnut Gulch (a) watershed in Arizona (AZ-WG), Fort Cobb (b) and Little Washita (c) watersheds in Oklahoma (FC-OK and LW-OK), and the Little River watershed in Georgia (d) (LR-GA). Yellow stars represent the locations of co-located precipitation and soil moisture monitoring stations, except for in the Walnut Gulch watershed, where yellow stars indicate the location of soil moisture monitoring stations and black circles indicate the location of precipitation stations. Streamflow gauges are indicated by black triangles in all watersheds, except at Fort Cobb where no stream gauge data were used and where the Fort Cobb Dam is marked by a black bar.

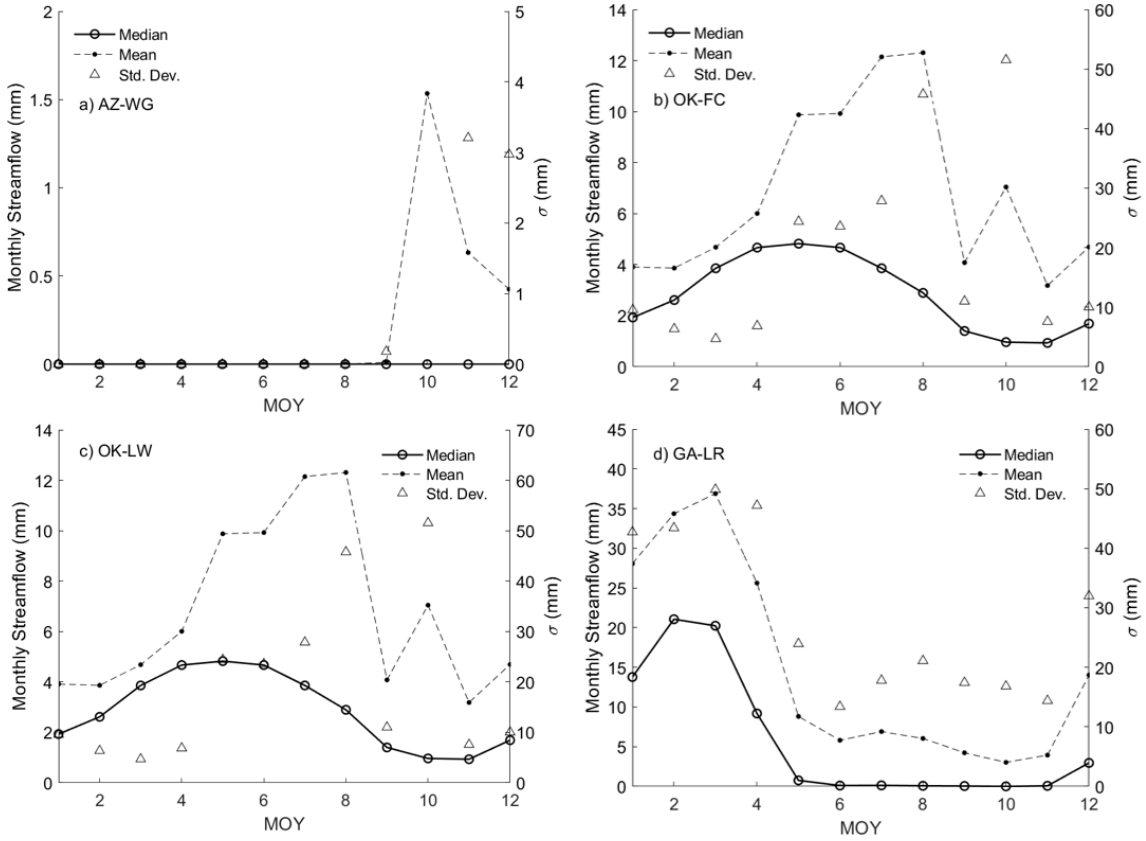

Figure 2. Mean and median monthly streamflow (Q) and the standard deviation of monthly streamflow values for AZ-WG (a), OK-FC (b), OK-LW (c), and GA-LR (d) for water years 2009-2017, 1994-2018, 1992-2018, and 1971-2015, respectively.

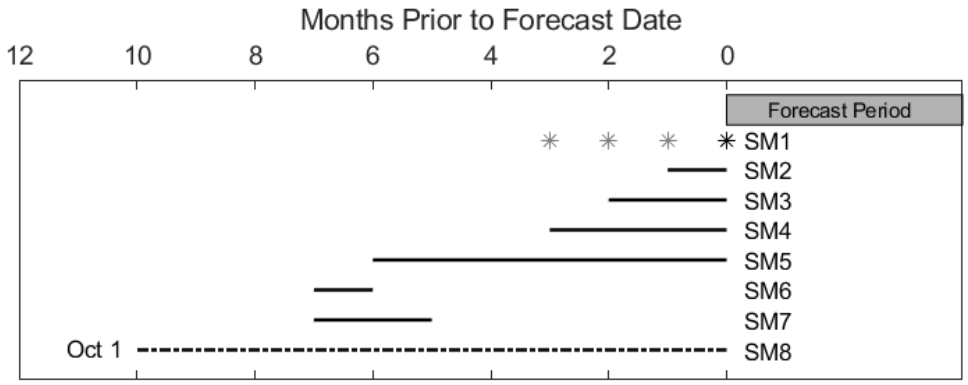

Figure 3. Soil moisture averaging time periods (black lines) and their position relative to the beginning of the forecast period for each watershed. Specific soil moisture averaging periods for each watershed/lead time combination are given in Table 2. The black star shown for SM1 indicates that the averaging period is the day of the forecast date for the 0-month lead time. Gray stars at SM1 indicate that the averaging period is the day of the forecast date at 1-, 2-, and 3-month lead times (results shown in Table 4). The dotted line shown for SM8 indicates that the total number of months considered in that averaging period varies between watersheds due to differing target forecast periods.

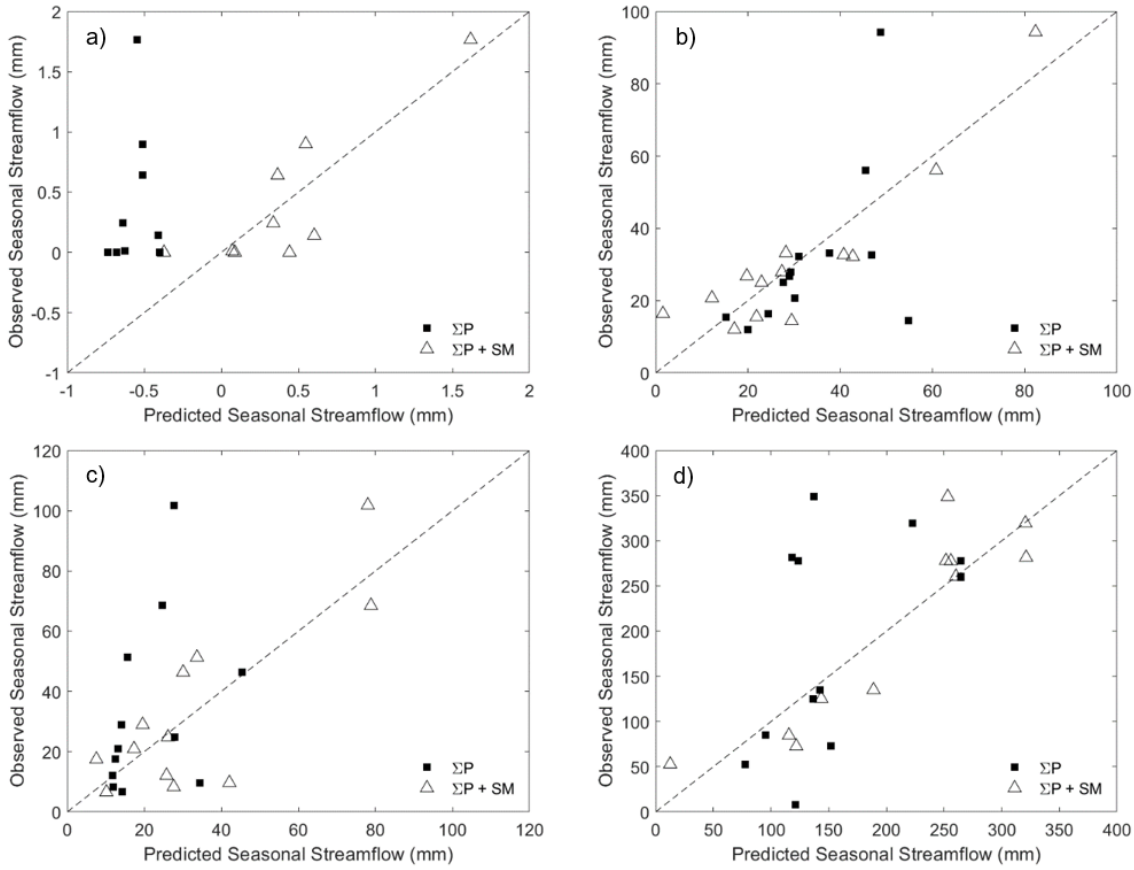

Figure 4. Observed and predicted seasonal streamflow volumes for baseline (black squares) and two-step (triangles) forecasts in the AZ-WG (a), OK-FC (b), OK-LW (c), and GA-LR (d) watersheds at the 0-month lead time. Dashed line is 1:1 line. Baseline forecasts were based only on cumulative precipitation prior to the forecast date (ΣP), whereas two-step forecasts included both ΣP and soil moisture (SM) information. Baseline forecasts for the AZ-WG and GA-LR watersheds did not meet the criteria for statistical validity, but baseline streamflow predictions are shown here to demonstrate improvements due to soil moisture data inclusion.

CHAPTER IV

INTEGRATING GROUND-BASED METEOROLOGICAL DATA AND REMOTELY-SENSED VEGETATION INDEX DATA TO ESTIMATE ROOT ZONE SOIL MOISTURE ACROSS DIVERSE VEGETATION TYPES

Briana M. Wyatt, Tyson E. Ochsner, and Chris B. Zou

ABSTRACT

Many soil moisture networks monitor only one land cover type, typically grassland, and the availability of in-situ soil moisture data in other land cover types is severely limited. Thus, spatial patterns and temporal dynamics of soil moisture in regions with heterogeneous land cover types remain poorly understood. The objective of this research was to determine how effectively root-zone soil moisture, represented as plant available water (PAW), can be estimated for diverse land cover types using a water balance model driven by high-resolution, remotely-sensed vegetation indices (VI) data and in-situ meteorological data. This was done by using VI data as a proxy for the basal crop coefficient, which is used to scale estimates of potential evapotranspiration within a simple water balance method. Plant available water dynamics under four different vegetation types were estimated relatively well using enhanced

vegetation index (EVI) data and normalized difference vegetation index (NDVI) data as proxies for the basal crop coefficient. Values of the correlation coefficients (r) between measured and modeled PAW ranged from 0.61 to 0.99 across four sites. Simulations were most accurate at the tallgrass prairie location, with mean absolute error (MAE) values of <40 mm. However, improved accuracy is needed for the remaining sites, where MAE values exceeded 55 mm in all cases. Our results provide preliminary evidence that the integration of remote sensing VI data may be usefully applied to estimate the soil moisture status under diverse unmonitored vegetation types.

INTRODUCTION

Soil moisture is an essential climate variable affecting near-surface temperature, hydrological processes, agricultural production, and the health of ecological systems (Ochsner et al. 2013; Wagner et al. 2007; Wagner et al., 2012). Soil moisture data from in-situ monitoring networks have been used to estimate deep drainage (Zhang et al., 2019; Wyatt et al., 2017), improve streamflow forecasts (Harpold et al., 2017), and improve agronomic decision making (Lollato et al., 2016). However, the majority of soil moisture data currently available from in-situ monitoring networks reflect conditions only under a single land cover type, typically grassland, and soil water conditions under other nearby land cover types, such as croplands or forests, may differ significantly from these measured values (Patrignani and Ochsner, 2018).

Unlike in-situ data, remotely sensed soil moisture products from satellites can provide global data which capture spatial and temporal variations in soil moisture across numerous vegetation types, but these data typically suffer from several limitations, including a shallow sensing depth (~5 cm), relatively coarse spatial resolution, and a limited ability to sense soil moisture under dense vegetation types such as forests (Mohanty et al. 2017; Peng et al. 2017; Kerr et al. 2001). The most accurate satellite soil moisture products are based on radiometers, which have footprints of >30 km (Entekhabi et al. 2010). Because vegetation types are often intermixed at smaller scales (< 1 km), variations in soil moisture caused by contrasting land cover types are not adequately captured by current remote-sensing soil moisture products.

A growing body of research shows the potential of higher resolution, remotely-sensed vegetation index (VI) data, such as those from NASA's Moderate Resolution

Imaging Spectroradiometer (MODIS) sensors, to close this gap in spatial scale and provide new insights into the effects of land cover type on soil moisture. The concept of using remotely-sensed VI data in mechanistic water and surface energy balance models has been frequently discussed in the literature (Hendrickx et al. 2016; Glenn et al. 2011; Glenn et al. 2010; Gonzalez-Dugo et al. 2009; Glenn et al. 2007), but the majority of land surface models were not designed to incorporate these data. Incorporating new data types into existing mechanistic models may not improve model results (Ford and Quiring 2013), and may actually decrease model performance due to overfitting issues (Transtrum and Qiu 2016). Land surface models which are capable of integrating VI data, such as those within the North American Land Data Assimilation System (NLDAS), have a crude conceptual representation of soil characteristics, allow only monthly VI inputs, and have a maximum resolution of ~1 km (Mitchell et al. 2004; Kumar et al. 2006).

The current research seeks to overcome these limitations by integrating meteorological data measured on the ground and remote sensing VI data into a simple water balance model based on the FAO-56 dual crop coefficient method (Allen et al., 1998) and comparing model-estimated plant available water (PAW) values to measured PAW at four in-situ monitoring locations under diverse land cover types. The goals of this research are: 1) to determine the effectiveness of using normalized difference vegetation index (NDVI) and enhanced vegetation index (EVI) data as proxies for the basal crop coefficient in the water balance simulations, 2) to discover which vegetation index leads to the most accurate plant available water estimates, and 3) to quantify differences in soil water dynamics due to differences in vegetation type.

MATERIALS AND METHODS

Monitoring Stations

Four locations throughout Oklahoma, each with a different dominant vegetation type, were chosen for modeling and as independent soil moisture monitoring locations to be used for model validation (Figure 1). Vegetation types at these sites include a mixed hardwood forest, a loblolly pine (*Pinus taeda*) plantation, rainfed (non-irrigated) cropland, and tallgrass prairie. In 2018, according to 500-m MODIS Land Cover Type 2 data, these locations were classified as grassland, needleleaf evergreen forest, cropland, and grassland, respectively. The misclassification of the mixed hardwood forest as grassland is likely a result of the small area of the forested site ($<500^2$ m^2), which is surrounded by grasslands and croplands (Figure 2).

At each monitoring location, arrays of soil moisture sensors (CS-655, Campbell Scientific, Inc., Logan, Utah) were installed in triplicate to monitor soil water storage in the profile. At the mixed hardwood forest, loblolly pine plantation, and cropland locations soil moisture sensors were installed in three profiles at depths of 5, 25, 60, and 100 cm. At these sites, sensor profiles were installed 6.1 m away from a central datalogger along headings separated by ~120° (Figure 3). This was done in order to maximize the distance between sensor profiles to reduce intercorrelation between soil moisture measurements. Soil cores were taken at the time of installation in each profile and at each depth (3 profiles per site X 4 depths per profile = 12 cores per site).

At the tallgrass prairie location, CS-655 soil moisture sensors installed for a previous project were used. Sensors were installed in triplicate at this location as well, but farther apart than at the other three monitoring locations (mean of 449 m apart, Figure 4).

At each tallgrass prairie monitoring profile, sensors were installed at 5, 10, 20, and 50 cm below the surface. As at the other sites, soil cores were collected from all soil profiles at the time of sensor installation and analyzed to estimate the soil volumetric water content at field capacity (-10 kPa, θ_{-10}) [$m^3\ m^{-3}$], water content at wilting point (-1500 kPa, θ_{-1500}) [$m^3\ m^{-3}$], bulk density [$g\ cm^{-3}$], and fractions of sand, silt, and clay.

Measurements of soil apparent dielectric permittivity (K_a) [-], and electrical conductivity (EC) [$dS\ m^{-1}$] were collected either every hour (tallgrass prairie sites) or half hour (all other sites) using the CS-655 sensors. Sensors were calibrated using Coyle-Lucien complex soil taken from a location near the tallgrass prairie site in 2013. The calibration equation used was

$$\theta = 0.107\sqrt{K_a} - 0.119\sqrt{EC} - 0.105 \quad (1)$$

where θ is the volumetric soil water content [$m^3\ m^{-3}$] (T. Ochsner, personal communication, December 2019). Using the volumetric water content values resulting from Equation 1 and site-specific soil hydraulic properties at each of these locations, we calculated mean (i.e., mean of three sensor profiles) daily plant available water (PAW) for all available dates. PAW values at these sites and at Oklahoma Mesonet stations were calculated by assuming soil moisture sensors were located at the center of a given soil layer (i.e., the data recorded by the sensor at 5 cm is representative of the condition of the layer from 0-10 cm, etc.), multiplying the reported volumetric water content by the thickness of that soil layer, and summing the totals for each layer. Due to datalogger storage limitations and remote site connectivity problems, portions of measured data are missing after the installation date at each site. Station installation dates are shown in Table 1.

Soil water balance model

The dual crop coefficient form of the FAO-56 method is a well-known empirical method used to estimate soil evaporation and crop transpiration (together, ET_c) using meteorological data and tabular crop coefficients (Allen et al., 1998). Inputs for the model include daily estimates of reference evapotranspiration (ET_o), which are calculated from measured wind speed, temperature, rainfall, incoming solar radiation, and relative humidity data; a basal crop coefficient (K_{cb}) curve which describes the daily ratio of the actual evapotranspiration to the reference evapotranspiration throughout the simulation period; plant height and rooting depth curves; soil sand and clay percentages, field capacity, and wilting point values; the fraction of soil covered by residue; and the soil moisture content at the beginning of the simulation. Daily ET_o values are calculated using the Penman-Monteith method as described in the FAO-56 procedure. A water stress coefficient (K_s), which reduces vegetation transpiration when the amount of available soil water drops below a defined threshold, and a soil evaporation coefficient (K_e), which reduces soil evaporation when the water content of the surface soil decreases, are calculated daily based on the estimated available soil water storage. Along with the K_{cb} values, the estimated K_s and K_e values are used to scale ET_o according to

$$ET_{c\_adj} = (K_s * K_{cb} + K_e)\, ET_0 \quad (2)$$

where ET_{c_adj} is the crop evapotranspiration, adjusted for soil water stress conditions (Allen et al., 1998).

ET_{c_adj} values are calculated as part of the daily water balance:

$$P = DP + RO + ET_{c\_adj} + D_r \quad (3)$$

where P is precipitation, DP is deep percolation, RO is surface runoff, and D_r is root zone depletion (i.e., change in root zone water storage) (Allen et al., 1998). Deep percolation is non-zero only on days when the soil water content exceeds field capacity and is estimated by

$$DP = P - RO - ET_{c_{adj}} - D_r \quad (4)$$

while D_r is estimated by

$$D_r = D_{r_{i-1}} - (P - RO) + ET_{c_{adj}} + DP \quad (5)$$

where $D_{r_{i-1}}$ is root zone depletion from the previous day. Additional calculations within the model include the estimation of the total available soil water (TAW), which is estimated by

$$TAW = (\theta_{-10} - \theta_{-1500}) * Z_r \quad (6)$$

where Z_r is the rooting depth [mm]. Finally, daily PAW values are estimated as

$$PAW = TAW - D_r \quad (7)$$

Irrigation inputs were not considered here because all of the study locations are rainfed. Additionally, for the sake of simplicity, surface runoff was assumed to be negligible for these nearly-level sites. It would be possible to estimate surface runoff using the NRCS curve number method and to incorporate those estimates into the model, but this was not done for the current study. Based on measured daily precipitation values as well as the hydrologic soil groups and estimated curve numbers of the study locations, surface runoff likely occurred on 0.5% of days at the mixed hardwood forest site, on 1.0% of days at the loblolly pine plantation, on 4.3% of days at the cropland, and on 3.9% of days at the tallgrass prairie site during the study period.

The FAO-56 method was developed for and has been traditionally applied in agricultural cropping systems, but the method has shown potential to estimate vegetation water use and soil water dynamics under diverse land covers types by using remote sensing vegetation indices data as a proxy for K_{cb} (Sanchez et al., 2010). Here, we applied the method at four locations in Oklahoma with diverse vegetation types for the period from January 2000-August 2019. Normalized difference vegetation index (NDVI) and enhanced vegetation index (EVI) data from the MODIS instruments aboard NASA's Aqua and Terra satellites and meteorological data from the Oklahoma Mesonet were used as the primary model inputs (Figure 1) (Huete et al., 1999; McPherson et al., 2007).

Geographical and Meteorological Inputs

Geographical inputs necessary for the model include site UTM coordinates, elevation, and longitude and latitude, which are used to adjust the psychrometric constant and incoming solar radiation by location. Precipitation records for each monitoring station are also required, as are daily estimates of reference evapotranspiration (ET_o). Estimates of ET_o were produced using daily data from the Oklahoma Mesonet station nearest each independent soil moisture location. Any missing records were filled using data from the next nearest Oklahoma Mesonet station (McPherson et al., 2007). If no data were available from the nearest station, remaining missing records were filled in using a linear interpolation. The distance between the Mesonet stations and the monitoring locations ranged from 0.13 km to 23.1 km (Figure 2, Figures 4-7, Table 1). The effects of non-reference (i.e., non-irrigated) ground cover on ET_o estimates were accounted for using daily dew point temperature and relative humidity data according to the method

described by Allen (1996). Dew point temperatures were calculated from daily temperature and relative humidity data as follows:

$$e_{sat} = 6.1365 * e^{\left(\frac{17.502*T_{min}}{240.97+T_{min}}\right)} \quad (8)$$

$$e = \left(\frac{RH}{100}\right) e_{sat} \quad (9)$$

$$T_{dew} = 240.97 * \log\left(\frac{\frac{e}{6.1365}}{17.502-\ln\left(\frac{e}{6.1365}\right)}\right) \quad (10)$$

where e_{sat} is the saturation vapor pressure [mb] at the minimum daily temperature, e is the actual vapor pressure [mb], T_{min} is the minimum daily temperature [°C], and RH is the relative humidity (Buck, 1981; Allen et al., 1998). This correction was made for days when the minimum observed air temperature was >2°C above the calculated dew point temperature, and the resulting dew point temperatures and relative humidity data were used to calculate adjusted daily maximum and minimum temperature values for use in the ET_o calculations according to the procedure described by Allen (1996). These corrections were necessary on 27% of days across all sites and resulted in a 2.7% decrease in ET_o, on average.

In addition to corrections for non-reference ground cover, precipitation records used in calculating ET_o at the forested sites were adjusted to account for canopy and understory interception, assuming 2 mm of interception lost at the onset of every precipitation event. This interception value is similar to that found by Zou et al. (2015), who reported canopy interception rates of 2.14-3.44 mm in eastern redcedar (*Juniperus virginiana*) woodlands. This adjustment was necessary because all precipitation data were collected at the nearest Mesonet station (i.e., outside the forested area) and are not necessarily representative of the precipitation experienced at the ground surface under the

forest canopy. This adjustment led to a decrease in total precipitation during the simulation period of 2782 mm (~141 mm yr^{-1}) at the mixed hardwood forest site and 3094 mm (~157 mm yr^{-1}) at the pine plantation site. While there may also be significant interception at the tallgrass prairie location during certain times of the year (Zou et al., 2015), due to the dynamic nature of the above ground vegetation, those effects were not considered here.

Remote Sensing Inputs

MODIS NDVI and EVI imagery at a 250-m resolution and 16-day return period were used here (MOD13Q1 and MYD13Q1 products). Because these images are available from either the Aqua or Terra satellite at 16-day intervals and because the satellite's return intervals are offset from one another by 8 days, a complete image is available every 8 days. EVI and NDVI are calculated as (Huete et al., 2008):

$$EVI = G\left(\frac{\rho_{NIR} - \rho_{red}}{\rho_{NIR} + C_1 * \rho_{red} - C_2 * \rho_{blue} + L}\right) \quad (11)$$

$$NDVI = \frac{(\rho_{NIR} - \rho_{red})}{(\rho_{NIR} + \rho_{red})} \quad (12)$$

where ρ are corrected or partially atmosphere-corrected surface reflectances of the near infrared (ρ_{NIR}), red (ρ_{red}), and blue (ρ_{blue}) bands, L is the canopy background adjustment that addresses NIR and red radiant transfer through a canopy, and C_1, C_2 are the coefficients of the aerosol resistance term, which uses the blue band to correct for aerosol influences in the red band (Huete et al., 2002). The coefficients adopted in the EVI algorithm are, L = 1, C_1 = 6, C_2 = 7.5, and G (gain factor) = 2.5 (Huete et al., 1994; Huete et al., 1997).

There is some evidence that EVI may be more suitable than NDVI for the current application for a number of reasons, including that EVI images are less likely to saturate when considering dense canopies due to the addition of the blue reflectance band (Gao et al., 2000). Additionally, EVI is designed to separate the background signal of the soil from that of the plant canopy, EVI is more responsive than NDVI to vegetation structural variations, and EVI data have been shown to be more highly correlated with ET than NDVI data (Gao et al., 2000; Wang et al., 2007).

All remote sensing data were downloaded using a custom script in the JavaScript API within the Google Earth Engine (GEE) Code Editor (Gorelick et al., 2017). This script defined a bounding rectangle around each monitoring station which contained only the dominant vegetation type based on Google Earth aerial imagery. Mean VI values for each area were calculated for each 16-day composite image, and a time series of VI values for each location was saved in a text file. After download, VI data were processed using a custom MATLAB script.

Raw EVI values were converted to K_{cb} values using two different approaches. The first was defined by:

$$K_{cb-EVI_1} = \frac{EVI - EVI_{min}}{EVI_{max} - EVI_{min}} \quad (13)$$

following the method described by Choudhury et al. (1994) and Glenn et al. (2010), where EVI is the mean observed EVI value of the defined area for each image, EVI_{min} is the minimum EVI for a given location during the study period, and EVI_{max} is the maximum EVI value for a given location during the study period. Additionally, a secondary EVI normalization was tested:

$$K_{cb-EVI_2} = \frac{EVI}{EVI_{max} - EVI_{min}} \quad (14)$$

This normalization is similar to the first, but differs in that it allows for $K_{cb\text{-}EVI_2}$ values greater than one, which is often observed in the original FAO-56 approach.

Similarly, K_{cb} values were calculated using NDVI data according to

$$K_{cb-NDVI} = 1.36NDVI - 0.03 \quad (15)$$

as described by Bausch and Neale (1987). Following the calculation of $K_{cb\text{-}EVI_1}$, $K_{cb\text{-}EVI_2}$, and $K_{cb\text{-}NDVI}$ at 8-day intervals, values were interpolated linearly between image dates to produce daily K_{cb} values for the simulation period similar to the method used by Sanchez et al. (2010) and Sanchez et al. (2012a).

Vegetation Characteristic Inputs

In addition to the data described above, the model requires the input of daily vegetation height and rooting depth data. Vegetation heights for the mixed hardwood forest site were assumed to be static and to be equal to 10.0 m, which lies within the range of tree heights in the cross timbers of Oklahoma reported by Oklahoma Forestry Services (2010). A mean tree height of 9.4 m was reported for the pine plantation location used in this study by Dipesh et al. (2014) and was used here, also assuming a static vegetation height. Dynamic daily vegetation heights for the tallgrass prairie site were estimated using crop growth curves and maximum vegetation heights for pasture reported by Allen et al. (1998). Dynamic daily vegetation heights for the cropland site were estimated by multiplying daily K_{cb} values by 2.0 m, the vegetation height for field corn reported by Allen et al. (1998). This method allowed the vegetation height to vary according to vegetation greenness rather than according to a defined growth curve, which was necessary due to the varying crop rotations implemented at the site and due to the

lack of crop type data in many years. The same method was used at the tallgrass prairie site, using a maximum plant height of 1.0 m based on observations at the field site.

Rooting depths for the two forested locations and for the cropland site were set equal to 1.2 m, the effective soil depth to which soil moisture content is measured by the installed sensors. The rooting depth used for the tallgrass prairie site was set to 0.65 m to match the soil moisture measurement depths at that location. The true rooting depth at the tallgrass prairie site is likely limited by the soil depth, which is < 30 cm in some places and commonly < 1.0 m. Vegetation height and rooting depth parameters for each site are given in Table 2.

Soil Property Inputs

Information regarding the soil properties of the modeled area is also required, including the depth of soil from which evaporation may occur (Z_e), θ_{-10} at the surface and for the full soil profile, θ_{-1500} at the surface and for the full soil profile, and soil volumetric water content on the first date of simulation. Z_e was calculated for each location based on the sand content of the surface soil as described in Allen et al. (1998) (Table 2). All of the necessary soil properties were estimated from soil cores taken at each monitoring site, and mean soil properties of the uppermost soil samples (5-cm depth) were used to represent the soil surface properties in the model.

Mean depth-weighted soil properties (i.e., mean values of the triplicate profiles' soil properties) were used to represent the soil physical properties of the full soil profile at each site within the model (Table 2). At the mixed hardwood forest, loblolly pine plantation, and cropland sites these depth-weighted properties were calculated by assuming that each soil moisture sensor was located at the center of a given soil layer

(i.e., the data recorded by the sensor at 5 cm is representative of the condition of the layer from 0-10 cm, etc.). At the tallgrass prairie site, due to the sensor installation depths, a trapezoidal integration was used to estimate profile soil properties to a depth of 65 cm. Soil moisture values on the first day of simulation were assumed to be the same as those at the nearest Oklahoma Mesonet station, or to be halfway between the depth-weighted θ_{-10} and θ_{-1500} values if no Mesonet data were available.

RESULTS AND DISCUSSION

ET_o estimates

Mean annual ET_o values at each location for the full simulation period are given in Table 3 and range from 1209 mm yr^{-1} in the loblolly pine plantation to 1412 mm yr^{-1} at the cropland site. Daily ET_o estimates ranged from 0.24 to 12.0 mm d^{-1} at the mixed hardwood forest location, from 0.29 to 9.55 mm d^{-1} at the loblolly pine plantation location, from 0.30 to 12.3 mm d^{-1} at the cropland location, and from 0.26 to 10.8 mm d^{-1} at the tallgrass prairie location. Smoothed mean daily ET_o values for each day of the year during the study period are shown in Figure 8. Mean daily ET_o peaked on the 192nd day of the year (July 10 or 11) in the loblolly pine plantation and peaked slightly later on the 201st day of the year (July 19 or 20) at the mixed hardwood forest, tallgrass prairie, and cropland sites.

Annual ET_o values found for the study sites are similar to those reported by prior studies. The mean annual ET_o value of 1209 mm yr^{-1} found at the loblolly pine plantation is higher than those reported in a prior study in southeastern Oklahoma, which reported ET_o values of ~900-1000 mm yr^{-1} (Hennessey et al., 2004). The ET_o values of 1341 mm

yr^{-1} estimated for the tallgrass prairie site and 1390 mm yr^{-1} for the hardwood forest site are significantly lower than the value of 1785 mm yr^{-1} reported by a study conducted in the same county as both stations (Wine and Hendrickx, 2013). The mean annual ET_o value of 1412 mm yr^{-1} estimated for cropland our study location is higher than the range of growing season (sum of fall, winter, and spring seasons) ET_o values of 728-959 mm reported by Lollato et al. (2018) for the same location, though the lack of ET_o values from Lollato et al. (2018) during the summer months may contribute significantly to this discrepancy.

K_{cb} curves

$K_{cb\text{-}EVI_1}$ values during the study period ranged from 0.0-1.0 for all vegetation types, by definition. $K_{cb\text{-}EVI_2}$ values ranged from 0.09 to 1.09 for mixed hardwood forest, 0.11 to 1.11 for the loblolly pine plantation, 0.0 to 0.99 for cropland, and 0.17 to 1.17 for tallgrass prairie. $K_{cb\text{-}NDVI}$ values ranged from 0.06 to 1.07 at the mixed hardwood forest, from 0.09 to 1.19 at the loblolly pine plantation, from 0.0 to 1.14 in the cropland, and from 0.16 to 1.07 at the tallgrass prairie. Mean daily K_{cb} values, as well as maximum and minimum K_{cb} values for each day of the year, are shown in Figure 9.

While K_{cb} trends in the two EVI-derived curves are similar, there are some notable differences between these curves and those derived from NDVI data. The loblolly pine plantation K_{cb} values are greater than all other K_{cb} values during the majority of the year in the NDVI-derived K_{cb} curve. This differs from the EVI-derived curves, where the loblolly pine plantation K_{cb} values were generally lower than those of the other vegetation types. Secondly, the shapes of the NDVI-derived curves for mixed hardwood

forest, loblolly pine plantation, and tallgrass prairie are different than those of the EVI-derived curves, with a plateau-like pattern during the late spring and summer rather than a brief peak followed by a slow decline like that of the EVI-derived curves.

There are also some notable similarities between the curves. Each of the three curve types show approximately the same rate and magnitude of K_{cb} increase at the onset of the growing season and each has approximately the same magnitude of change in K_{cb} throughout the year. Additionally, the cropland curves for all three K_{cb} estimation methods are remarkably similar, unlike the curves of the other three vegetation types. The mean cropland K_{cb} curve shows little change throughout the calendar year, with small peaks near day 100, day 175, and day 320 in all K_{cb} curves. The relatively constant cropland mean K_{cb} values and multiple small peaks throughout the year in Figure 9 are likely due to the production of crops with different peak growth periods during different years of the study period (e.g., winter wheat versus sorghum).

An example of different seasonal K_{cb} curves for cool season (winter wheat) and warm season (sorghum) crops is shown in Figure 10. This figure shows the different peaks in K_{cb} values between crop types, with peak K_{cb} values for winter wheat occurring in late April and early May in all instances and peak K_{cb} values in early July for sorghum. In both crops, K_{cb} dynamics are similar regardless of the vegetation index data used, with the exception of a second peak in K_{cb} in mid-August for sorghum when considering $K_{cb\text{-}NDVI}$. The magnitude of K_{cb} values is higher for the $K_{cb\text{-}NDVI}$ curves than for the EVI-derived curves, likely as a result of the use of an empirical K_{cb} estimation equation rather than a normalization.

The K_{cb} curves for the study locations are similar to those in prior studies which estimated the basal crop coefficient using VI data. Sanchez et al. (2012a) also used Equation 15 to estimate K_{cb}, and reported values ranging from near zero to ~0.75 for barley cropland during a single growing season. In general, the K_{cb} values found here are slightly higher than those reported by Sanchez et al. (2012a). The minimum K_{cb} value at the cropland site was rarely near zero (Figure 9), and the range of maximum cropland K_{cb} values (0.99 -1.14) found here is slightly higher that found by Sanchez et al. (2012a). The same study reported K_{cb} values ranging from zero to ~0.5 for grassland, which is much lower than the maximum value of >1.0 found in this current study. However, it is important to note that Sanchez et al. (2012a) considered only one growing season, while the current study considers nearly 20 years of VI data. Campos et al. (2017) used the soil adjusted vegetation index (SAVI) to estimate K_{cb} for a site under maize and soybean rotation and found that K_{cb} reached a maximum value of 0.95 under maize and 0.90 under soybean. These values are more comparable to the maximum K_{cb} values found for the cropland site (Figure 9).

The dual crop coefficient method has been most commonly applied to cropland and grassland locations, and to our knowledge, no comparable studies have been carried out in forested ecosystems that would allow for a comparison of K_{cb} curves at the mixed hardwood forest and loblolly pine plantation sites. However, Allen et al. (1998) suggests a year-round K_{cb} value of 1.0 for conifer trees, which is comparable to the maximum K_{cb} values found at the loblolly pine plantation site using the current K_{cb} estimation methods. Additionally, Figure 9 suggests that even for evergreen species the K_{cb} value is not

constant and fluctuates seasonally, which could lead to incorrect estimates of ET_{c_adj} when using a constant K_{cb} value.

ET_{c_adj} estimates

Smoothed mean daily ET_{c_adj} curves for the study period are shown in Figure 11. Annual ET_{c_adj} values estimated using $K_{cb\text{-}EVI_1}$ ranged from 1114 to 1438 mm yr^{-1} for the mixed hardwood forest site; from 590 to 1166 mm yr^{-1} for the loblolly pine plantation site; from 495 to 1028 mm yr^{-1} for the cropland site; and from 563 to 893 mm yr^{-1} for the tallgrass prairie site. Annual ET_{c_adj} values estimated using $K_{cb\text{-}EVI_2}$ ranged from 1048 to 1318 mm yr^{-1} for the mixed hardwood forest site; from 584 to 1193 mm yr^{-1} for the loblolly pine plantation site; from 592 to 1020 mm yr^{-1} for the cropland site; and from 570 to 928 mm yr^{-1} for the tallgrass prairie site. Annual ET_{c_adj} values estimated using $K_{cb\text{-}NDVI}$ ranged from 960 to 1233 mm yr^{-1} for the mixed hardwood forest site; from 565 to 1205 mm yr^{-1} for the loblolly pine plantation site; from 491 to 998 mm yr^{-1} for the cropland site; and from 571 to 941 mm yr^{-1} for the tallgrass prairie site.

Mean estimated annual ET_{c_adj} ranged from 740 mm yr^{-1} in the tallgrass prairie to 1198 mm yr^{-1} in the mixed hardwood forest using $K_{cb\text{-}EVI_1}$; from 753 mm yr^{-1} in the tallgrass prairie to 1115 mm yr^{-1} in the mixed hardwood forest using $K_{cb\text{-}EVI_2}$; and from 756 mm yr^{-1} in the tallgrass prairie to 1037 mm yr^{-1} in the mixed hardwood forest using $K_{cb\text{-}NDVI}$ (Table 3). ET_{c_adj} values were greatest using $K_{cb\text{-}EVI_1}$, followed by $K_{cb\text{-}EVI_2}$, then $K_{cb\text{-}NDVI}$. The greatest mean annual ET_{c_adj} across all K_{cb} estimation methods was found for the mixed hardwood forest location, which is likely due to the higher K_{cb} values at this location (Figure 9). The lowest ET_{c_adj} values across all K_{cb} estimation methods were

found at the tallgrass prairie location, which may be because the specified rooting depth for the tallgrass prairie site was the shallowest among all the study locations (Table 2).

Current estimates of ET_{c_adj} compare relatively well with prior estimates of evapotranspiration (ET) in Oklahoma across vegetation types, with the exception of the hardwood forest site, which has unrealistically high ET_{c_adj} values that require further investigation. Prior work has estimated annual ET in Oklahoma grasslands ranging from to 640-810 mm yr^{-1} (Burba and Verma, 2005). The current mean annual ET_{c_adj} values (740 mm yr^{-1} to 756 mm yr^{-1}) fall within the range of these prior estimates. Additionally, the mean ET_{c_adj} value of 750 mm yr^{-1} is very similar to that reported by Sun et al. (2018), who measured a single-year ET value of 728 mm using an eddy covariance system installed nearby the independent tallgrass prairie monitoring site.

Wagle et al. (2019) reported seasonal ET values ranging from 652-734 mm and a single-year total ET value of ~900 mm for a non-irrigated alfalfa field in central Oklahoma. These values are fairly similar to the mean annual ET_{c_adj} values found at the cropland site, which ranged from 787 mm yr^{-1} to 796 mm yr^{-1} (Table 3). Additionally, similar ET rates were found under agricultural land in central Oklahoma by Liu et al. (2010), who reported an annual value of 778 mm yr^{-1}, and by Burba and Verma (2005), who measured ET in winter wheat in north-central Oklahoma using an eddy covariance system and found annual values ranging from 710 mm to 750 mm.

Liu et al. (2010) reported an annual ET value of 854 mm in forest systems in north-central Oklahoma, which is slightly lower than estimated ET_{c_adj} at the loblolly pine site and much lower than estimated ET_{c_adj} estimated for the mixed hardwood forest. Doughty et al. (2016) reported ET values estimated from MODIS satellite data of 650 mm yr^{-1} to >

900 mm yr^{-1} in evergreen forest in southeast Oklahoma, which is slightly lower than the ET_{c_adj} values estimated here for the pine plantation (918 mm yr^{-1} to 946 mm yr^{-1}). Hennessey et al. (2004) reported ET values of ~600-800 mm yr^{-1} in a loblolly pine plantation in southeastern Oklahoma, values which are also slightly lower than those found in the present study.

Comparison of modeled and measured PAW

Model-estimated PAW for the study period (considering all K_{cb} estimation methods) ranged from 0-59 mm under mixed hardwood forest, from 0-291 mm under pine, from 0-247 mm under cropland, and from 0-72 mm under tallgrass prairie. Mean daily PAW values estimated by the model for each vegetation type are shown in Figure 12, and measured and estimated PAW are shown in Figure 13. Mean daily PAW was greatest under the mixed hardwood forest when using $K_{cb\text{-}NDVI}$ (12.0 mm), followed by $K_{cb\text{-}EVI_2}$ (11.6 mm) and then $K_{cb\text{-}NDVI}$ (11.4 mm). Mean daily PAW was greatest under the loblolly pine plantation when using $K_{cb\text{-}EVI_1}$ (127 mm), followed by $K_{cb\text{-}EVI_2}$ (116 mm) and then $K_{cb\text{-}NDVI}$ (105 mm). Mean daily PAW was greatest under the cropland when using $K_{cb\text{-}EVI_2}$ (80.0 mm), followed by $K_{cb\text{-}EVI_1}$ (78.2 mm) and then $K_{cb\text{-}NDVI}$ (67.8 mm). Mean daily PAW was greatest under the tallgrass prairie when using $K_{cb\text{-}EVI_1}$ (26.3 mm), followed by $K_{cb\text{-}EVI_2}$ (23.1 mm) and then $K_{cb\text{-}NDVI}$ (22.1 mm).

The model was able to estimate PAW dynamics relatively well at all sites. The greatest Pearson correlation coefficient (r) values (considering all K_{cb} estimation methods) were found for the loblolly pine plantation site (mean r = 0.99), and the lowest values were found for the mixed hardwood forest site (mean r = 0.61). Values of r for the

loblolly pine plantation were 0.99 for all K_{cb} methods, indicating a high level of agreement between model estimated and measured PAW dynamics regardless of the vegetation index data type or K_{cb} estimation method used. However, this high correlation value is likely caused, in part, by the short data record used for comparison and a relative lack of changes in PAW during that time (Figure 13). Values of *r* for mixed hardwood forest were 0.61 in all cases, indicating moderate levels of agreement between measured and estimated PAW (Table 4, Figure 13). Values of *r* for the cropland site range from 0.91 to 0.92, indicating good model performance at this site (Table 4, Figure 13). Values of *r* for the tallgrass prairie site range from 0.72 to 0.78, indicating moderately good model performance at the site.

The range of *r* values seen here is comparable to those found by Schnur et al. (2010), who found *r* values from 0.74 to 0.94 when applying their trained linear regression model to estimate 0-50 cm soil moisture values at distant, unmonitored sites using NDVI data. Our findings are also similar to those reported by Owe et al. (1988), who found an *r* value of 0.82 for their model, which used microwave brightness temperature and NDVI to estimate soil moisture at an unmonitored location. Overall, the soil water balance model was able to capture PAW dynamics moderately well regardless of K_{cb} estimation method, but these findings may be a result of the short data records available at most of the sites. For example, the loblolly pine plantation has the shortest data record available for comparison with the model outputs and has the greatest correlation values in all cases, while the tallgrass prairie site has the longest data record available and has the second lowest *r* values in all cases. These comparisons will likely become more meaningful in the future as more measured data are collected at each site.

While the model was able to predict soil water dynamics relatively well at most sites, it was not able to accurately estimate the magnitude of plant available water values. NSE values ranged from -4.76 to -0.16, indicating poor model performance at all sites (Table 4). Possible NSE values range from -∞ to 1.0, with a value of 1.0 indicating perfect model performance and values less than zero indicating that the mean of the observed data is a better predictor than the model-estimated values (Moriasi et al., 2007). The greatest level of agreement between measured and modeled PAW values based on the NSE metric was found for the loblolly pine plantation site (mean NSE across all K_{cb} estimation methods = -0.96), and the worst agreement was found for the mixed hardwood forest site (mean NSE across all K_{cb} estimation methods = -4.69). No NSE values are greater than zero, indicating that at all locations the mean observed PAW value is a better predictor than model-estimated PAW. As described above, these results are likely impacted by the limited data records at each site, and would likely change given a longer data record.

Mean absolute error (MAE) ranged from 37.6 mm to 90.3 mm, with the greatest MAE values across all K_{cb} estimation methods found for the cropland and loblolly pine plantation sites (mean MAE = 70.9 mm in both cases) and the lowest mean MAE values across all K_{cb} estimation methods found at the tallgrass prairie site (mean MAE = 39.0 mm) (Table 4). Mean bias error (MBE) ranged from 33.4 mm to 90.3 mm, with the greatest MBE observed for the loblolly pine plantation site (mean MBE = 70.9 mm) and the lowest MBE found for the mixed hardwood forest (mean MBE = 33.6 mm). MBE values reported here are higher than those found by Patrignani and Ochsner (2018), who used the dual crop coefficient method to estimate root zone PAW to a depth of 80 cm

under winter wheat in Oklahoma and found MBE values ranging from -7.9 mm to 5.7 mm. It should be noted that the lower MAE and MBE values found for the tallgrass prairie site may be a result of the shallower rooting depth used as this site, since the amount of available water calculated within the model is directly related to the rooting depth (see Equation 6). Regardless of this distinction, even the current simulations with the lowest amounts of error have MBE values greater than those reported by prior work.

The ratio of the root mean square error to the standard deviation of observed data, or RSR, ranged from 1.07 to 2.39 (Table 4). RSR values range from zero to a large positive value, where a value of zero indicates no error and therefore perfect model simulation. Moriasi et al. (2007) provided the following performance ratings for RSR values found for models using a monthly time step: $0.00 \leq RSR \leq 0.50$ are very good, $0.05 \leq RSR \leq 0.60$ are good, $0.60 \leq RSR \leq 0.70$ are satisfactory, and $RSR > 0.70$ are unsatisfactory. Given these definitions, none of the current model simulations are considered to be satisfactory; however, Moriasi et al. (2007) does note that less strict criteria should be used when modeling at time step smaller than one month, such as the daily simulations considered in the present study.

Comparison of PAW measurements from independent monitoring stations and Mesonet

Finally, we compared measured PAW under each vegetation type to measured PAW at the nearest Mesonet station in order to determine differences in PAW dynamics and magnitude under different land cover types (Table 5). The greatest Pearson correlation coefficient (*r)* value was found for the loblolly pine plantation site ($r = 0.91$), and the lowest value was found for the cropland site ($r = 0.48$). The low correlation

between PAW at the cropland site and the nearby Oklahoma Mesonet station is likely a result of the dichotomous nature of soil moisture dynamics under cool-season crops (such as winter wheat) and warm-season native grasses growing near the Mesonet station (Patrignani and Ochsner, 2018). NSE values ranged from -197 for the cropland site to 0.56 for the mixed hardwood forest, indicating that PAW measured at Mesonet stations and PAW measured under the different vegetation types are more closely related at some sites than at others (Table 5). The mixed hardwood forest and tallgrass prairie locations had positive NSE values, indicating that there is a meaningful relationship between Mesonet PAW and independent station PAW at those locations, but given the small amount of measured data currently available, the nature of this relationship is difficult to determine.

Mean absolute error (MAE) ranged from 22.8 mm to 210 mm, with the greatest MAE found for the cropland and lowest MAE found for the mixed hardwood forest site (Table 5). Mean bias error ranged from -183 mm to 6.7 mm, with the greatest MBE observed for the loblolly pine plantation and the lowest MBE found for the mixed hardwood forest. The ratio of the root mean square error to the standard deviation of observed data ranged from 0.94 to 19.0 (Table 5). Given the RSR definitions given above, none of the Mesonet stations are considered to have satisfactorily reflected PAW conditions at the independent monitoring stations. Overall, the dynamics of PAW between Mesonet and independent monitoring station are moderately well-correlated, but there are often large differences in measured PAW between the stations, which highlights the need for improved estimations of soil moisture under these diverse vegetation types.

By comparing the results shown in Tables 4 and 5, it is possible to determine whether PAW under each vegetation type is better represented by the model estimates or by the soil water conditions measured at the nearest Oklahoma Mesonet station. Values of *r* are greater at the mixed hardwood forest and tallgrass prairie sites when comparing measured PAW at the independent stations with the nearest Mesonet station, indicating that at these sites PAW measured at the independent site is more aligned with PAW data from the Mesonet than with model-estimated PAW. However, the *r* value found for the tallgrass prairie site when comparing independent and Mesonet PAW (Table 5) is only slightly higher than the *r* value found for the site when comparing independent PAW and model-estimated PAW (Table 4, difference of 0.01). Additionally, model-estimated PAW values lead to lower amounts of error than the Mesonet PAW data at this site (mean MAE of 39.0 mm [Table 4] versus MAE of 42.6 mm [Table 5]).

Despite the fact that the soil water balance model is not able to estimate the magnitude of PAW accurately, model-estimated PAW is a better indicator of actual conditions at the at the loblolly pine plantation and the cropland sites than are PAW data from the nearest Mesonet station. At these sites, model-estimated PAW has higher correlation coefficients; less negative NSE values; and lower MAE, MBE, and RSR values. As mentioned above, the especially low correlation between Mesonet and measured PAW values at the cropland location is likely due to the patterns of soil moisture dynamics under cool-season crops (such as winter wheat) versus those under warm-season native grasses.

Impact of K_{cb} estimation method on accuracy of model-estimated PAW

Overall, the least model error was observed when using the $K_{cb\text{-}EVI_1}$ crop coefficient curves (Table 4). Mean Pearson correlation values for each K_{cb} estimation method ranged from 0.81 to 0.82, and no single simulation *r* value was below 0.61, indicating that model performance was acceptable for all K_{cb} estimation methods (Moriasi et al., 2007). Mean MAE values were lowest when considering $K_{cb\text{-}EVI_1}$ (58.1 mm), followed by $K_{cb\text{-}EVI_2}$ (60.8 mm), followed by $K_{cb\text{-}NDVI}$ (68.6 mm). The better performance observed for simulations using the $K_{cb\text{-}EVI}$ crop curves may be a result of the improved performance of EVI data in dense canopy covers, the ability of EVI data to separate the soil and plant canopy signals, and the greater responsiveness of EVI data to canopy structural variations (Gao et al., 2000; Wang et al., 2007).

The FAO-56 method has historically been used to estimate ET rather than PAW, and for this reason few studies have compared FAO-56 estimated and measured soil moisture values. One study in Spain used the $K_{cb\text{-}NDVI}$ relationship (Eq. 15) to estimate soil moisture in an area with vegetation types including rainfed cereals, irrigated crops, forests, pasture, and vineyards and found *r* values ranging from 0.68 to 0.91 (Sanchez et al., 2010). Another study in Spain used the same $K_{cb\text{-}NDVI}$ method and found *r* values of 0.85 for barley and 0.88 for grass (Sanchez et al., 2012a). A third study used Landsat NDVI data and the same $K_{cb\text{-}NDVI}$ method over a 1300 km^2 area and found that model-estimated soil moisture and soil moisture measured at 19 monitoring locations were highly correlated, with *r* values ranging from 0.92 to 0.97 (Sanchez et al, 2012b). The range of *r* values reported by these studies (0.68 to 0.97) is comparable to the range of *r* values found by the present study (0.61 to 0.99), but the present simulations require

further improvements and testing before the method may be used to accurately model PAW under the diverse vegetation types considered here.

CONCLUSIONS AND FUTURE WORK

In general, model PAW estimates were well-correlated with measured PAW values, despite a large discrepancy in PAW magnitude at all study sites. This is particularly of note because the FAO-56 method was developed specifically for cropping systems, but our results indicate that, with further improvements, the method may be used to produce useful estimates of PAW when applied in other vegetation types. In the future, we plan to refine the approach developed here and to create a distributed model which applies the method over larger areas (i.e., county or state scale). This will involve gathering MODIS EVI, NDVI, and land cover type image time series to estimate K_{cb} curves; gathering soil property information and meteorological data from large-scale databases; modifying existing programs to handle spatially explicit data and perform quality control on these images; and applying the method developed here for each pixel within the desired area.

ACKNOWLEDGEMENTS

Support for this work was provided by the USGS 104(b) program and the Oklahoma Water Resources Center Berry Fellows Program.

REFERENCES

Allen, R. G. 1996. Assessing integrity of weather data for reference evapotranspiration estimation. Journal of Irrigation and Drainage Engineering. American Society of Civil Engineers, 112(2), 97-106.

Allen, R. G., et al. 1998. Crop evapotranspiration- Guidelines for computing crop water requirements-FAO Irrigation and drainage paper 56. FAO, Rome 300(9): D05109.

Bausch, W. C. and C. M. Neale. 1987. Crop coefficients derived from reflected canopy radiation: a concept. Trans. ASAE 30(3): 703-709.

Buck, Arden L. 1981. New equations for computing vapor pressure and enhancement factor. Journal of Applied Meteorology, 20(12), 1527-1532.

Burba, G. G. and S. B. Verma. 2005. Seasonal and interannual variability in evapotranspiration of native tallgrass prairie and cultivated wheat ecosystems. Agricultural and Forest Meteorology 135(1): 190-201.

Campos, I., et al. 2017. Reflectance-based crop coefficients REDUX: For operational evapotranspiration estimates in the age of high producing hybrid varieties. Agricultural Water Management 187: 140-153.

Choudhury, B.J., N.U. Ahmed, S.B. Idso, R.J. Reginato, and C.S.T. Daughtry. 1994. Relations between evaporation coefficients and vegetation indices studied by model simulations. Remote Sensing of Environment 50(1):1-17.

Dipesh, K.C., R.E. Will, T.B. Lynch, R. Heinemann, and R. Holeman. 2014. Comparison of loblolly, shortleaf, and pitch X loblolly pine plantations growing in Oklahoma. Forest Ecology 61(3):540-547.

Doughty, R. X. Xiao, Y. Qin, Y. Zhang. 2016. Responses of evapotranspiration and gross primary production of forests and grasslands to drought in the Kiamichi watershed of southeast Oklahoma. Oklahoma Governor's Water Conference. http://www.eomf.ou.edu/media/gisday/posters/Doughty-Kiamichi-Drought-ResiliencyXiaoRuss.pdf Accessed 21 November 2019.

Entekhabi, D., et al. 2010. The soil moisture active passive (SMAP) mission. Proceedings of the IEEE 98(5): 704-716.

Ford, T. W. and S. M. Quiring 2013. Influence of MODIS-Derived Dynamic Vegetation on VIC-Simulated Soil Moisture in Oklahoma. Journal of Hydrometeorology 14(6): 1910-1921.

Gao, X., et al. 2000. Optical–biophysical relationships of vegetation spectra without background contamination. Remote Sensing of Environment 74(3): 609-620.

Glenn, E. P., et al. 2007. Integrating remote sensing and ground methods to estimate evapotranspiration. Critical Reviews in Plant Sciences 26(3): 139-168.

Glenn, E. P., et al. 2010. Vegetation index methods for estimating evapotranspiration by remote sensing. Surveys in Geophysics 31(6): 531-555.

Glenn, E. P., et al. 2011. Vegetation index-based crop coefficients to estimate evapotranspiration by remote sensing in agricultural and natural ecosystems. Hydrological Processes 25(26): 4050-4062.

Gonzalez-Dugo, M., et al. 2009. A comparison of operational remote sensing-based models for estimating crop evapotranspiration. Agricultural and Forest Meteorology 149(11): 1843-1853.

Gorelick, N., Hancher, M., Dixon, M., Ilyushchenko, S., Thau, D., & Moore, R. 2017. Google Earth Engine: Planetary-scale geospatial analysis for everyone. Remote Sensing of Environment.

Harpold, A. A., et al. 2017. Does including soil moisture observations improve operational streamflow forecasts in snow-dominated watersheds? JAWRA Journal of the American Water Resources Association 53(1): 179-196.

Hendrickx, J. M. H., et al. 2016. Benchmarking optical/thermal satellite imagery for estimating evapotranspiration and soil moisture in decision support tools. JAWRA Journal of the American Water Resources Association 52(1): 89-119.

Hennessey, T. C., et al. 2004. Long-term growth and ecophysiological responses of a southeastern Oklahoma loblolly pine plantation to early rotation thinning. Forest Ecology and Management 192(1): 97-116.

Howell, A.T., et al. 1997. Seasonal and maximum daily evapotranspiration of irrigated wheat, sorghum, and corn- Southern High Plains. Transactions of the ASAE 40(3): 623-634.

Huete, A. R., Liu, H. Q., Batchily, K., & van Leeuwen, W. J. D. 1997. A comparison of vegetation indices over a global set of TM images for EOS-MODIS. Remote Sensing of Environment, 59, 440–451.

Huete, A., et al. 1999. MODIS vegetation index (MOD13). Algorithm theoretical basis document 3: 213.

Huete, A., Justice, C., & Liu, H. 1994. Development of vegetation and soil indices for MODIS-EOS. Remote Sensing of Environment, 49, 224–234.

Huete, A., K. Didan, T. Miura, E.P. Rodriguez, X. Gao, and L.G. Ferreira. 2002. Overview of the radiometric and biophysical performance of the MODIS vegetation indices. Remote Sensing of Environment 83(1-2): 195-213.

Huete, A.; Didan, K., van Leeuwen, W., Miura, T.; Glenn, E. MODIS vegetation indices. In Land Remote Sensing and Global Environmental Change: NASA's Earth Observing System and the Science of ASTER and MODIS 2008, in press.

Kerr, Y. H., et al. 2001. Soil moisture retrieval from space: The Soil Moisture and Ocean Salinity (SMOS) mission. Geoscience and Remote Sensing, IEEE Transactions on 39(8): 1729-1735.

Kumar, S. V., et al. 2006. Land information system: An interoperable framework for high resolution land surface modeling. Environmental Modelling & Software 21(10): 1402-1415.

Liu, Wenjuan, Y. Hong, S.I. Khan, M. Huang, B. Vieux, S. Caliskan, and T. Grout. 2010. Actual evapotranspiration estimation for different land use and land cover in urban regions using Landsat 5 data. Journal of Applied Remote Sensing 4(1):1-15.

Lollato, R. P., et al. 2016. Prediction of plant available water at sowing for winter wheat in the Southern Great Plains. Agronomy Journal 108(2): 745-757.

Lollato, R.P., T.E. Ochsner, D.B. Arnall, T.W. Griffin, and J.T. Edwards. 2018. From field experiments to regional forecasts: upscaling wheat grain and forage yield response to acidic soils. Agronomy Journal 111(1):287-302.

McPherson, R. A., et al. 2007. Statewide monitoring of the mesoscale environment: A technical update on the Oklahoma Mesonet. Journal of Atmospheric and Oceanic Technology 24(3): 301-321.

Mitchell, K. E., et al. 2004. The multi-institution North American Land Data Assimilation System (NLDAS): Utilizing multiple GCIP products and partners in a continental distributed hydrological modeling system. Journal of Geophysical Research: Atmospheres 109(D7).

Mohanty, B. P., et al. 2017. Soil moisture remote sensing: state-of-the-science. Vadose Zone Journal 16(1).

Moriasi, D., et al. 2007. Model evaluation guidelines for systematic quantification of accuracy in watershed simulations. Trans. Asabe 50(3): 885-900.

Ochsner, T. E., et al. 2013. State of the art in large-scale soil moisture monitoring. Soil Science Society of America Journal 77(6): 1888-1919.

Oklahoma Forestry Services. 2015. Oklahoma Forest Resource Assessment. http://www.forestry.ok.gov/Websites/forestry/Images/Oklahoma%20Forest%20Resource%20Assessment,%20FINAL%20FOR%20WEB.pdf. Accessed 20 November 2019.

Owe, M., et al. 1988. Estimating surface soil moisture from satellite microwave measurements and a satellite derived vegetation index. Remote Sensing of Environment 24(2): 331-345.

Patrignani, A. and T. E. Ochsner. 2018. Modeling transient soil moisture dichotomies in landscapes with intermixed land covers. Journal of Hydrology 566: 783-794.

Peng, J., et al. 2017. A review of spatial downscaling of satellite remotely sensed soil moisture. Reviews of Geophysics.

Sánchez, N., et al. 2010. Combining remote sensing and in situ soil moisture data for the application and validation of a distributed water balance model (HIDROMORE). Agricultural Water Management 98(1): 69-78.

Sánchez, N., et al. 2012a. Water balance at plot scale for soil moisture estimation using vegetation parameters. Agricultural and Forest Meteorology 166: 1-9.

Sánchez, N., J. Martínez-Fernández, M. Rodríguez-Ruiz, E. Torres, and A. Calera. 2012b. A simulation of soil water content based on remote sensing in a semi-arid Mediterranean agricultural landscape. Spanish Journal of Agricultural Research 10(2):521-532.

Schnur, M. T., et al. 2010. Estimating root zone soil moisture at distant sites using MODIS NDVI and EVI in a semi-arid region of southwestern USA. Ecological Informatics 5(5): 400-409.

Sun, X., et al. 2018. Effect of vegetation on the energy balance and evapotranspiration in tallgrass prairie: a paired study using the eddy-covariance method. Boundary-Layer Meteorology.

Transtrum, M. K. and P. Qiu. 2016. Bridging mechanistic and phenomenological models of complex biological systems. PLOS Computational Biology 12(5): e1004915.

Wagle, Pradeep, P.H. Gowda, and B.K. Northup. 2019. Dynamics of evapotranspiration over a non-irrigated alfalfa field in the Southern Great Plains of the United States. Agricultural Water Management 223. doi: https://doi.org/10.1016/j.agwat.2019.105727

Wagner, W., et al. 2007. Operational readiness of microwave remote sensing of soil moisture for hydrologic applications. Hydrology Research 38(1): 1-20.

Wagner, W., W. Dorigo, R. de Jeu, D. Fernandez, J. Benveniste, E. Haas, and M. Ertl. 2012. Fusion of active and passive microwave observations to create an essential climate variable data record on soil moisture. ISPRS Annals of the Photogrammetry, Remote Sensing and Spatial Information Sciences, Volume I-7.

Wang, X., et al. 2007. Different responses of MODIS-derived NDVI to root-zone soil moisture in semi-arid and humid regions. Journal of hydrology 340(1): 12-24.

Wine, M. and J. Hendrickx. 2013. Biohydrologic effects of eastern redcedar encroachment into grassland, Oklahoma, USA. Biologia. 68: 1132.

Wyatt, B. M., et al. 2017. Useful drainage estimates obtained from a large-scale soil moisture monitoring network by applying the unit-gradient assumption. Vadose Zone Journal 16(6).

Zhang, Y., et al. 2019. Estimating deep drainage using deep soil moisture data under young irrigated cropland in a desert-oasis ecotone, Northwest China. Vadose Zone Journal 18(1).

Zou, C.B., G.L. Caterina, R.E. Will, E. Stebler, and D. Turton. 2015. Canopy interception for a tallgrass prairie under juniper encroachment. PLOS One 10(11). doi: 10.1371/journal.pone.0141422.

Table 1. Site information, including latitude and longitude, distance to the nearest Oklahoma Mesonet station, elevation above sea level, long-term mean daily maximum temperature (T_{max}), long-term mean daily minimum temperature (T_{min}), long-term mean annual precipitation (P), and the year in which soil moisture sensors were installed.

Site	Latitude, Longitude	Elevation	Distance to Mesonet	T_{max}, T_{min}	P	Year Installed
	deg.	m	km	°C	mm	
Loblolly Pine Plantation	34.03, -94.82	110	23.1	23.9, 11.0	1159	2019
Mixed Hardwood Forest	36.00, -97.04	292	1.00	22.3, 9.92	873	2018
Cropland	35.03, -97.91	328	0.13	23.1, 9.36	812	2018
Tallgrass Prairie	36.06, -97.21	327	0.47	22.1, 9.43	884	2012

Table 2. Depth of soil subject to evaporation (Z_e), soil volumetric water contents at field capacity (θ_{-10}) and wilting point (θ_{-1500}) for the surface layer and sub-surface, mean depth-weighted sand and clay contents, maximum vegetation height (h_{max}), and maximum rooting depth (Z_{r_max}) at each monitoring location.

Site	Sand	Clay	θ_{-10}	θ_{-1500}	Z_e	h_{max}	Z_{r_max}
	%	%	$m^3\ m^{-3}$	$m^3\ m^{-3}$	m	m	m
Loblolly Pine Plantation	36.9	20.9	0.28, 0.33	0.03, 0.09	0.13	10.0	1.20
Mixed hardwood forest	86.1	4.23	0.09, 0.07	0.02, 0.02	0.11	9.40	1.20
Cropland	21.3	24.5	0.31, 0.32	0.10, 0.11	0.14	2.00	1.20
Tallgrass Prairie	11.0	22.5	0.30,0.32	0.13, 0.21	0.13	1.00	0.65

Table 3. Mean annual reference evapotranspiration (ET_o) and adjusted crop evapotranspiration (ET_{c_adj}) for each vegetation type and basal crop coefficient (K_{cb}) estimation method. ET_o values are independent of vegetation characteristics and do not differ between K_{cb} estimation methods.

K_{cb} method	Site	ET_o	ET_{c_adj}
		mm	mm
$K_{cb\text{-}EVI_1}$	Loblolly Pine Plantation	1209	918
	Mixed Hardwood Forest	1390	1198
	Cropland	1412	788
	Tallgrass Prairie	1341	740
$K_{cb\text{-}EVI_2}$	Loblolly Pine Plantation	1209	931
	Mixed Hardwood Forest	1390	1115
	Cropland	1412	787
	Tallgrass Prairie	1341	753
$K_{cb\text{-}NDVI}$	Loblolly Pine Plantation	1209	946
	Mixed Hardwood Forest	1390	1037
	Cropland	1412	796
	Tallgrass Prairie	1341	756

Table 4. Pearson correlation coefficient (*r*), Nash-Sutcliffe Efficiency (NSE), mean absolute error (MAE), mean bias error (MBE), and the ratio of the root mean square error to the standard deviation of observed data (RSR) calculated by comparing daily plant available water estimated by the water balance model using $K_{cb\text{-}EVI_1}$, $K_{cb\text{-}EVI_2}$, and $K_{cb\text{-}NDVI}$ curves and measured plant available water at each independent monitoring site.

K_{cb} method	Site	*r*	NSE	MAE	MBE	RSR
		-	-	mm	mm	-
$K_{cb\text{-}EVI_1}$	Loblolly pine plantation	0.99	-0.16	56.2	56.2	1.07
	Mixed hardwood forest	0.61	-4.76	69.6	33.8	2.39
	Cropland	0.91	-1.03	69.0	37.7	1.42
	Tallgrass prairie	0.78	-1.01	37.6	37.4	1.42
$K_{cb\text{-}EVI_2}$	Loblolly pine plantation	0.99	-0.63	66.2	66.2	1.27
	Mixed hardwood forest	0.61	-4.68	69.1	33.5	2.38
	Cropland	0.91	-0.99	68.3	37.3	1.41
	Tallgrass prairie	0.73	-1.25	39.6	39.3	1.50
$K_{cb\text{-}NDVI}$	Loblolly pine plantation	0.99	-2.07	90.3	90.3	1.74
	Mixed hardwood forest	0.61	-4.63	68.8	33.4	2.37
	Cropland	0.92	-1.36	75.3	41.2	1.53
	Tallgrass prairie	0.72	-1.31	40.0	39.8	1.52

Table 5. Pearson correlation coefficient (*r*), Nash-Sutcliffe Efficiency (NSE), mean absolute error (MAE), mean bias error (MBE), and the ratio of the root mean square error to the standard deviation of observed data (RSR) calculated by comparing plant available water measured under each land cover type and measured plant available water at the Oklahoma Mesonet station nearest the monitoring site.

Site	*r*	NSE	MAE	MBE	RSR
	-	-	mm	mm	-
Loblolly Pine Plantation	0.91	-45.3	186	-183	6.75
Mixed Hardwood Forest	0.80	0.56	22.8	6.7	1.01
Cropland	0.48	-197	210	-115	19.0
Tallgrass prairie	0.79	0.12	42.6	33.8	0.94

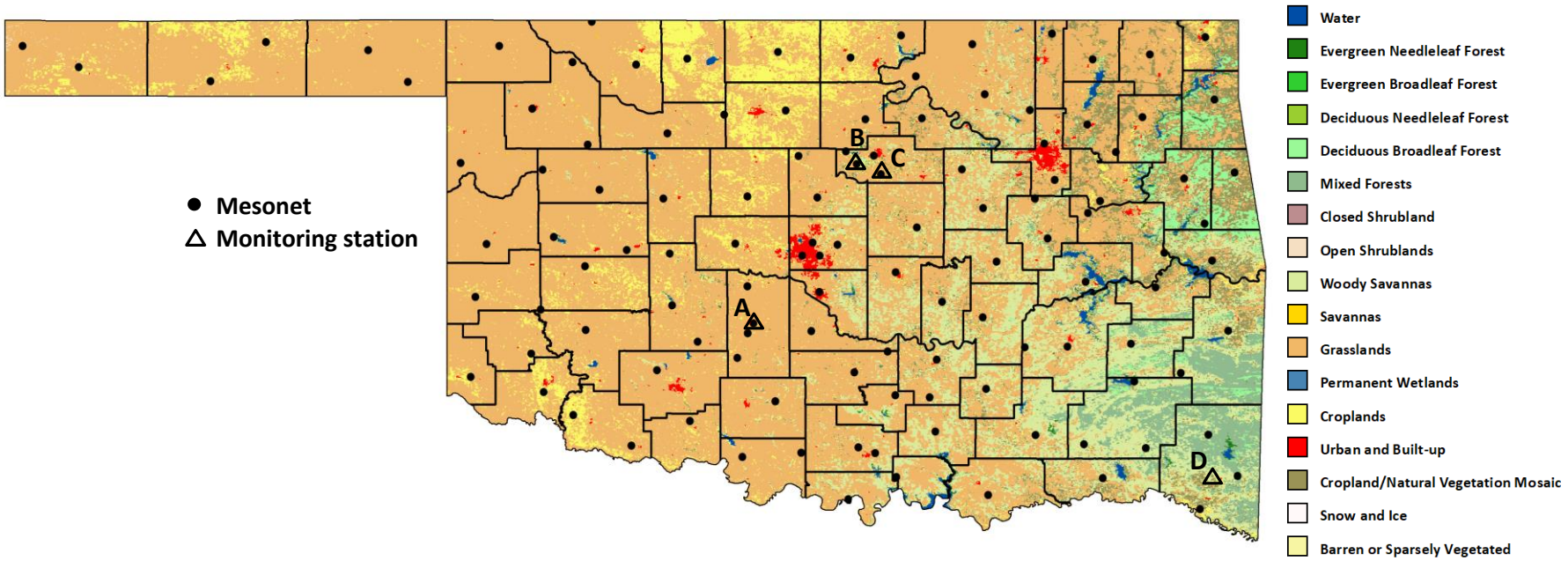

Figure 1. Map of MODIS land cover types (500-m resolution) and county boundaries in Oklahoma, active Oklahoma Mesonet locations (circles), and locations of independent soil moisture monitoring stations under various vegetation types (triangles).

Figure 2. Mixed hardwood forest and Perkins Oklahoma Mesonet station locations.

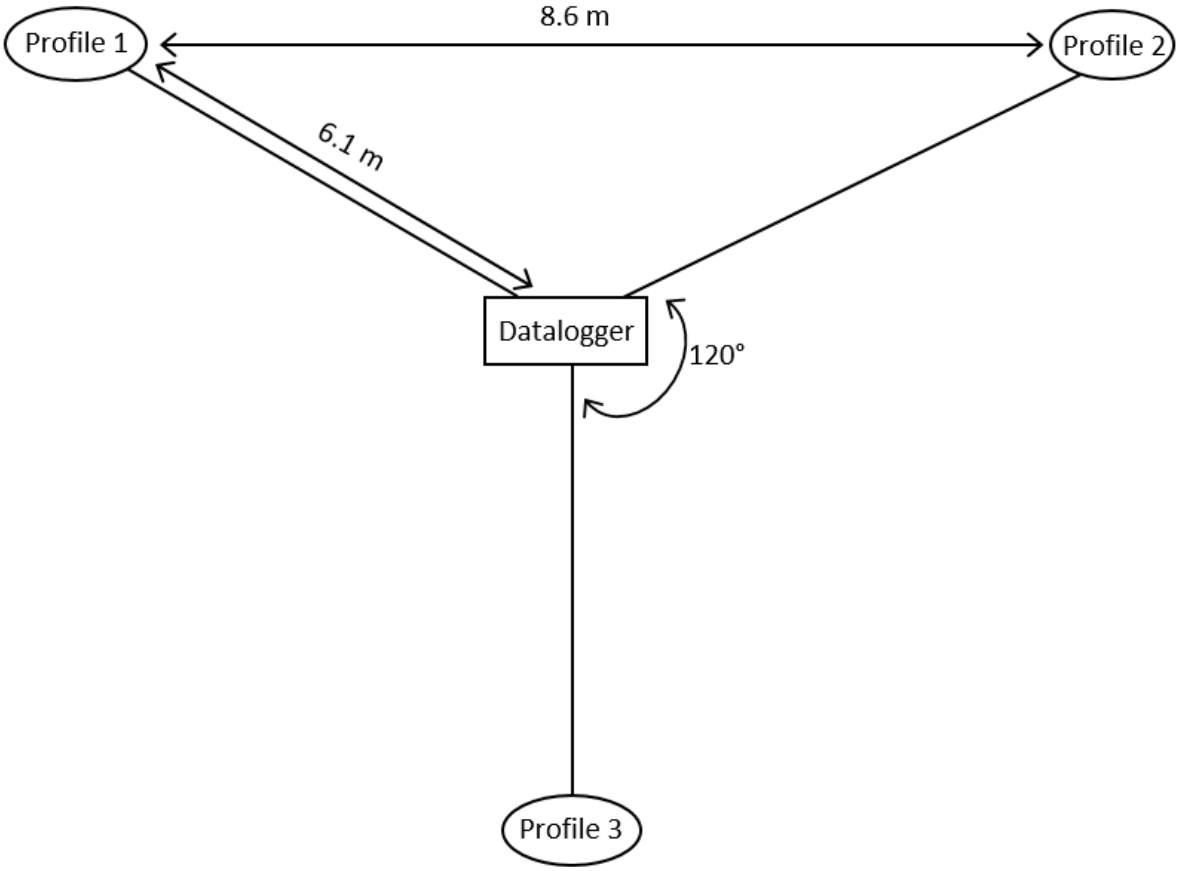

Figure 3. Diagram of soil moisture monitoring station layout.

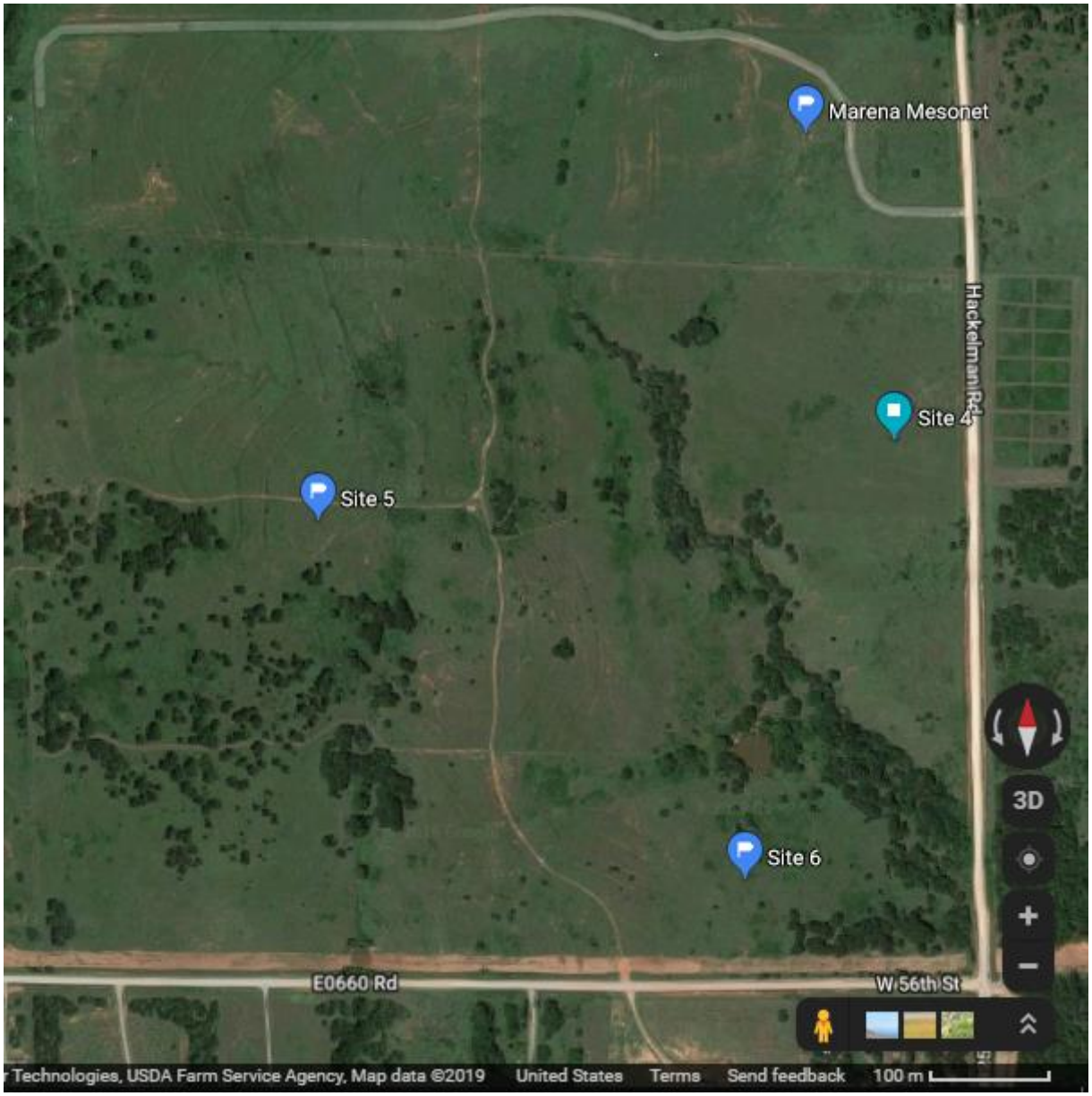

Figure 4. Tallgrass prairie monitoring locations and Marena Oklahoma Mesonet station location.

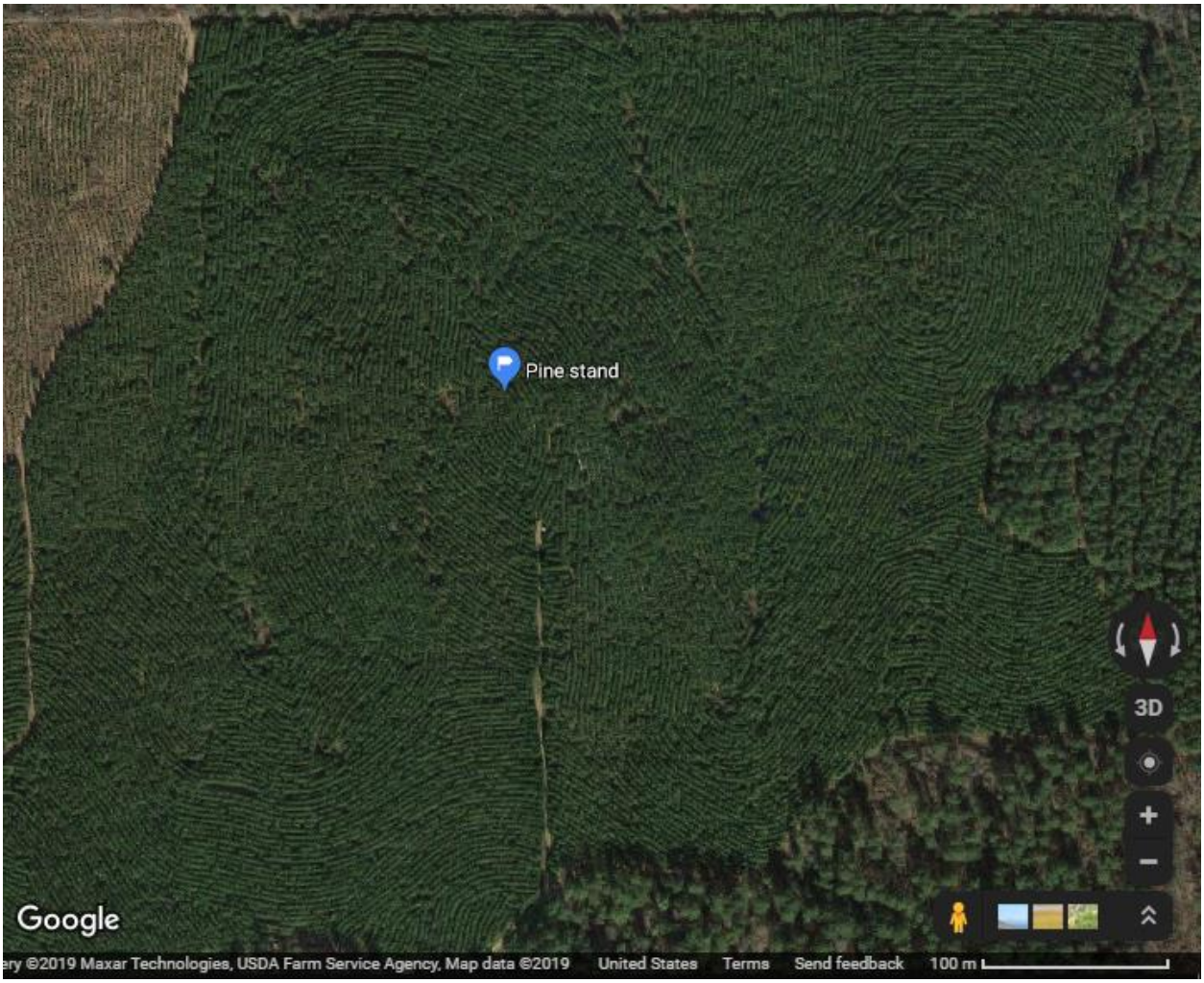

Figure 5. Loblolly pine plantation monitoring site location.

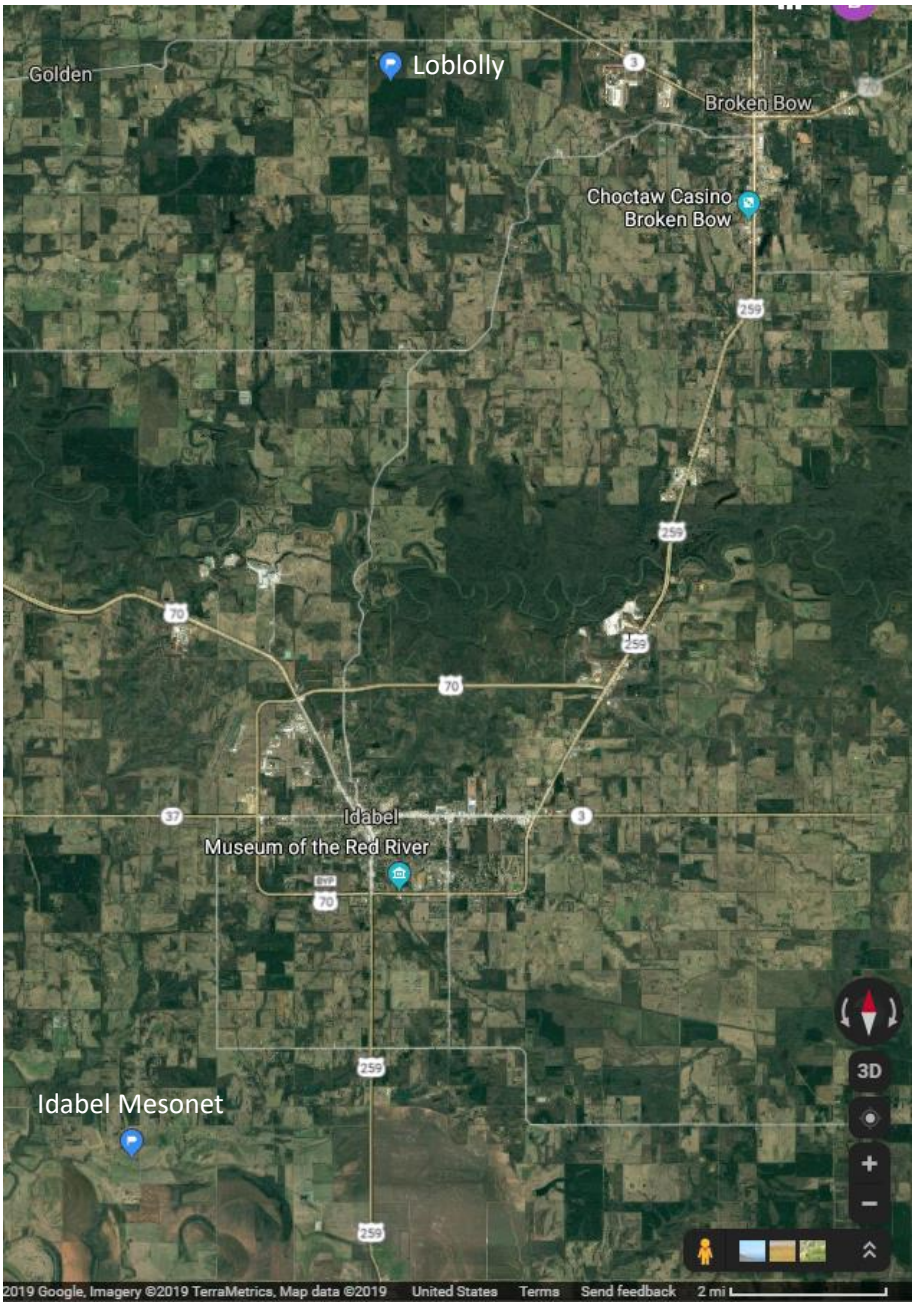

Figure 6. Loblolly pine plantation monitoring site (upper blue marker) and Idabel Mesonet (lower blue marker) locations.

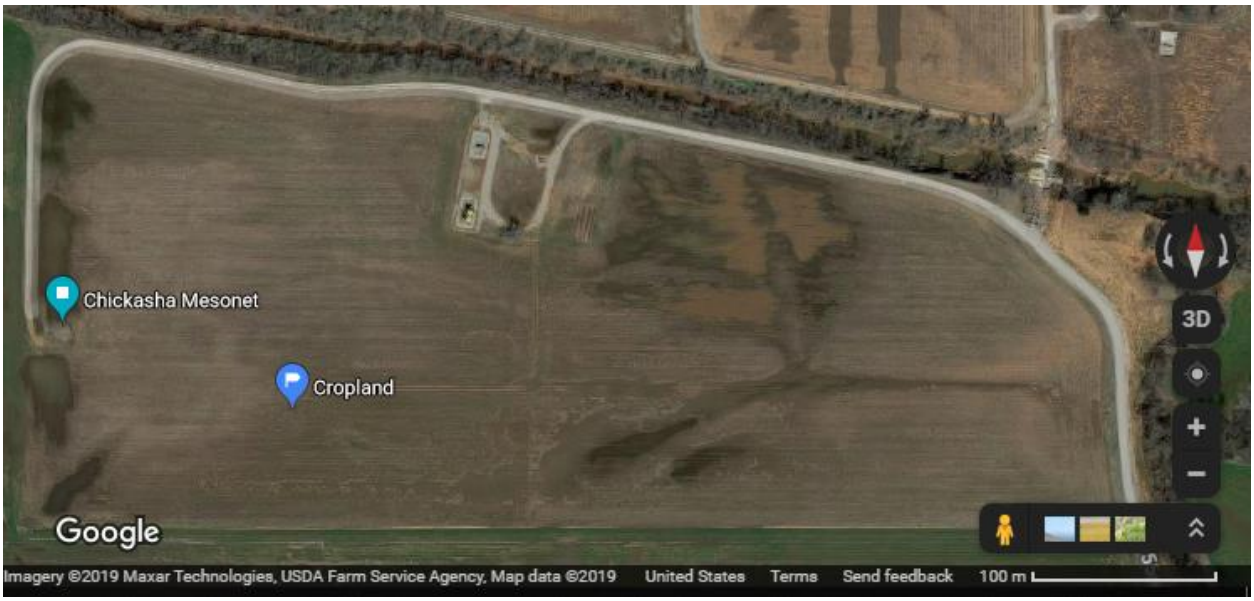

Figure 7. Cropland monitoring site and Chickasha Oklahoma Mesonet location.

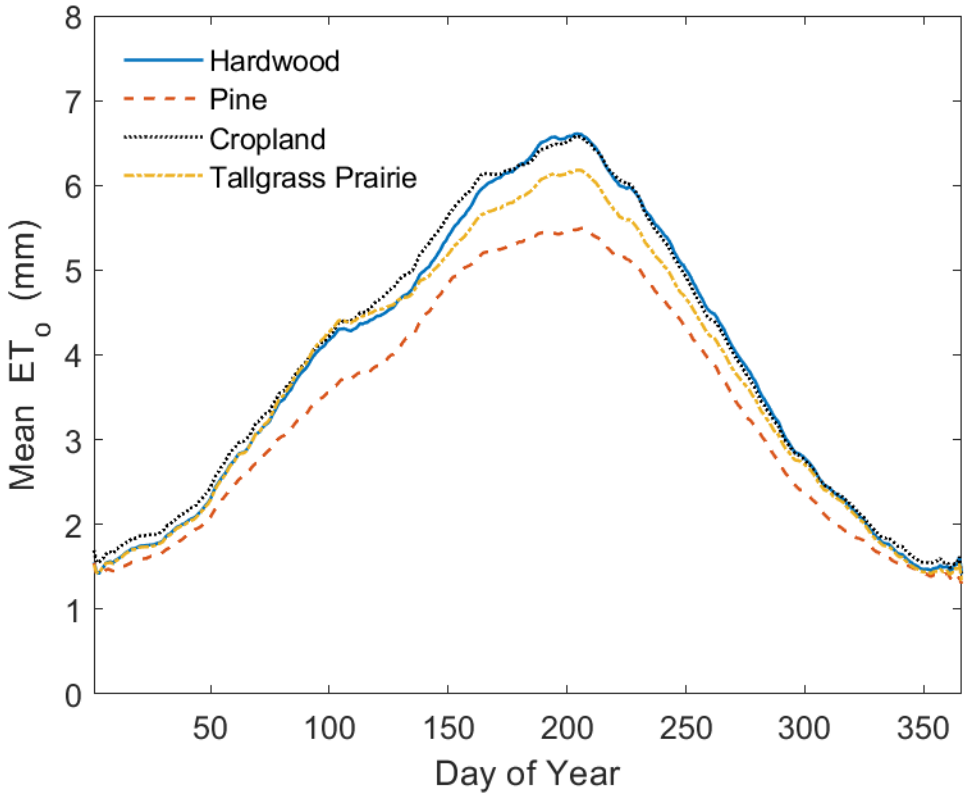

Figure 8. Daily mean reference evapotranspiration (ET_o) by site, smoothed using a 30-day centered moving average.

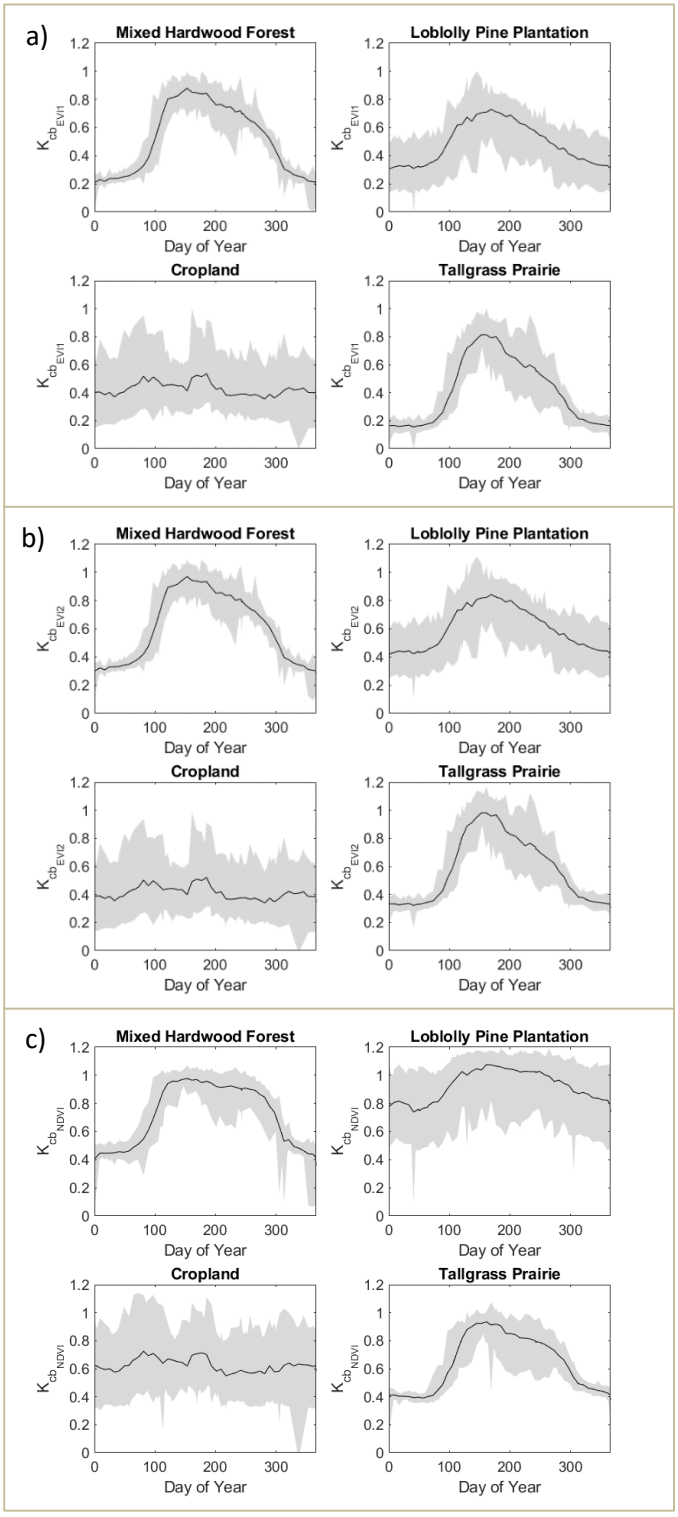

Figure 9. Mean daily $K_{cb\text{-}EVI_1}$ (a), $K_{cb\text{-}EVI_2}$ (b), and $K_{cb\text{-}NDVI}$ (c) for each vegetation type for Jan 2000-Aug 2019. The gray shaded areas represent the full range of daily K_{cb} values.

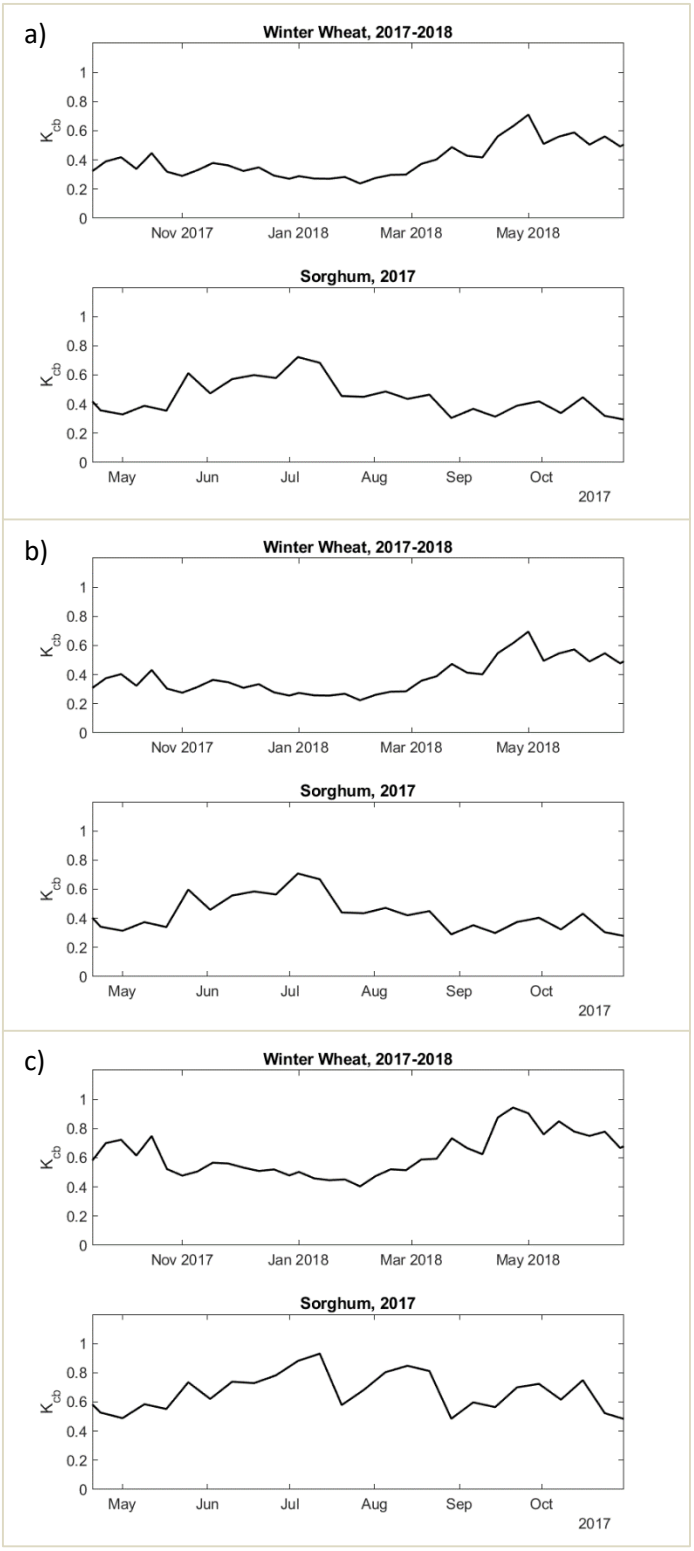

Figure 10. Examples of growing season K_{cb} curves for a cool season crop (winter wheat) and a warm season crop (sorghum) derived from $K_{cb\text{-}EVI_1}$ (a), $K_{cb\text{-}EVI_2}$ (b), and $K_{cb\text{-}NDVI}$ (c) data.

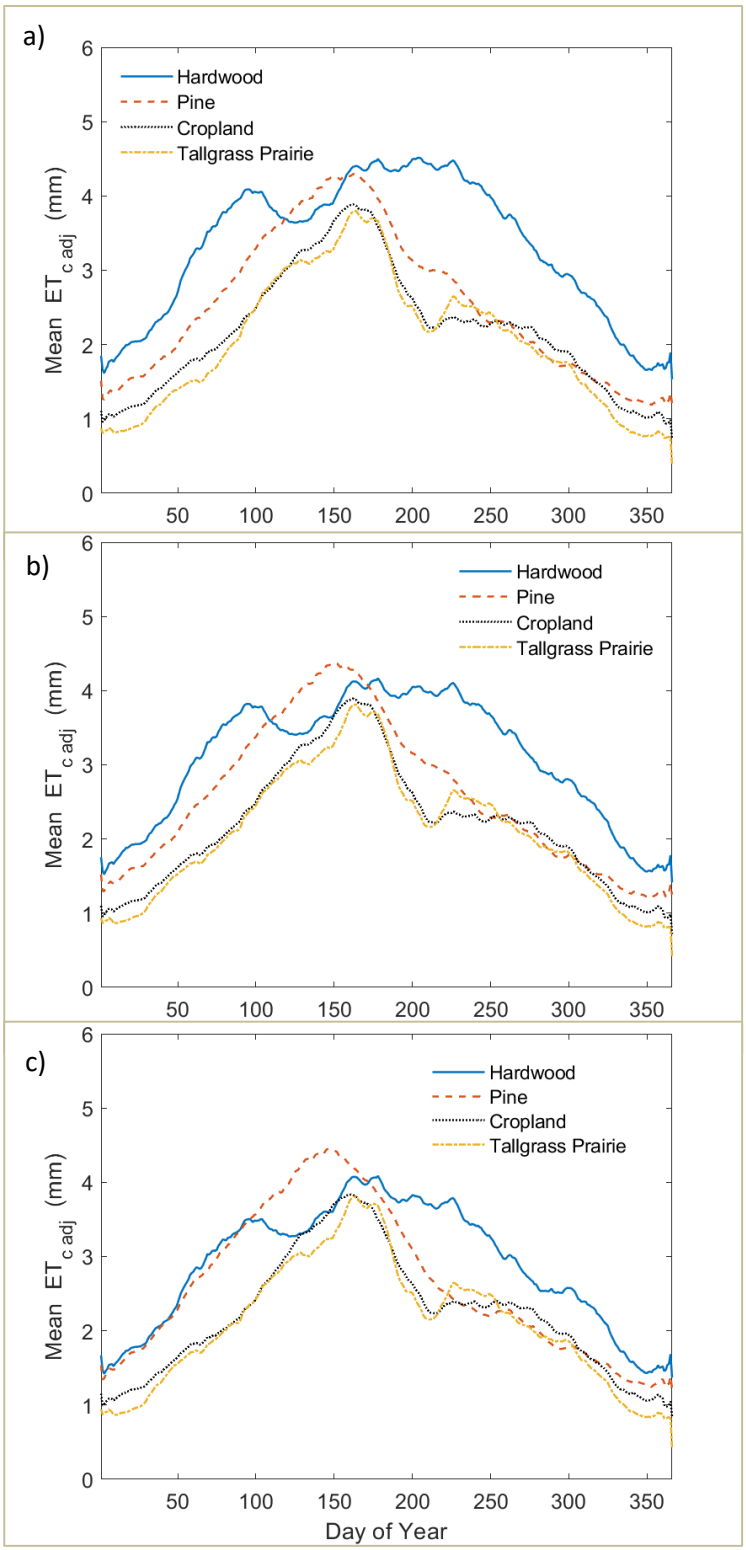

Figure 11. Mean daily evapotranspiration (ET_{c_adj}) as estimated by the FAO-56 dual crop coefficient method using $K_{cb\text{-}EVI_1}$ (a), $K_{cb\text{-}EVI_2}$ (b), and $K_{cb\text{-}NDVI}$ (c), smoothed using a 30-day centered moving average.

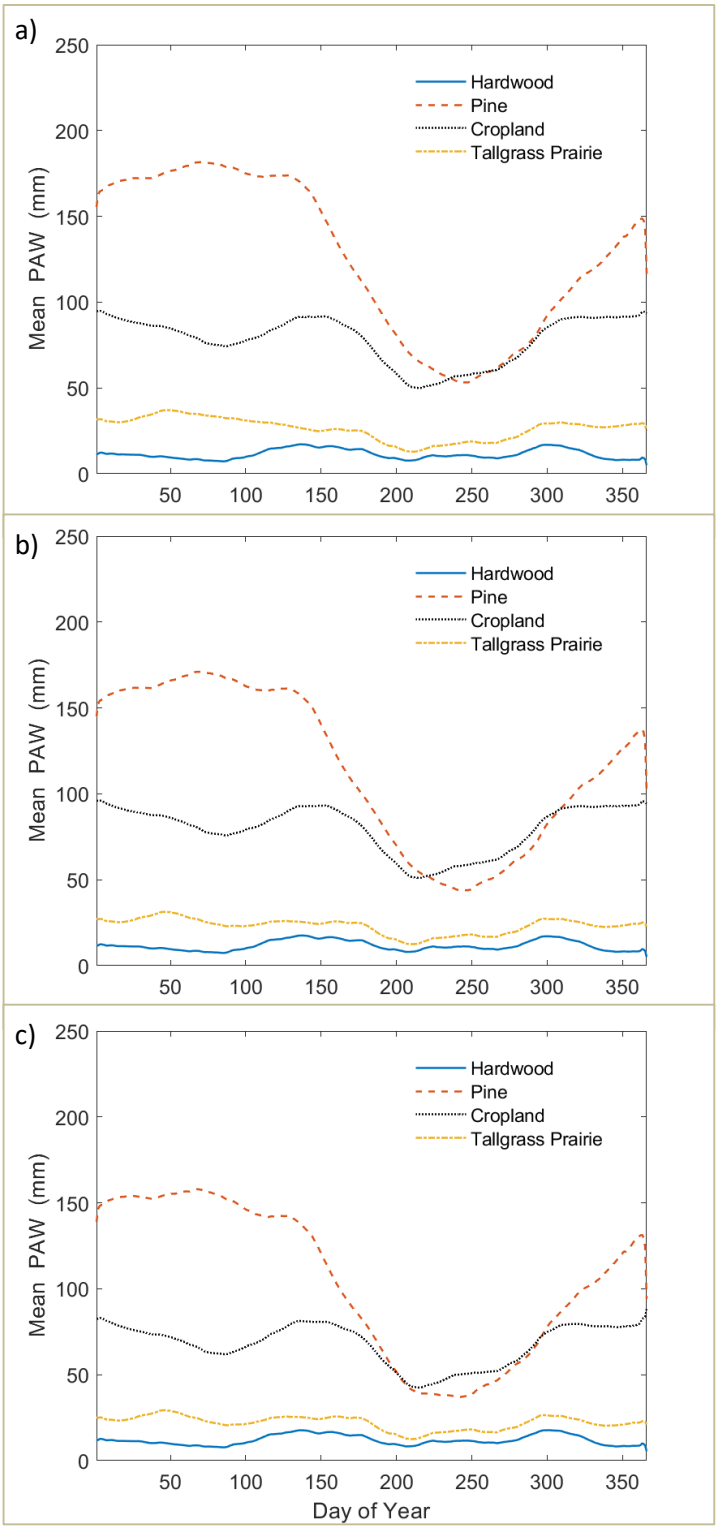

Figure 12. Mean daily plant available water as estimated by the FAO-56 dual crop coefficient method using $K_{cb\text{-}EVI_1}$ (a), $K_{cb\text{-}EVI_2}$ (b), and $K_{cb\text{-}NDVI}$ (c), smoothed using a 30-day centered moving average.

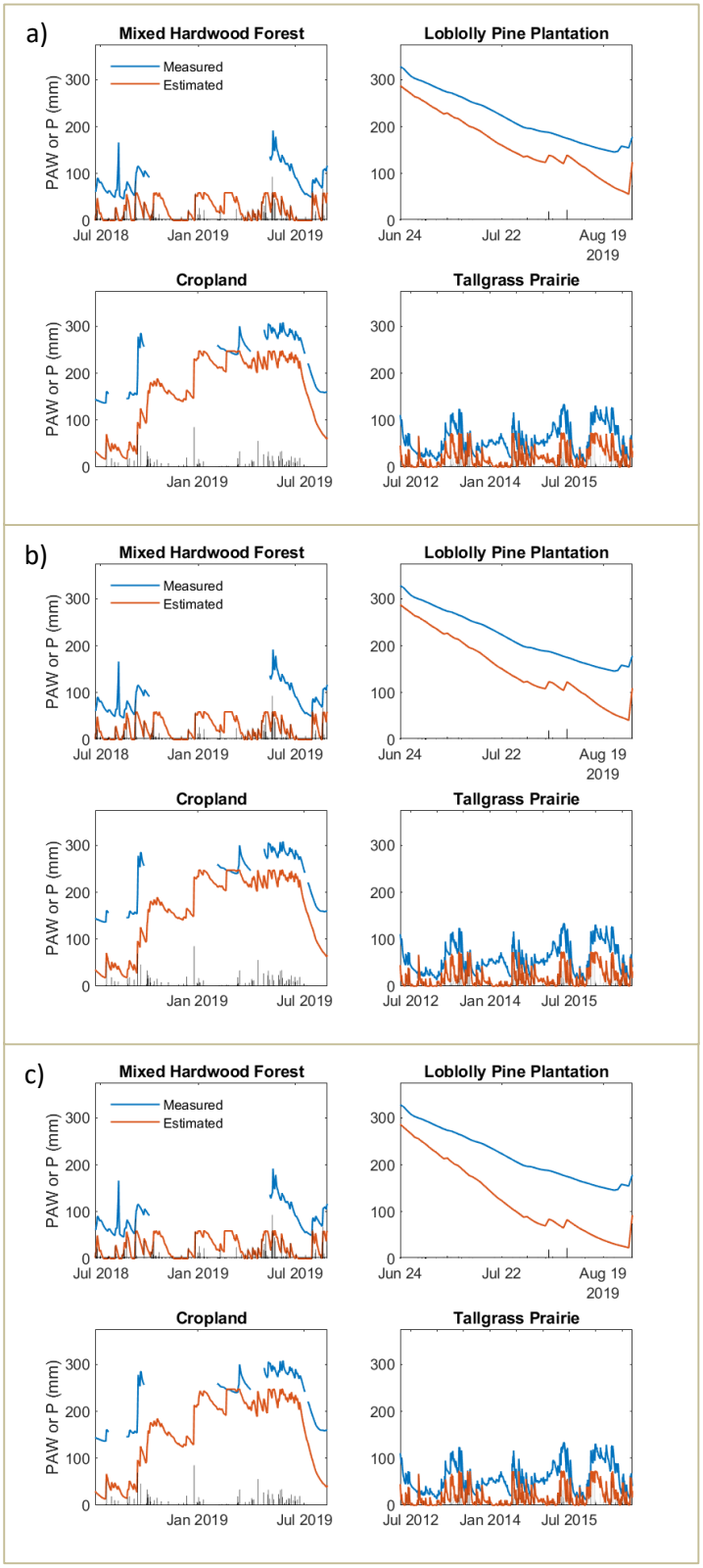

Figure 13. Daily precipitation (P), measured PAW under each vegetation type, and estimated PAW estimated using $K_{cb\text{-}EVI_1}$ (a), $K_{cb\text{-}EVI_2}$ (b), and $K_{cb\text{-}NDVI}$ (c).

CHAPTER V

GENERAL CONCLUSIONS

Soil moisture is a critical variable influencing groundwater recharge, rainfall-runoff partitioning, and plant water uptake. In this dissertation, soil moisture data were applied to i) estimate potential groundwater recharge over 17 years at 78 locations throughout Oklahoma and ii) improve the accuracy of streamflow forecasts in four rainfall-dominated watersheds in order to enhance surface water resource management. The estimation of soil moisture under diverse vegetation types using a simple water balance approach was also demonstrated.

In the first study I investigated the usefulness of long-term soil moisture data and soil physical properties for estimating potential groundwater recharge throughout Oklahoma. I found that soil moisture data can be used, along with a unit-gradient assumption, to estimate potential groundwater recharge, and that estimates from the method align well with estimates of recharge reported in prior publications for several major aquifers in the state. Additionally, I used a calibrated soil water flow model to verify our findings at four focus sites and found that modeled and estimated potential groundwater recharge rates agree more closely at dry sites than at wet ones. The potential groundwater recharge rates presented represent the first state-wide estimates of recharge

since the 1980's and may be useful for future hydrological studies in the state.

In the second study I applied a well-known statistical streamflow forecasting model typically used in the snow-dominated West in four rainfall-dominated watersheds in order to determine if the inclusion of soil moisture data leads to improved forecast accuracy. My results show that forecasts based on precipitation data alone explain, at best, 27% of variability in seasonal streamflow, while forecasts which include soil moisture data explain 67-83% of variability in seasonal streamflow volumes at the 0-month lead time. These forecasts have strong potential for improving surface water management in rainfall-dominated regions.

The third study looked at the potential of using remotely-sensed vegetation index data and measured meteorological data in a soil water balance model based on the FAO-56 dual crop coefficient method in order to estimate soil moisture under diverse vegetation types. The study focused on four common vegetation types in Oklahoma – mixed hardwood forest, loblolly pine plantation, cropland, and tallgrass prairie. My results show that the model is able to capture soil moisture dynamics relatively well under all of the study vegetation types, but that further adjustments are needed to order to improve model accuracy.

VITA

Briana M. Wyatt

Candidate for the Degree of

Doctor of Philosophy

Dissertation: MEASURING AND MODELING DEEP DRAINAGE, STREAMFLOW, AND SOIL MOISTURE IN OKLAHOMA

Major Field: SOIL SCIENCE

Biographical:

Education:

Completed the requirements for the Doctor of Philosophy in Soil Science at Oklahoma State University, Stillwater, Oklahoma in December 2019.

Completed the requirements for the Master of Science in Plant and Soil Sciences at Oklahoma State University, Stillwater, Oklahoma in May 2015.

Completed the requirements for the Bachelor of Science in Environmental Science at Oklahoma State University, Stillwater, Oklahoma in May 2013.

Experience:

Graduate Research Associate, Department of Plant and Soil Sciences, Oklahoma State University, Stillwater, OK. Supervisor: Dr. Tyson Ochsner. 2015-2019.

Graduate Research Assistant, Department of Plant and Soil Sciences, Oklahoma State University, Stillwater, OK. Supervisor: Dr. Tyson Ochsner. 2013-2015.

Professional Memberships:

American Geophysical Union; Soil Science Society of America; American Society of Agronomy